POLITECNICO
DI TORINO

Thermodynamic analysis in a scroll expander in an ORC system

Master's Thesis in Mechanical Engineering

Candidate

Matteo Silvano

Supervisor

Daniela Misul

Co-Supervisors

Mirko Baratta

Mohsen MosayebNezhad

A.Y. 2017-2018

Aknowledgments (ringraziamenti)

Ringrazio innanzitutto la professoressa Daniela Misul e il professor Mirko Baratta per avermi dato la possibilità di svolgere questo lavoro di tesi su un argomento innovativo e interessante.

Ringrazio Mohsen MosayebNezhad per la sua disponibilità, il suo supporto e il suo buon umore durante il lavoro.

Table of contents

1. Introduction 1

2. Technology description 3

2.1. Microturbines 3

2.2. ORC systems 5

2.3. Scroll Expander 11

3. Energy Modelling 15

3.1. Expander model 16

3.2. ORC system model 28

3.3. Efficiencies definitions 29

3.4. Assumptions 29

3.4.1. Original model assumptions 29

3.4.2. Micro-turbine assumptions 30

4. Studied configurations 32

4.1. Single-loop configuration 32

4.1.1. Scroll Assumptions 33

4.1.2. Plant Assumptions 34

4.2. Double-loop configuration 35

4.2.1. Configuration design 35

4.2.2. Scrolls assumptions 36

4.2.3. Plant assumptions 37

5. Results and discussion 37

5.1. Single-loop configuration 39

5.1.1. Design conditions 39

5.1.2. Parametric Analysis 40

5.2. Double-loop configuration 52

5.2.1. Design conditions 52

5.2.2. Parametric Analysis 53

5.3. Diagrams of the working fluids in design conditions 64

5.4. Discussion 65

6. Conclusion 66

7. Bibliography 67

Appendix: Double-loop configuration code 70

Nomenclature

A	area	[m^2]
AU	heat transfer coefficient	[W/K]
cp	specific heat	[J/kg K]
h	specific enthalpy	[J/kg]
$\dot{M}$	mass flow rate	[kg/s]
N	rotational speed	[rpm]
P	pressure	[Pa]
$\dot{Q}$	heat transfer rate	[W]
r	ratio	[-]
s	specific entropy	[J/kg K]
t	temperature	[°C]
u	specific internal energy	[J/kg]
v	specific volume	[m^3/kg]
$\dot{V}$	volume flow rate	[m^3/s]
w	specific work	[J/kg]
$\dot{W}$	power	[W]

Greek symbols

α	coefficient	[-]
Δ	difference	[-]
η	efficiency	[-]
γ	isentropic exponent	[-]

Subscripts

ad	adapted
amb	ambient
calc	calculated
comp	compressor
crit	critical
dis	discharge
elmec	electromechanical
ex3	end of isochoric expansion
ex2	after mixing with leakage flow
ex	exhaust
exp	expander
in	internal
is	isentropic
leak	leakage
loss0	constant losses
loss1	mechanical losses
loss2	electrical losses
mot	motor
n	nominal
oh	overheated
p	constant pressure
s	‘‘swept”
sh	shaft
su	suction conditions
su1	scroll suction
thr	throat
v	volume
w	wall

Figure index

Figure 1: Capstone C30 microturbine structure[2]. 4

Figure 2. Functional diagram of the C30 microturbine. 5

Figure 3: Photograph of a fixed Scroll. 12

Figure 4: Fabrication parameters of the scroll 13

Figure 5: Critical clearances of the machine [18]. 14

Figure 6: Description of the expansion process[19]. 15

Figure 7: Scroll design and chamber volume as function of angle [20]. 16

Figure 8: Schematic of the scroll expander model. 17

Figure 9: Representation of the entire expansion process in the P-V diagram. 22

Figure 10: Under (left)/ over(right)-expansion losses on P-V diagram 23

Figure 11: Flow chart of the model [5]. 28

Figure 12: Schematic of the scroll expander integrated into an ORC system 28

Figure 13: Single-loop configuration 33

Figure 14: Double-loop configuration 35

Figure 15: Mass flow-rate. 41

Figure 16: Leakage mass flow-rate. 42

Figure 17: Mass flow-rate and leakage. 43

Figure 18: Utility water mass flow-rate and leakage. 44

Figure 19: Utilities water mass flow-rate 45

Figure 20: Electrical power output and net power output 46

Figure 21: Exhaust fluid temperature. 47

Figure 22: Electrical efficiency. 48

Figure 23: Isentropic efficiency. 49

Figure 24: Total pump power supplied. 50
Figure 25: Pumps power supplied. 51
Figure 26: Mass and leakage flow rate in expander 1 53
Figure 27: Total pump power supplied. 54
Figure 28: Mass flow rate in expander 1 and 2. 55
Figure 29: Utility water mass flow rate. 56
Figure 31: Net electrical power output 57
Figure 32: Heat flow towards the ambient ($\dot{Q}_{amb}$) 58
Figure 33: Temperature at the expander exhaust 59
Figure 34: Electrical efficiency. 60
Figure 35: Isentropic efficiency 61
Figure 36: Pump total power 62
Figure 37: Pumps power. 63
Figure 38: T-s diagram of isopentane in thermodynamic cycle 64
Figure 39: Isobutane T-s diagram in thermodynamic cycle 64

List of Tables

Table 1. Microturbine technology comparison [1]. 3

Table 2: Input parameters of original model 30

Table 3: C30 microturbine parameters 31

Table 4: Properties of possible working fluids [25] 32

Table 5: Scroll Assumptions in Single-loop configuration 33

Table 6: Plant assumption 34

Table 7: First scroll assumptions (isopentane) 36

Table 8: Second Scroll assumptions (isobutane) 36

Table 9: Plant assumptions for double-loop configuration 37

Table 10: Results of single-loop configuration in design conditions 39

Table 11 : Results of double-loop configuration in design conditions 52

Table 12: Efficiency gain 65

Abstract

More and more people are finding that distributed energy solutions are the answer for their power resource challenges. Distributed energy comes in many forms. Renewables such as solar and wind are top-of-mind when most people think of distributed resources, but natural gas fed micro-CHP is often a good fit too, because it adds reliability to the system and is a consistent source of power. On the other hand, an organic Rankine cycle (ORC) allows the effective use of low temperature heat sources, offering an advantageous efficiency for small-scale applications. Therefore, ORC add-on could be a promising solution for micro-CHP applications. This thesis project aims to improve energy efficiency of a natural gas-fired 30kW microturbine system by recovering waste heat of the turbine and converting it to the useful shaft work using an ORC system. Results show that an electrical efficiency of 13.6% could be achieved in one of the proposed ORC systems, and so implementation of this solution could be beneficial to recover heat from exhaust gas of microturbine.

1. Introduction

In recent history, mankind has been struggling to find more efficient ways to produce, deliver and consume energy. Norms and legislations are leading the pace to this eco-friendly revolution, and the technological background has never been so challenging. Nowadays, producing from a resource must not only be cost-effective, but also, to a certain extent, be respectful of the environment. Greenhouse gas effect and pollutant emissions are worrying authorities and public opinion and several nations have started a massive energy renewable policy to limit emissions.

Interest in ensuring reliable power and controlling energy costs has led to a rise in distributed power generation. Industrial complexes, military bases, college campuses, as well as great companies and other facilities are taking advantage of the value of generating their own electricity, along with the flexibility it offers. A variety of technologies are available to generate electricity at or near where it will be used, including microturbines, internal combustion engines, solar panels, wind turbines, combined heat and power systems, and organic Rankine cycle (ORC) systems. Moreover, advances in microgrid technology have allowed more facilities to generate their own power, which is either islanded or connected to a larger grid.

Building new plants of any generating technology is a difficult and crucially important aspect of the electrical power business. Nevertheless, operating a plant is what really brings in revenue. Operating them efficiently can make the difference between profit and loss, particularly in competitive markets. In an operating environment, plant efficiency is a paramount feature for a power plant, no matter where the generation comes from. For fossil-fuel plants, also efficiency is key to reducing greenhouse gas emissions. A major efficiency goal for fossil-fueled plants is heat rate improvement. The fewer heat it takes to generate a kilowatt-hour of electrical energy, the less fuel is needed and the more money that flows to the bottom line. Combined heat and power (CHP) and waste heat recovery using organic Rankine cycle (ORC) systems are other interesting ways to optimize energy systems. The

CHP working principle consists in using heat carried by exhaust gases from fossil combustion systems that would otherwise be wasted. These flue gases could come from coal or biomass-fueled boiler or exhaust from a gas turbine or reciprocating engine, to produce steam and/or hot water for various industrial or commercial needs. The process can increase efficiency of the combined system significantly, which saves money on fuel and reduces overall emissions. On the other hand, ORC allows for the effective use of low temperature heat sources, offering an advantageous efficiency for small-scale applications. The heat sources can be of different origins, such as solar energy, natural gas, biomass, ground heat source and waste heat. Since ORC operates at lower pressures and temperatures, it reduces the cost, system complexity, and alleviates some safety concerns. Thus, an organic Rankine cycle (ORC) add-on could be a promising solution for micro-CHP applications.

The aim of this Master Thesis is to fully understand the working principle of a scroll expander, integrated within an Organic Rankine Cycle (ORC) plant, coping with different input parameters. Scroll expanders are volumetric machines commonly used in the refrigeration and air-conditioning industry and they often work as compressors (for fridges, tanks, etc…). If appropriately modified, these applications are mainly used to extract energy that would otherwise be waisted in the ambient, which allows very low efficiencies of the machine. Organic Rankine Cycles (ORC) systems are commonly coupled with these types of machines. In this study, two configurations of ORC have been investigated. Geometrical features have been set as parameters and the results have been commented. The present work examines the viability of utilization of such system and it is organized as follows: Section 2 presents an overview on microturbine technology, ORC system, and scroll expander. In Section 3, particular attention will be paid on the code used to model the machine's expansion process. In Section 4 an explanation of the studied configurations is given. in Section 5 the results are presented and commented.

2. Technology description

2.1. Microturbines

Microturbines can be considered as small, closely packed, high-speed turbo-generators that are able to generate energy in different forms, namely electricity and heat. The basic application of microturbines is to be found in aircraft auxiliary power systems, diesel engine turbochargers, and automotive designs. Microturbines are usually recuperated and are single-stage and single-shaft. Furthermore, they are quite close to each other in terms of most significant parameters as shown in Table 1.

Table 1. Microturbine technology comparison [1].

Turbine model/Parameters	$\dot{W}_{net}$ [kW]	η_{el} [%]	$T_{exhaust}$ [°C]	P_{fuel} [bar]
MTT	3	17	[-]	~3
Capstone C30	30	26	275	~4
Capstone C65	65	29	309	5.17
Ansaldo AE-T100	100	30	325	6
Capstone C200	200	33	280	5.17
FlexEnergy GT250S	250	30	256	5.51
FlexEnergy GT333S	333	32	267	6.2
Aurelia A400	400	40	185	7

Given these indicators, it has therefore been concluded that microturbines are optimized to an acceptable level and if any major modifications would be done, this would either be costly or risky. As an example, redesigning a turbine with a lower pressure ratio and an increased turbine inlet temperature (TIT) and recuperation ratio might lead to an increased efficiency, but it must be pointed

out that such a turbine would not only have unsatisfactory heat recovery capabilities but also would be relatively expensive due to the special materials required [1].

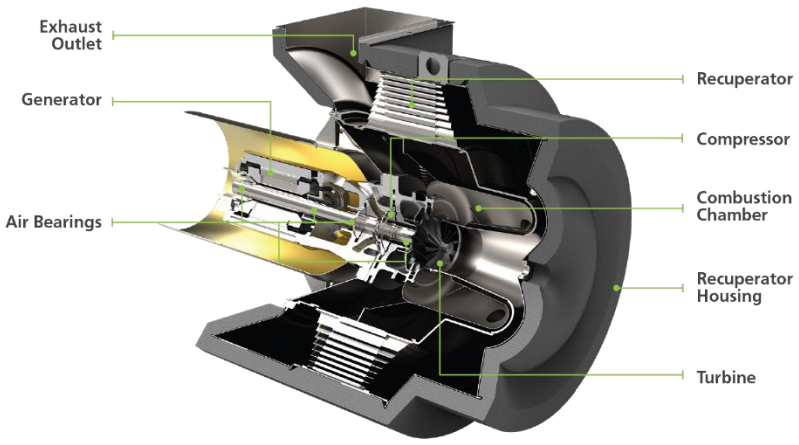

Figure 1: Capstone C30 microturbine structure[2].

Microturbine operation is described by a Brayton cycle. Figure 2 schematizes this cycle, in which the compressor first raises the air's atmospheric pressure to the required pressure. The compressed combustion air then passes through a non-mixing heat exchanger called a recuperator.

The recuperator enables the microturbine to use a portion of the exhaust thermal energy in order to preheat the combustion air. Thanks to the use of preheated air in the combustion phase, less fuel needs to be injected in order to guarantee the exhaust temperature which is required for expansion across the turbine. As a result, an increase in the overall fuel-to-electrical efficiency of the machine is to be expected.

In the next step of the Brayton cycle, the preheated and compressed air is led into a combustor, mixed with fuel and burned. This combustion process is highly exothermal and therefore releases heat. The discharge gases are subsequently expanded through a turbine in order to drive the rotation of the central shaft on which are assembled the compressor and the permanent magnet generator. Because

the turbine, compressor, and alternator are mounted on the same rotating shaft, they turn at the same angular speed to generate electrical power while permanently introducing air to sustain the overall process. The faster the machine's shaft spins in the magnetic field the more electrical power is generated in the alternator. Output power conditioning is generally realized by using inverter-based power electronics.

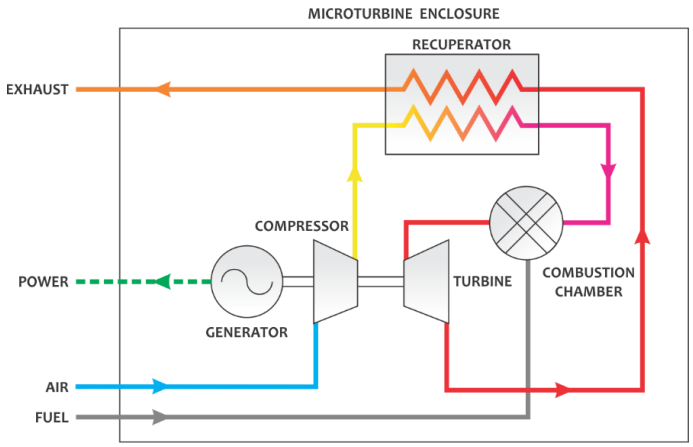

Figure 2. Functional diagram of the C30 microturbine.

2.2. ORC systems

The working principle of the ORC system is similar to that of the Rankine cycle. In this cycle, the working fluid is pumped to an evaporator where it is vaporized. Then it passes through an expansion device (which in this case is a scroll expander), and then through a condenser where it is re-condensed.

In the ideal cycle, the expansion is isentropic, and the evaporation and condensation processes are isobaric. In a real cycle, however, the presence of irreversibilities lowers the cycle efficiency. Those irreversibilities mainly occur in:

Expansion: Only a part of the energy recoverable from the pressure difference is transformed into useful work. The other part is converted into heat and is lost. The efficiency of the expander is defined by comparison with an isentropic expansion.

Exchangers: The fluid passes through a lengthy and sinuous path which guarantees good heat exchange but leads to pressure drops. This decreases the amount of power recoverable from the cycle.

ORC systems involve cycles in which the thermodynamic and physical properties of the working fluid are changed in order to obtain useful mechanical work. The ORC layout is in a way less complex than the one of the ordinary steam Rankine cycle: in such a process the water-steam drum connected to the boiler is no longer necessary and one single heat exchanger can be utilized to realise fluid preheating, vaporization and superheating phases. The development of micro ORC technologies, suitable for residential applications (a few kW), has received significant attention over the last years, even though a satisfactory efficiency is still a challenge [3].

Organic fluids tend to remain superheated when the expansion is terminated. It must be said that superheating is not as essential in ORC cycles as it is in steam cycles. In fact, in organic Rankine cycles with turbines, as the fluid does not condensate the risk of damaging turbine blades is mitigated; this allows to extend the machine's lifetime to 30 years instead of 15–20 years for normal steam turbines. In steam Rankine cycles, because of superheating constraint, the inlet temperature of the turbine should be higher than 450 °C to avoid droplets impact on the rotating components during the expansion. This implies higher thermal stresses in the boiler and on the turbine blades as well as a higher cost, as more energy and materials are required.

The low boiling point of a selected organic operating fluid enables to recover heat at much lower temperature during the lower heat recovery phase, which is an advantage. Regarding the components' dimensions, in a common steam cycle, the steam density is incredibly low in the low-pressure part of the cycle. Since pressure drops increase at the same rate as the velocity squared, the high-volume flow rate needs to have an increased hydraulic diameter of the pipes and adapted heat exchangers. Similarly, the turbine diameter is generally proportional to the volume flow rate. ORC cycles tolerate the use of once-through boilers, which avoids steam drums and recirculation units. This is mainly due

to the smaller density discrepancy between vapor and liquid for what concerns high-molecular-weight organic substances.

Pump power consumption is proportional to the liquid volume flow rate and to the pressure drop between outlet and inlet. It can be exposed in terms of the Back Work Ratio (BWR), which is usually defined as the pump power consumption divided by the turbine output power. In a steam Rankine cycle, the water flow rate is quite low and the BWR fluctuates around 0.4%. For a high temperature ORC using toluene, the typical value is 2–3%. For a low temperature ORC using HFC-134a, values higher than 10% are commonly faced. In a general way, the lower the critical temperature, the higher the BWR.

In a steam cycle, pressures of 60–70 bar and thermal stresses in the high-pressure process increase the technological cost of the boiler. In an ORC, pressure generally does not exceed 30 bar and the working fluid is not vaporized directly by the heat source (e.g. a biomass burner) but thanks to a heat transfer loop. The heat recovery is therefore easier since thermal oil can be at ambient pressure, and the necessity of an on-site steam boiler operator is prevented.

To by-pass air intrusion in the cycle, a condensing pressure higher than atmospheric pressure is highly advisable. Water has a condensing pressure generally lower than 0.1 bar absolute, which makes it difficult to use. On the contrary, low operating temperature organic fluids such as HFC-245fa, HCFC-123 or HFC-134a do meet this requirement. Organic fluids with a relatively high critical temperature on the other hand, such as hexane or toluene, are below atmospheric pressure at ambient temperature and so should be used cautiously.

Water as a working fluid has many advantages if compared to organic fluids. Its main assets are its abundance (which means lower cost), non-toxicity, non-flammability, its respect for the environment (low Global Warming Potential and null Ozone Depleting Potential), chemical stability (working fluid is not deteriorated in case of hot spot in the evaporator), and low viscosity (and so lower losses and higher heat exchange coefficients). On the other hand, steam cycles are normally not perfectly

sealed: water is lost as a consequence of leakage, drainage or boiler blow-down. That is why a water-treatment system must be included in the power plant to supply the cycle with pure deionized water. The plant should be provided with a deaerator to avoid corrosion of metallic parts due to the fact that oxygen might be present in the cycle.

Very often in steam cycles, the pressure ratio and the enthalpy drop over the turbine are considerable, so that turbines with several expansion stages are widely used. In ORC cycles, the enthalpy drop is quite smaller, and single or two-stage turbines are usually employed, which entails lower costs. Another consequence of the lower enthalpy drop of organic fluids is lower rotating speeds and therefore lower tip speed. A lower rotating speed allows direct coupling with the alternator without reduction gear (this is advantageous for low power-range plants), while the low tip speed diminishes the stress on the turbine blades and by that simplifies their design.

The efficiency of current high temperature Organic Rankine Cycles does not exceed 24%. Typical steam Rankine cycles show a thermal efficiency higher than 30%, but with a more complex cycle design (in terms of number of components or size) [4].

Over the past few years, ORC systems designed for micro-CHP installations have been investigated [5]–[7]. Qiu et al. [8] have made a review of the different ORC expansion machines and came to the conclusion that scroll expanders are particularly appropriate for micro-CHP systems which do not exceed 10 kWe. Peterson et al. [9] analyzed a scroll expander using several working fluids and achieved a variety of experimental results. Liu et al. [10] performed some simulation on a scroll expander coupled to an alternator in an ORC system to transform a thermal energy source, consisting of high pressure vapor, into electricity. The most important component in a domestic-application ORC system is the device that produces power. Small-scale ORC systems should be provided with an efficient expander which must also be cost-effective. Scroll machines are highly efficient, with little vibration, low noise level, simple design, and they are commonly used as compressors in the refrigeration industrial sector. Scroll expanders have all the benefits of scroll machines that are used

as compressors; they could therefore be an acceptable alternative for use in small-scale ORC systems. So far, a number of researchers have explored the use of expanders in ORC systems. Tadashi et al. [11] have investigated and tested the losses occurring in a scroll expander and have demonstrated that the efficiency could be as high as 75%. Zanelli et al. [12] built an ORC unit to perform some testing on a scroll expander modified from a commercial scroll compressor. Peterson et al. [9] also tested a scroll expander, obtaining an isentropic efficiency of 45%–50% when using refrigerant R123 as the working fluid. Yanaqisawa et al. [13] analyzed another scroll expander by choosing water mixed with air as the working fluid. They eventually found out that the performance output results of the expander were independent from the water-to-air volume ratio. Hiwata et al. [14] studied a scroll profile in order to monitor the axial load in a scroll expander and diminish the leakage losses during the expansion process. The studies that have been carried out have confirmed that leakage flow and heat transfer during the expansion process, as well as suction and discharge losses are the predominant factors that affect a scroll expander's efficiency. Even though the expander is a main component in the ORC, it has not been widely available for domestic-scale applications. An alternative approach that is generally considered is to use a more common refrigeration scroll compressor in reverse, as expander.

The review of the relevant literature showed that many aspects related to the ORC systems have been thoroughly investigated. However, to the best of author's knowledge utilization of scroll expander in an ORC system using cascade configuration integrated to a microturbine unit has not been studied and scrutinized yet. It is clear, from what has been said, that an appropriate working fluid should be chosen to enhance the performance of the machine. When selecting the most appropriate working fluid, the following guidelines and indicators should be considered carefully.

First of all, the thermodynamic performance has to be taken into account. The efficiency and/or power generated should be as high as possible for a predetermined heat source and heat sink temperatures. This performance is correlated to a certain amount of interdependent thermodynamic properties of

the working fluid such as critical point, acentric factor, density, specific heat, etc. It is not evident to calculate an optimized value for each thermodynamic property of interest independently. The usual approach consists in simulating the cycle with a thermodynamic model while controlling the behavior of different candidate working fluids.

Another factor that needs to be considered is the isentropic saturation vapor curve: in normal blade turbines a negative saturation vapor curve entails the formation of small droplets in the last phase of the expansion. The vapor must therefore be superheated when it arrives to the turbine inlet port to avoid blades damage. In the case of a positive saturation vapor curve, a recuperator can be used. As a result, cycle efficiency can be increased. One of the most indispensable factors is the necessity to have high vapor density: this parameter is of paramount importance mainly for fluids which have a very low condensing pressure (e.g. silicon oils). Low density is equivalent to a major volume flow rate: the size of the heat exchangers has therefore to be increased to limit excessive pressure drops. This has an important consequence on the overall cost of the system. It should however be noted that greater volume flow rates enable a simpler design in the case of turboexpanders, for which size is not a crucial issue. Normally, greater pressures lead to higher investment costs and technical complexity. That is why it is preferable to have lower pressures, which however must guarantee a satisfying power output. However, the low pressure is to be higher than the ambient pressure so as to avoid air intrusion into the cycle. Thus, the condensing gauge pressure has to be positive.

Another interesting characteristic of organic fluids is their low speed of sound. As a result, this speed is reached much sooner in an ORC than in a conventional steam cycle and constitutes an important advantage, as high Mach numbers correspond to higher irreversibilities and therefore lower turbine polytropic efficiencies.

In contrast to water, organic substances are known to suffer chemical deterioration and decomposition at relatively high temperatures. So, the maximum heat source temperature is limited by the chemical stability of the working fluid. Obviously, the melting point is bound to be lower than the lowest

temperature during the year to avoid the working fluid to freeze. The cycle has also to withstand safety compliance features which comprise two main points: its toxicity and flammability. The ASHRAE Standard 34 classifies refrigerant fluids in safety categories and can be used for the assessment of a working fluid of interest. Another critical chemical parameter is Low Ozone Depleting Potential (ODP). The ODP of current organic fluids is either equal to zero or very close to it, since non-null ODP substances have been progressively being phased-out in line with the Montreal Protocol. Greenhouse Warming Potential (GWP) is of capital concern and must be kept as low as possible. GWP is measured to the GWP of CO2 as a base, chosen as unity. Although some refrigerants can attain a GWP value as high as 1000, there is currently no legislation regarding the use of high GWP fluids. Last but not least, in order to choose the appropriate organic fluid, its cost cannot be neglected. The best condition is to have a working fluid with high availability and low cost: organic fluids already used in refrigeration or in the chemical sector are easily purchasable and low-priced.

2.3. Scroll Expander

Scroll compressors are volumetric machines that are commonly used in the industry, especially in refrigerating cycles. However, recently they have been also used in organic Rankine cycle (ORC) systems as expanders. The main advantages of this device is its simplicity and the fact that its components are commercially available [5]. Whereas large industrial ORC systems use turbomachinery components similar to those widely utilized in typical fossil-fuel-fired power generation plants, the main issue to develop ORC technology in the order of 1–100kW is in the accurate selection of an acceptable expander, given the unavailability of commercial turbines at this scale [15]. Prediction of scroll expander operation is therefore important to analyze and design the equipment.

A scroll expander is a volumetric machine which comprises an orbiting scroll and a fixed scroll. The scrolls face each other with a certain gap tolerance. The thermal machine itself has a wide working

range in terms of admissible pressure, rotational speed and power output. It has advantages of few moving parts, little vibration, low noise and simple structure. Moreover, the scroll machine as compressor is a well acknowledged technology that has been extensively applied in refrigeration and air-conditioning industry. In Figure 3 is exposed a photograph taken in Politecnico di Torino's Macchine laboratory, starring a fixed scroll of the machine (in this case, a compressor).

Figure 3: Photograph of a fixed Scroll.

Scroll expander has been applied in Organic Rankine Cycle (ORC) based Waste Heat Recovery (WHR) due to its high efficiency, compactness and low cost. As early as 1993, Toyota used a scroll expander as an energy conversion device on an Internal Combustion engine WHR system. The results indicated that, when using R123 under ambient temperature of 25°C, 3% overall efficiency improvement was achieved [16].

By developing manufacturing technologies and constantly spurring innovation and improvements, the scroll technology has become more and more present in the residential and commercial markets. Up to 2015, the production of the scroll compressors has exceeded 100 million since 2006 [17].

The geometrical modeling of the scroll machine is a part that has a crucial importance for the determination of the scroll machine's thermodynamic state, leakage, forces, heat transfer coefficients,

mechanical losses, etc. As a result, a precise geometrical model is to be thoroughly established and some fabrication parameters need to be established. It must include the measure of the principal parameters such as chamber volume and leakage area.

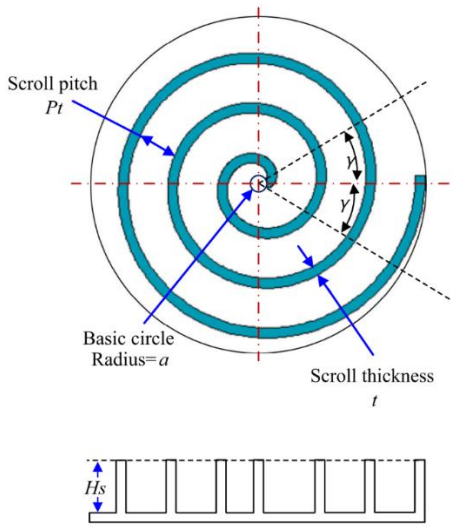

Figure 4: Fabrication parameters of the scroll

Generally, the refitted scroll expanders (which are the ones obtained by modifying scroll compressors) have a low efficiency due to suction/discharge pressure losses, mechanical losses (from bearings), over-and under-expansion losses, leakage, heat transfer losses, etc.

To optimize the performance of the expander and to limit under-expansion and over-expansion losses, this built-in volume ratio has to match the operating points of interest. Nevertheless, volume expansion ratios reached in Rankine cycle systems are usually greater than those attained in vapor compression refrigeration systems. That is why it is worth developing adapted designs of such expanders, instead of retrofitting existing compressors. It must be stated that piston alternating expanders are more suitable for applications with high expansion ratios because their structure allows remarkably elevated internal built-in volume ratios.

A major issue associated with the use of a volumetric machine is its lubrication system. One possible solution consists in keeping an oil separator at the expander outlet. In such a case, unlike the compressor use, an oil pump to drive the separated oil back to the expander suction is mandatory. Another solution would be to circulate the oil mixed with the refrigerant through the cycle and to provide the evaporator exhaust with an oil separator. The separated oil reaches the bearings, while the lubrication of the two spirals of the scroll machine depends on the efficiency of the separator. Another option would be to use oil-free machines, but these generally show poor volumetric performance and high leakage as consequence of larger tolerances between moving mechanical parts. In this thesis project, in order to simplify the cycle and have a more compact installation (no oil pump) the cycle has been considered oil-free.

In some operating conditions, liquid could probably be present at the end of the expansion phase. This is a significant problem for piston expanders, but not at all for scroll expanders, since they can generally tolerate a considerable liquid mass fraction without damaging. Among the multiple critical points that are faced during the design of this type of machine, a few are worth being deeply investigated. In particular, the unavoidable leakages that occur in the working cycle have to be limited by reducing as much as possible the radial clearance and the tip seal clearance, which are responsible for the losses of internal power. Clearance are however necessary to prevent the issue of mechanical friction resistance, which would decrease shaft work and would maybe lead to seizure. Figure 5 illustrates the two main types of leakage that are present in a scroll expander.

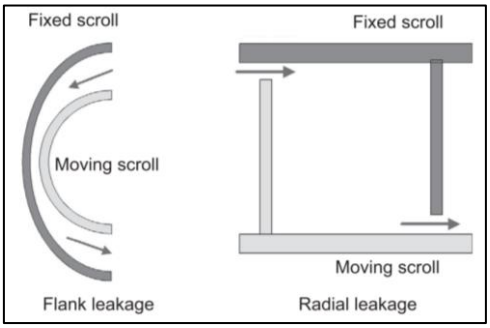

Figure 5: Critical clearances of the machine [18].

3. Energy Modelling

Scroll compressors are volumetric machines that are commonly used in the industry, especially in refrigerating cycles. However, they also can be used in Organic Rankine Cycles (ORC) as expanders, which is a process that involves vapor that must be heated by a hot gas usually in low grade heat recovery systems. In the expander mode, the orbiting spiral turns on the opposite direction with respect to the compressor mode. The main advantages of this cycle are essentially its impressive simplicity and the fact that its components are not niche products. The working fluid is generally a substance that has a lower ebullition temperature than water in order to require less energy for the fluid phase transformation. Although this technology exists, it has not been widely used in the industry and several studies involving different working fluids are in process. Scrolls are particularly suitable for small ORC applications as they allow to have limited flow rates and can tolerate also a two-phase condition, due to the reduced rotational speed, if compared to a turbomachine. Some of the researchers found out that the performance of the scroll is highly influenced by mechanical losses and fluid leakages, in different operating conditions.

A scroll expander is a machine that is mainly composed by an orbiting scroll, a fixed scroll, an inlet port and an exhaust port. The fluid in the chamber volume expands and mechanical work is produced (Figure 6) due to the difference between the pressures on the scroll flanks that produce a resulting force not aligned with the center of the fixed scroll (torque is therefore generated).

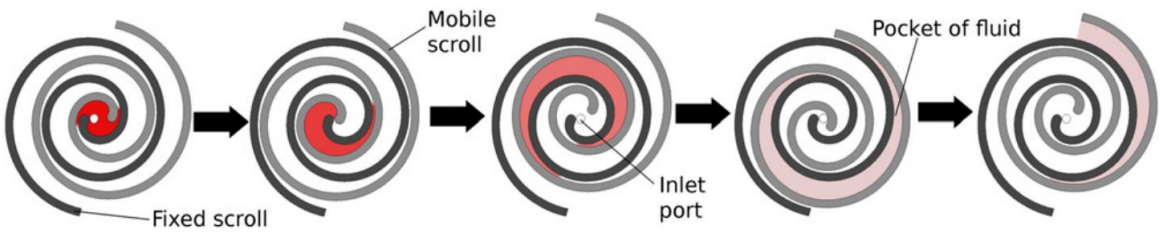

Figure 6: Description of the expansion process[19].

The volumes involved are variable during the normal operating conditions as the expansion process needs to take place (Figure 7, right). The two scrolls are almost tangent to each other; yet there is no contact between the parts, thanks to an accurate design of parts and precise manufacturing tolerances (Figure 5, left).

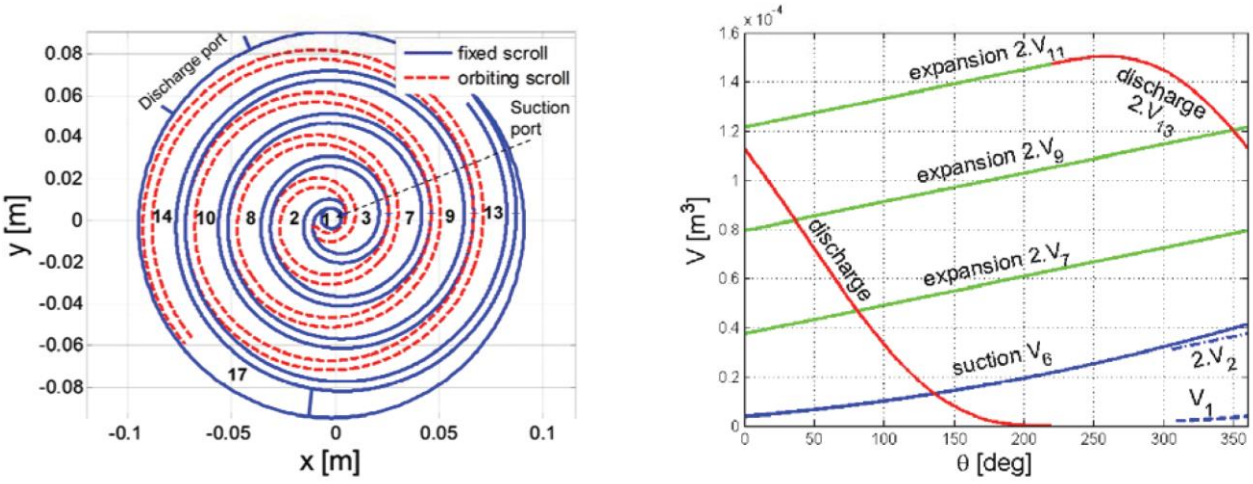

Figure 7: Scroll design and chamber volume as function of angle [20].

3.1. Expander model

The following semi-empirical model is based on a hermetic scroll compressor studied by Winandy et al.[21] as presented in Figure 8. The code has then been investigated by Lemort et al.[19] and perfectioned in order to be suitable for a scroll expander using EES (Engineering Equation Solver) software, the same used in this work. Details about the validation process are presented in Figure 11. The thermodynamic transformation model has been considered in the following order:

Adiabatic supply pressure drop: It corresponds to the pressure drop encountered at the inlet port.

Isobaric supply cooling-down: the chamber increases its volume at constant pressure so the temperature decreases.

Adiabatic and reversible expansion to the adapted pressure imposed by the built-in volume ratio of the machine: during this phase the machine generates work.

Adiabatic expansion at a constant machine volume: when the chamber faces the exhaust port, the pressure in the chamber is likely to be higher than the exhaust environment pressure.

Adiabatic mixing between supply and leakage flows: leakages are not participating to work production, but they must be considered in the thermodynamic process.

Isobaric exhaust cooling-down or heating-up: The fluid can be either cooled or heated, depending on its exhaust thermodynamic conditions with respect to the exhaust environment conditions.

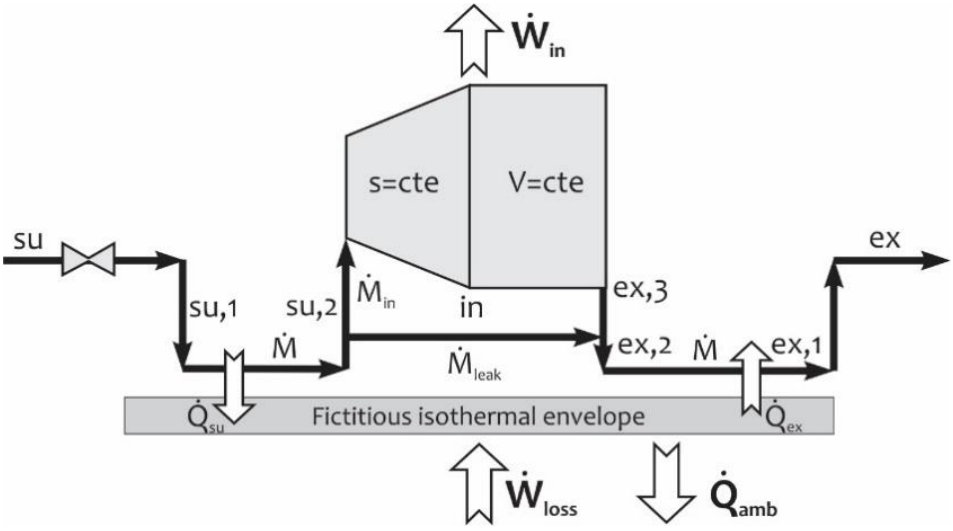

Figure 8: Schematic of the scroll expander model.

Supply Status

The fluid supply is in over-heated conditions, so there is a positive difference between the fluid temperature and the saturation temperature of the fluid at the same pressure.

$$\Delta T_{oh,su_0,exp} = T_{su_0,exp} - T_{sat,su_0,exp} \tag{1}$$

Assuming that the pressure losses in the supply pipe can be neglected:

$$P_{su,exp} = P_{su_0,exp} \tag{2}$$

Supply Pressure Drop su →su1

The cross-sectional inlet port area A_{su} is a parameter that still has to be identified. As the model is stationary, A_{su} represents an average area of the suction port during all the suction phase.

The cross-sectional area of the nozzle throat can be written as:

$$A_{thr,su} = \pi \cdot \frac{d_{su}^{\,2}}{4} \tag{3}$$

Pressure drop

The pressure drop is calculated as it would be computed in a converging nozzle in which an isentropic flow is present.

$$\Delta P_{su,exp} = \frac{\left[\frac{\dot{M}_{exp,guess}}{A_{thr,su}}\right]^2}{\frac{2}{v_{su,exp}}} \tag{4}$$

The pressure $P_{su_1,exp}$ at the beginning of the suction process is determined:

$$P_{su_1,exp} = P_{su,exp} - \Delta P_{su,exp} \tag{5}$$

The pressure losses at the inlet can be expressed by the ratio:

$$r_{p,su,exp} = \frac{P_{su_1,exp}}{P_{su,exp}} \tag{6}$$

Filling factor

The filling factor is always higher than the unitary value and is computed as:

$$\varphi = \frac{\dot{M}_{exp}}{\dot{M}_{th}} = 1 + \frac{\dot{M}_{leak}}{\dot{M}_{th}} \tag{7}$$

Throat section properties

The velocity is calculated, from the mass flow definition, as:

$$C_{thr,su} = \frac{\dot{M}_{exp,guess}}{A_{thr,su}} \cdot v_{thr,su} \tag{8}$$

The throat final enthalpy is determined considering only enthalpies and final kinetic energy in the energy balance equation (Eq.(9)).

$$h_{thr,su} = h_{su,exp} - \frac{C_{thr,su}^{\ 2}}{2} \tag{9}$$

Supply cooling down: su1 → su2

Heat capacity rate, which will be an important parameter in the following analysis can be calculated as:

$$\dot{C}_{su_1,exp} = \dot{M}_{exp,guess} \cdot cp_{su_1,\exp} \tag{10}$$

Heat transfer coefficient relationship between the nominal and the effective value can be written as:

$$AU_{su,exp} = AU_{su,exp,n} \cdot \left[\frac{\dot{M}_{exp,guess}}{\dot{M}_{exp,n}} \right]^{0.8} \tag{11}$$

Where $AU_{su,\exp,n}$ is the heat transfer coefficient that corresponds to the nominal mass flow rate $\dot{M}_n$. This expression is derived from the Reynold's analogy for a turbulent flow through a pipe. It has therefore been assumed that fluid properties remain unchanged. Exhaust heat transfer assumptions are very similar to these assumptions.

The number of transfer units is described by the equation below.

$$NTU_{su,exp} = \frac{AU_{su,exp}}{\dot{C}_{su_1,exp}} \tag{12}$$

The effectiveness is therefore:

$$\varepsilon_{su,exp} = 1 - \mathrm{e}^{-NTU_{su,exp}} \tag{13}$$

The heat rate has to be considered with the effectiveness of the heat exchange process. So it can be calculated as:

$$\dot{Q}_{su,exp} = \varepsilon_{su,exp} \cdot \dot{C}_{su_1,exp} \cdot \left[T_{su_1,exp} - T_{w,exp,guess} \right] \tag{14}$$

Suction phase is isobaric, as shown in the following identity.

$$P_{su_2,exp} = P_{su_1,exp} \tag{15}$$

According to the first law of thermodynamics, by neglecting kinetic terms:

$$h_{su_2,exp} = h_{su_1,exp} - \frac{\dot{Q}_{su,exp}}{\dot{M}_{exp,guess}} \tag{16}$$

Mass flow rate

The correlation between rotational speed and the output electrical power (Eq.(17)) is obtained from the alternator's manufacturer [19].

$$rpm_{exp} = 3007 + 0.02155 \cdot \dot{W}_{el,exp,guess} + 0.000002091 \cdot \dot{W}^2_{el,exp,guess} \tag{17}$$

The volumetric flow rate is defined as:

$$\dot{V}_{s,exp} = \frac{rpm_{exp}}{60} \cdot V_{s,exp} \tag{18}$$

Where $V_{s,\mathrm{exp}}$ is the swept volume in expander mode. It is equal to the one in compressor mode $V_{s,\mathrm{comp}}$ divided by the built-in volume ratio of the machine $r_{v,\mathrm{in}}$ (see Figure 9). The useful mass flow rate is consequently determined:

$$\dot{M}_{in} = \frac{\dot{V}_{s,exp}}{v_{su_2,exp}} \tag{19}$$

Leakage flow rate

A scroll Expander has two leakage paths: the radial leakage is caused by a gap between the bottom of the top plate and the scrolls; the flank leakage (tangential) is due to a gap between the flanks of the scrolls. In this model, the totality of leakage paths are gathered into a unique virtual leakage clearance, which area has been determined. The pressure at the inlet of the leakage nozzle is $P_{su_2,\exp}$.

$$P_{crit} = P_{su_2,exp} \cdot \left[\left(\frac{2}{\gamma+1} \right)^{\left(\frac{\gamma}{\gamma-1} \right)} \right] \tag{20}$$

The critical pressure ratio can be evaluated as:

$$r_{p,crit} = \frac{P_{su_2,exp}}{P_{crit}} \tag{21}$$

The following identity (Eq.(22)) implies neglecting pressure losses at the exhaust. The outlet port is sufficiently large to state this assumption.

$$P_{ex_3,exp} = P_{ex,exp} \tag{22}$$

The throat pressure in the nozzle is stated as the maximum between exhaust pressure and critical pressure [5].

$$P_{thr} = MAX\left[P_{ex_3,exp}; P_{crit} \right] \tag{23}$$

By applying first law of thermodynamics, with the due simplifications,

$$C_{thr} = \sqrt{2 \cdot \left(h_{su_2,exp} - h_{thr} \right)} \tag{24}$$

The mass flow rate is then easily determined:

$$\dot{M}_{leak} = A_{leak} \cdot \frac{C_{thr}}{v_{thr}} \tag{25}$$

The leakage total area is represented by the empirical correlation (Eq. (26)) used by Lemort et al.[19].

$$A_{leak} = (0,6845 - 0,11635604 \cdot (10 - \frac{P_{su,exp}}{10^5}) \quad (26)$$

Total flow

The total mass flow rate has to take into account also the leakages that do not contribute to mechanical work generation.

$$\dot{M}_{exp} = \dot{M}_{in} + \dot{M}_{leak} \quad (27)$$

Isentropic expansion: su2 → in

The specific volume of the working fluid at the end of the isentropic expansion process is calculated as follows:

$$v_{in,exp} = r_{v,in} \cdot v_{su_2,exp} \quad (28)$$

While $r_{v,in}$ is defined as the ratio between V_{in} and $V_{su,2}$ (initial and final volumes of the isentropic expansion process) as it is illustrated in Figure 9.

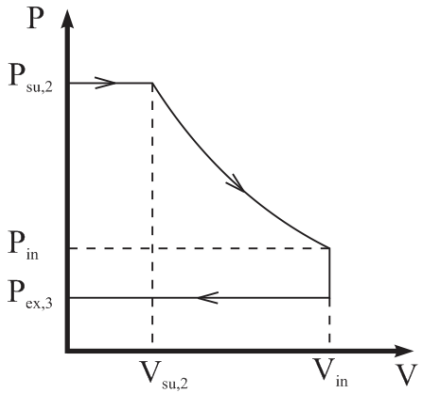

Figure 9: Representation of the entire expansion process in the P-V diagram.

In the previous figure, it can be noticed that the expander is operating with an under-expansion process, which means that useful work is lost. However, another possible issue can be caused by over-expansion process, which also leads to a work loss and therefore must be avoided (Figure 10).

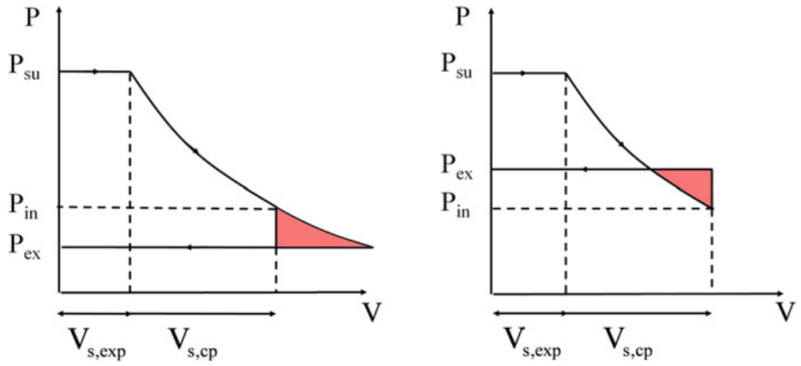

Figure 10: Under (left)/ over(right)-expansion losses on P-V diagram

The internal work referred to mass, if we neglect kinetic terms, is expressed as:

$$w_{exp,1} = h_{su_2,exp} - h_{in,exp} \tag{29}$$

The built-in pressure ratio is calculated as the ratio between the pressure at the end of suction and the pressure at the end of isentropic expansion.

$$r_{p,in} = \frac{P_{su_2,exp}}{P_{in,exp}} \tag{30}$$

Isochoric Expansion

The final part of the cycle is characterized by an isochoric expansion. In fact, as soon as the fluid faces the exhaust port, the difference between chamber pressure and exhaust pressure leads to a constant volume expansion, which produces still a small amount of work.

$$w_{exp,2} = v_{in,exp} \cdot (P_{in,exp} - P_{ex_3,exp}) \tag{31}$$

The enthalpy at the end of the latter expansion is

$$h_{ex_3,exp} = h_{in,exp} - w_{exp,2} \tag{32}$$

Total work referred to mass is calculated as:

$$w_{in,exp} = w_{exp,1} + w_{exp,2} \tag{33}$$

Power

The internal power can be defined as:

$$\dot{W}_{in,exp} = \dot{M}_{in} \cdot w_{in,exp} \tag{34}$$

The power lost as mechanical friction is calculated as the sum of mechanical power lost in the pipes (loss0) and the power lost in the machine (here a value of 0.1 has been adopted).

$$\dot{W}_{loss_1} = \dot{W}_{loss_0} + \alpha \cdot \dot{W}_{in,exp} \tag{35}$$

Where α is a predetermined coefficient, which accounts for mechanical losses [19].

The power available at the shaft is expressed as:

$$\dot{W}_{sh,exp} = \dot{W}_{in,exp} - \dot{W}_{loss_1} \tag{36}$$

Mechanical efficiency of the expander is defined as shaft power over internal power.

$$\eta_{mec} = \frac{\dot{W}_{sh,exp}}{\dot{W}_{in,exp}} \tag{37}$$

Electrical Power

The electrical power losses are related to the difference between the rotation speed at which the electric machine should work and the speed of the expander and are calculated according to the formula given by the electrical machine's manufacturer [19].

$$\dot{W}_{loss_2} = 198.7 + 0.4553 \cdot rpm_{rel} + 0.03699 \cdot rpm_{rel}^{\,2} \tag{38}$$

The electrical power obtained is calculated as:

$$\dot{W}_{el,exp} = \dot{W}_{sh,exp} - \dot{W}_{loss_2} \tag{39}$$

Power conversion efficiency is defined as:

$$\eta_{gen} = \frac{\dot{W}_{el,exp}}{\dot{W}_{sh,exp}} \tag{40}$$

The power losses can then be added to form a total power loss value:

$$\dot{W}_{loss} = \dot{W}_{loss_1} + \dot{W}_{loss_2} \tag{41}$$

Electromechanical efficiency is defined as:

$$\eta_{elmec} = \frac{\dot{W}_{el,exp}}{\dot{W}_{in,exp}} \tag{42}$$

Mixing with leakage at exhaust: ex3 → ex2

At the exhaust, the main flow mixes with leakage fluid in an adiabatic way (Eq. (43)), according to an enthalpy balance.

$$h_{ex_2,exp} = \frac{\dot{M}_{in} \cdot h_{ex_3,exp} + \dot{M}_{leak} \cdot h_{su_2,exp}}{\dot{M}_{exp}} \tag{43}$$

Exhaust cooling down: ex2 → ex1

The heat capacity rate is still expressed, similarly to Eq.(8), as:

$$\dot{C}_{ex_2,exp} = \dot{M}_{exp} \cdot cp_{ex_2,exp} \tag{44}$$

The heat transfer coefficient has been obtained with the same expression used in Eq.(11).

$$AU_{ex,exp} = AU_{ex,exp,n} \cdot \left[\frac{\dot{M}_{exp}}{\dot{M}_{exp,n}} \right]^{0.8} \tag{45}$$

The definitions of ε and NTU are still applicable:

$$NTU_{ex,exp} = \frac{AU_{ex,exp}}{\dot{C}_{ex_2,exp}} \tag{46}$$

$$\varepsilon_{ex,exp} = 1 - e^{-NTU_{ex,exp}} \tag{47}$$

The heat rate stars an iterative value of temperature and is expressed by Eq.(48).

$$\dot{Q}_{ex,exp} = \varepsilon_{ex,exp} \cdot \dot{C}_{ex_2,exp} \cdot \left(T_{ex_2,exp} - T_{w,exp,guess} \right) \tag{48}$$

The enthalpy therefore obtained by the application of first law of thermodynamics is described in Eq.(49).

$$h_{ex_1,exp} = h_{ex_2,exp} - \frac{\dot{Q}_{ex,exp}}{\dot{M}_{exp}} \tag{49}$$

Heat Balance over the expander

The main heat transfer in a scroll expander happens between:

- The expander's envelope and the fluid in the supply and exhaust ports, where the shell and the scrolls are introduced as a metallic envelope of uniform temperature T_w.
- The scrolls and the fluid in the suction, expansion end discharge chambers.
- The shell and the ambient air.

The total heat rate exchanged with ambient air is formed by three main terms: the suction term, the exhaust term and the mechanical term (components frictions).

$$\dot{Q}_{amb,exp} = \dot{Q}_{su,exp} + \dot{Q}_{ex,exp} + \dot{W}_{loss} \tag{50}$$

The fictitious envelope averaged temperature is calculated in Eq.(51) and it has a consistent influence on the heat transfer to the ambient.

$$T_{w,exp} = \frac{\dot{Q}_{amb,exp}}{AU_{amb,exp}} + T_{amb,exp} \tag{51}$$

Energy balance check

The final error is defined as Eq.(52) and should be minimized for accurate results:

$$residual = \dot{M}_{exp} \cdot \left(h_{su_0,exp} - h_{ex,exp} \right) - \dot{W}_{el,exp} - \dot{Q}_{amb,exp} \tag{52}$$

Performance

$$w_{is,exp} = h_{su,exp} - h_{ex,exp} \tag{53}$$

Where $w_{is,\exp}$ the isentropic work is referred to mass produced by the expansion.

The isentropic efficiency is defined by the ratio of the internal work and the isentropic work (Eq.(54)).

$$\eta_{is} = \frac{w_{in,exp}}{w_{is,exp}} \tag{54}$$

Eq.(55) represents the pressure ratio (PR) between suction port and exhaust:

$$PR = \frac{P_{su,exp}}{P_{ex,exp}} \tag{55}$$

Eq. (56) represents the theoretical mass flow rate which is defined as the ratio between volumetric flow rate and specific volume at the suction.

$$\dot{M}_{th} = \frac{\dot{V}_{s,exp}}{v_{su,exp}} \tag{56}$$

The previous model has been validated experimentally by Lemort et al. [19] with a maximum deviation of 2%. The uncertainty on output temperatures is 0,5 K while the uncertainty regarding output power is of 15W, which are both acceptable values. For further clarification, the parameter identification process is illustrated in a concise flow-chart diagram in Figure 11.

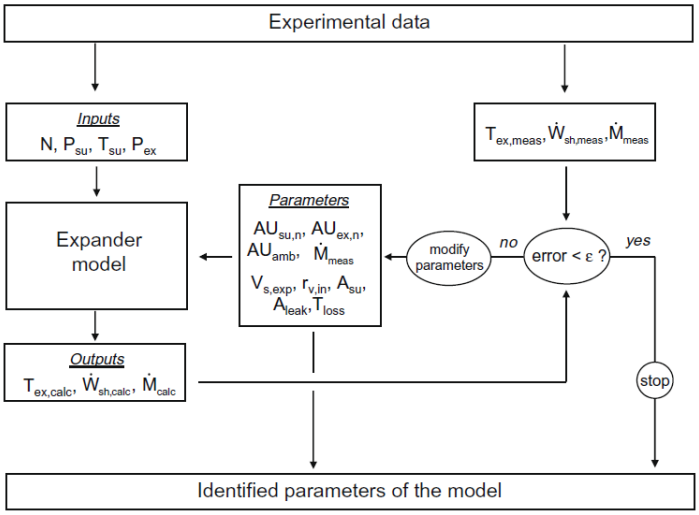

Figure 11: Flow chart of the model [5].

3.2. ORC system model

The power plant is very similar to a normal Rankine Cycle, with the difference that a different working fluid is used. As a matter of fact, in this application organic substances are used instead of highly pure water. Figure 12 demonstrates integration of the scroll expander into an Organic Rankine Cycle. One of the most peculiar things about the cycle illustrated and the model used is the isothermal envelope, which is fictitious, as it does not physically exist, but it is a more effective way to perceive the heat transmitted to ambient air and to have an idea of the thermal efficiency of the machine.

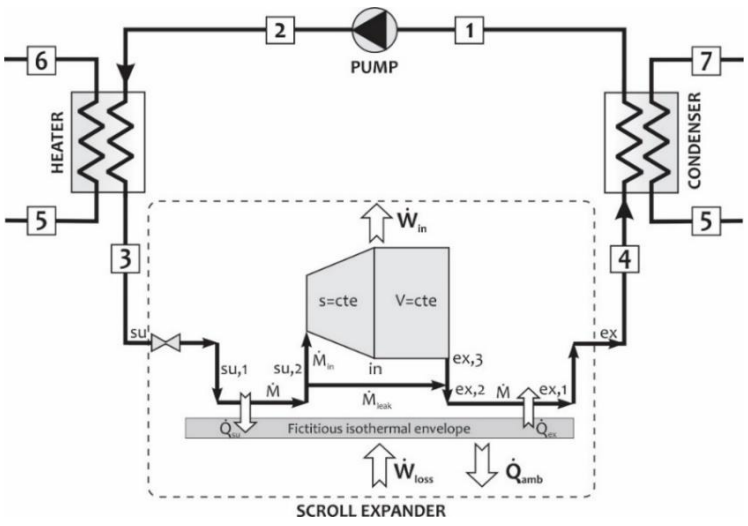

Figure 12: Schematic of the scroll expander integrated into an ORC system

Pump absorbed electrical power is calculated as:

$$\dot{W}_{pump} = \dot{M}_{exp} \cdot \frac{v_1(P_2 - P_1)}{\eta_{pump}} \tag{57}$$

Net electrical work is defined as:

$$\dot{W}_{net} = \dot{W}_{el,exp} - \dot{W}_{pump} \tag{58}$$

The amount of thermal energy introduced to the boiler load can be obtained using Eq. (59):

$$\dot{Q}_{evaporator} = \dot{M}_{exp} \cdot (h_3 - h_2) \tag{59}$$

3.3. Efficiencies definitions

The efficiencies of the different systems have been defined and calculated in the following way:

$$\eta_{el} = \frac{\dot{W}_{net}}{\dot{Q}_{in}} \tag{60}$$

$$\eta_{CHP} = \frac{\dot{W}_{net} + \dot{Q}_{recovered}}{\dot{Q}_{in}} \tag{61}$$

$$\eta_{overall} = \frac{\dot{W}_{net,total} + \dot{Q}_{recovered}}{\dot{Q}_{combustion}} \tag{62}$$

Where $\dot{W}_{net}$ is the net electric power, $\dot{W}_{net\_total}$ is the total net output produced by the microturbine and the scroll expander, $\dot{Q}_{recovered}$ is the total heat recovered by the system. In the denominator, there is the energy provided by the gas combustion $\dot{Q}_{combustion}$ or the energy available from exhaust gas from microturbine $\dot{Q}_{in}$.

3.4. Assumptions

3.4.1. Original model assumptions

The input values given to the original model are presented in Table 2. These values have then been modified in order to increase power and have a more convenient system from a thermodynamic

point of view, for this particular application, which includes the integration to a microturbine. If the same conditions were to be kept, the enthalpy of the exhaust gases would be extracted in an unsatisfactory way and the power output would be too low to invest sensibly in this technology.

Table 2: Input parameters of original model

Symbol	Value	UOM	Parameter
$P_{su,exp}$	$1.6 \cdot 10^6$	[Pa]	Supply Pressure
$P_{ex,exp}$	$2.8 \cdot 10^5$	[Pa]	Exhaust Pressure
$T_{su,exp}$	139	[°C]	Supply Temperature
$T_{amb,exp}$	34	[°C]	Ambient Temperature
A_{leak}	$1.383 \cdot 10^{-6}$	[m^2]	Leakage Area
A_{su}	$3 \cdot 10^{-5}$	[m^2]	Suction Port Area
$r_{v,in}$	2.85	[dim]	Built-in Volume Ratio
V_{s,exp,cm^3}	22.4	[cm^3]	Swept Volume (Displacement)
$AU_{amb,exp}$	3.4	[W/K]	Heat Transfer Coefficient with ambient air
$AU_{su,exp,n}$	30	[W/K]	Nominal Heat Transfer Coefficient in suction
$AU_{ex,exp,n}$	30	[W/K]	Nominal Heat Transfer Coefficient in exhaust
$\dot{M}_{r,exp,n}$	0.1	[kg/s]	Nominal Flow Rate
$\dot{W}_{loss,0}$	0	[W]	Power lost in pipes
α	0.1	[dim]	Mechanical losses Coefficient
rpm	3000	[rpm]	Angular speed of the generator

3.4.2. Micro-turbine assumptions

A CAPSTONE C30 microturbine has been used in its design conditions and delivers the conditions described in Table 3. Temperature and mass flow rate have been taken from capstone technical reference [22]. The specific heat value has been calculated by the EES software in order to have a sensible value, according to a non-ideal combustion with 10% excess of air. The gas turbine produces the power required for air and fuel compressor, as well as a surplus of mechanical power.

The isentropic efficiency of the gas turbine is defined as follows:

$$\eta_{GT} = \frac{h_{in} - h_{out}}{h_{in} - h_{out,s}} \tag{63}$$

Accordingly, the internal power produced by the gas turbine can be defined as:

$$\dot{W}_{GT} = \dot{M}_g (h_{in} - h_{out}) \tag{64}$$

And the electric power is obtained as:

$$\dot{W}_{EL} = \eta_M \times \eta_{EL} (\dot{W}_{GT} - \dot{W}_C) \tag{65}$$

Where η_M and η_{EL} are mechanical and electrical efficiencies, respectively.

$$\dot{Q}_{combustion} = \dot{m}_{CH_4} \cdot LHV_{CH_4} \tag{66}$$

Where $\dot{m}_{CH_4}$ is the fuel mass flow rate and LHV_{CH_4} is the lower heating value of the fuel.

N.B. This last value has been estimated thanks to the electrical efficiency, which is known, and the electrical net power output. The LHV has been assumed to be equal to 50 MJ/kg which is the average value for commercial methane.

The microturbine parameters are reported in Table 3.

Table 3: C30 microturbine parameters

Symbol	Value	UOM	Parameter
T_{18}	275	[°C]	Exhaust temperature
$\dot{M}_g$	0,31	[kg/s]	Exhaust gas mass flow rate
cp_g	1100	[J/(kg·K)]	Specific heat
$\dot{W}_{EL}$	30000	[W]	Power output
$\dot{Q}_{combustion}$	115385	[W]	Heat rate delivered
$\dot{m}_{CH4}$	2.31	[g/s]	Fuel mass flow rate

4.Studied configurations

4.1. Single-loop configuration

The previous model of the expander has been used to describe a single loop ORC system for domestic application. Such a cycle has very basic elements such as condenser, evaporator and expander. The condensing heat is recovered through a water circuit thanks to a highly efficient heat exchanger. In the proposed system, exhaust gas of a 30 kW microturbine heats up an intermediate water loop using the first heat recovery exchanger (HX1). To fulfill this scope, two working fluids have been chosen, one for the first loop, the other for the second loop presented in Section 4.2. The working fluids have been identified according to their thermodynamic properties that had to match system property and because their range of operating temperatures is very suitable for this particular application, provided that a water-loop is introduced. In particular, Heberle and Brüggemann [23] published an exergy-based analysis aimed at selecting the working fluid in an organic Rankine cycle. They concluded that working fluids with lower critical temperatures, for example isopentane and isobutane, are more appropriate for power generation within an ORC system [24]. As a matter of fact, they have much lower GWP than other refrigerants, which makes them even more suitable for our purposes. Table 4 summarizes the properties of the two fluids above mentioned.

Table 4: Properties of possible working fluids [25]

Working fluid	R227ea	Isobutane	R245fa	Isopentane
T_c [K]	374.9	407.81	427.16	460.35
P_c [MPa]	2.93	3.63	3.65	3.38
Global Warming Potential	2900	3	820	11

Global Warming Potential (CO_2)=1

In the proposed configuration, the water loop has been introduced to transfer thermal energy recovered from the exhaust gas to the evaporator of the ORC system (HX1). In this way, the working fluid (in our case isopentane) receives the thermal energy at a lower temperature, which is more

appropriate for this kind of application with organic fluids. It must be pointed out that water has been kept liquid for safety reasons by pressurizing the ducts. That is why temperatures higher than 100°C are reached. In this configuration, as in the one in the following section, the heat losses of the exchanger towards the ambient have been neglected. Heat exchangers have therefore been assumed to be adiabatic. After having tried different inlet pressures and temperatures, the ones presented in Figure 13 have been chosen as a good compromise between the working fluids characteristics and the results obtained. Moreover, pinch point temperature difference are acceptable and are always higher than 5°C.

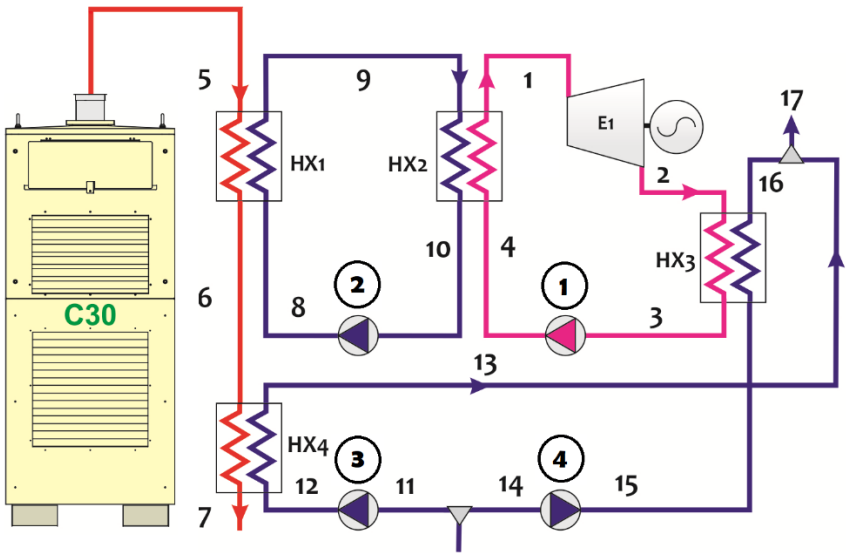

Figure 13: Single-loop configuration

4.1.1. Scroll Assumptions

Table 5: Scroll Assumptions in Single-loop configuration

Symbol	Value	UOM	Parameter
$P_{su,\,exp}$	$1.2 \cdot 10^{6}$	[Pa]	Supply pressure
$P_{ex,\,exp}$	$4 \cdot 10^{5}$	[Pa]	Exhaust pressure
$T_{su,\,exp}$	140	[°C]	Supply temperature
$T_{amb,\,exp}$	34	[°C]	Ambient temperature
A_{leak}	$9.172 \cdot 10^{-7}$	[m^2]	Leakage area
A_{su}	$6 \cdot 10^{-5}$	[m^2]	Suction port area
$r_{v,\,in}$	2.85	[dim]	Built-in volume ratio

$V_{s,\,exp,\,cm^3}$	45	[cm^3]	Swept volume (Displacement)
$AU_{amb,\,exp}$	3.4	[W/K]	Heat transfer coefficient with ambient air
$AU_{su,\,exp,\,n}$	30	[W/K]	Nominal heat transfer coefficient in suction
$AU_{ex,\,exp,\,n}$	30	[W/K]	Heat transfer coefficient in exhaust
$\dot{M}_{exp,\,n}$	0.1	[kg/s]	Nominal flow rate
$\dot{W}_{loss0}$	0	[W]	Power lost in pipes
α	0.1	[dim]	Coefficient

4.1.2. Plant Assumptions

The plant assumptions are reported in Table 6.

Table 6: Plant assumption

Symbol	Value	UOM	Parameters
$\dot{M}_{water}$	0.1	[kg/s]	Water-loop mass flow rate
T_9	150	[°C]	Water temperature
P_9	6	[Bar]	Water pressure
T_7	75	[°C]	Exhaust gas temperature
P_7	1.013	[Bar]	Exhaust gas pressure
T_1	140	[°C]	Scroll supply temperature
P_1	1.2	[MPa]	Scroll supply pressure
T_{12}, T_{15}	15	[°C]	Utility input temperature
T_{13}, T_{16}	60	[°C]	Utility output temperature
η_{Cond_P}	0.99	[-]	Pressure efficiency of condenser (HX3)
η_{HT_HX}	0.98	[-]	Pressure efficiency of HT heat exchanger
η_{LT_HX}	0.97	[-]	Pressure efficiency of LT heat exchanger

It must be stated that enthalpy losses in heat exchangers and in pipes have been neglected, as it has been noted that high efficiency heat exchangers have been used, coupled to a satisfactory pipes insulation material. The pressure efficiencies have been reported according to [24]. The exhaust gas pressure has been assumed equal to the atmospheric one, without any type of aftertreatment system.

Pressure P_1 has been chosen because it is the most suitable one at the chosen temperature as it allows to not excessively over-heat the organic fluid. Temperature T_1 has been chosen as the maximum temperature that can be delivered from the heat exchanger, considering a pinch point of 10°C.

Temperatures T_{10} T_{13}, T_{15}, T_{16} have been chosen as typical water grid temperatures that can be encountered in residential applications. Pressure P_9 has been implemented to avoid water evaporation that would increase pump power consumption.

4.2. Double-loop configuration

4.2.1. Configuration design

The configuration which has been described so far has clearly shown a lack of efficiency. In order to improve this efficiency and increase it to at least 10%, the plant has been modified and another loop with another expander has been introduced. Performance is therefore expected to increase especially in terms of net power obtainable. The new configuration has been designed and simulated. The working fluids (isopentane, isobutane) have been chosen, as mentioned before, according to a logic of exergy minimization and the same pressures and temperatures have been chosen, in order to verify how much of the water utility flow rate is lost with respect to the previous case. This alternative configuration is reported in Figure 14. In the next figure, the circled numbers are indicating the number of the pumps that are reported in the results part.

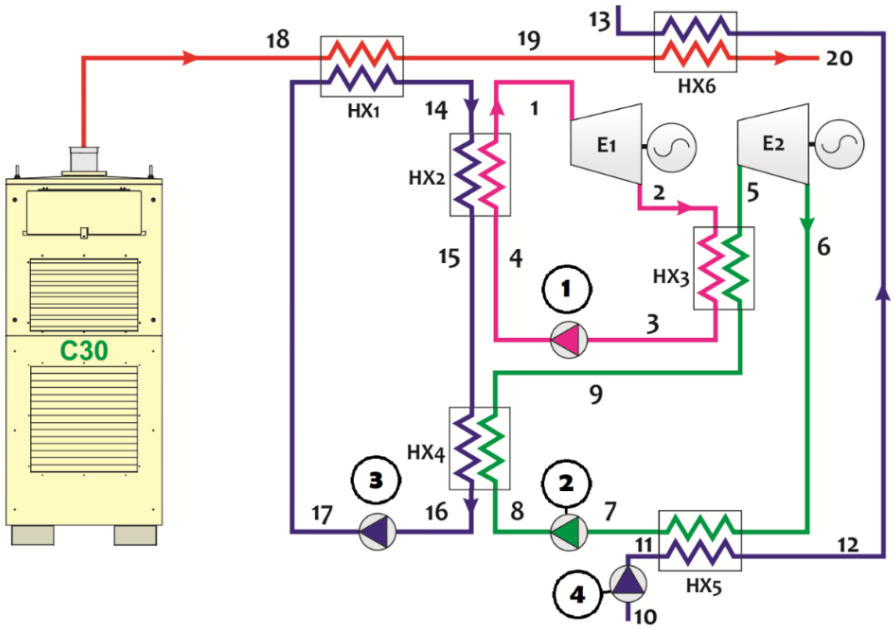

Figure 14: Double-loop configuration

The water loop has been kept and another heat exchanger has been introduced for preheating of isobutane in second loop. The goal of this configuration is to increase significantly the power output without decreasing too much the water utility mass flow rate. Thanks to the interesting thermodynamic properties of organic fluids, this objective can be achieved, as these types of fluids require low quantities of heat for their phase transformation.

4.2.2. Scrolls assumptions

The assumptions of the first scroll have been chosen in order to optimize performance without attaining abnormal or dangerous pressures, since this application is though for domestic use and therefore requires some safety measures. The temperature at the inlet has been considered as the maximum temperature for the working fluid to operate. In our case, two-phase conditions have not been explored, so the fluid is always oversaturated at the expander exhaust. The pressure matching has been chosen after several trial and error tests that have led to these particular values which are in line with what is found in technical literature. The numerical assumptions are reported in Table 7 and Table 8.

Table 7: First scroll assumptions (isopentane)

Symbol	Value	UOM	Parameter
$P_{su,\ exp1}$	$1.2 \cdot 10^{6}$	[Pa]	Supply pressure
$P_{ex,\ exp1}$	$4 \cdot 10^{5}$	[Pa]	Exhaust pressure
$T_{su,\ exp1}$	140	[°C]	Supply temperature

Table 8: Second Scroll assumptions (isobutane)

Symbol	Value	UOM	Parameter
$P_{su,\ exp2}$	$1.4 \cdot 10^{6}$	[Pa]	Supply Pressure
$P_{ex,\ exp2}$	$4.5 \cdot 10^{5}$	[Pa]	Exhaust Pressure
$T_{su,\ exp2}$	100	[°C]	Supply Temperature

4.2.3. Plant assumptions

Table 9: Plant assumptions for double-loop configuration

Symbol	Value	UOM	Parameters
$\dot{M}_{water}$	0.1	[kg/s]	Water-loop mass flow rate
T_{14}	150	[°C]	Water temperature
P_{14}	6	[Bar]	Water pressure
T_{20}	75	[°C]	Exhaust gas temperature
P_{20}	1.013	[Bar]	Exhaust gas pressure
T_{10}	15	[°C]	Utility input temperature
T_{13}	60	[°C]	Utility output temperature
η_{Cond_P}	0.99	[-]	Pressure loss efficiency of condenser (HX5)
η_{HT_HX}	0.98	[-]	Pressure loss efficiency of HT heat exchanger
η_{LT_HX}	0.97	[-]	Pressure loss efficiency of LT heat exchanger

4.2.4. Heat exchangers and pumps

The source of energy of the whole cycle are the exhaust gases (red line in Figure 14). The two heat transfers in the exchangers where the exhaust gases are flowing are described by these equations:

HX1

$$\dot{M}_g \cdot (h_{18} - h_{19}) = \dot{M}_{water} \cdot (h_{14} - h_{17}) \tag{67}$$

HX6

$$\dot{M}_g \cdot (h_{19} - h_{20}) = \dot{M}_{cw} \cdot (h_{13} - h_{12}) \tag{68}$$

The heat balance is therefore respected, so heat exchangers are assumed to be large enough to transfer all the enthalpy flux from a fluid to the other, and enough small to neglect ambient heat losses.

The cycle process is described as follows:

Loop 1:

The working fluid (isopentane) is heated-up by pressurized liquid water in a non-mixing heat exchanger (HX2) in order to have a superheated working fluid at the expander's inlet. The heat balance is as follows:

The fluid then expands in the scroll expander and produces work. It is then condensed and saturated in HX3 according to the following equation:

$$\dot{M}_{\exp 1} \cdot (h_2 - h_3) = \dot{M}_{\exp 2} \cdot (h_5 - h_9) \tag{70}$$

$$\dot{M}_{\exp 1} \cdot (h_1 - h_4) = \dot{M}_{water} \cdot (h_{14} - h_{15}) \tag{69}$$

It is then pumped from point 3 to 4 in order to compensate the pressure losses in the circuit. The equation used to describe the pumping effect on enthalpy is:

$$h_4 = h_3 + v_3 \cdot (P_4 - P_3) \tag{71}$$

Loop 2:

The working fluid (isobutane) is heated-up by condensing isopentane in a non-mixing heat exchanger (HX3) in order to have a superheated working fluid at the expander's inlet. The enthalpy balance is the same as Eq.(70). Then the working fluid expands in the second scroll machine and produces additional work. It is then condensed and saturated in another heat exchanger where cold water arrives from the water grid at 15°C. The heat balance in exchanger HX5 is the following:

$$\dot{M}_{\exp 2} \cdot (h_6 - h_7) = \dot{M}_{cw} \cdot (h_{12} - h_{11}) \tag{72}$$

The fluid is subsequently pumped according to the same equation already described (Eq.(71)), and that has been used for every pump in the plant. From point 8 to 9 the fluid is pre-heated by the water in heat exchanger HX4. The heat balance is as follows:

$$\dot{M}_{\exp 2} \cdot (h_9 - h_8) = \dot{M}_{water} \cdot (h_{15} - h_{16}) \tag{73}$$

It has been assumed that the heat exchangers are highly efficient and strongly isolated from the ambient so that there are no enthalpy losses towards the ambient during heat transfer phase. Due to the small mass flow rates it is considered that heat balance is achieved successfully.

5. Results and discussion

5.1. Single-loop configuration

5.1.1. Design conditions

In Table 10 the results of design condition for single-loop configuration have been reported. Comments on this part are present in Section 5.4.

Table 10: Results of single-loop configuration in design conditions

Symbol	Value	UOM	Parameters
T_{ex}	107.8	[°C]	Scroll exhaust temperature
T_w	111.6	[°C]	Fictitious envelope temperature
$\dot{M}_{water}$	100	[g/s]	Water-loop mass flow rate
$\dot{M}_{cw}$	344	[g/s]	Total Water utility mass flow rate
$\dot{M}_{cw1}$	189	[g/s]	Water utility mass flow rate(1)
$\dot{M}_{cw2}$	155	[g/s]	Water utility mass flow rate(2)
$\dot{M}_{exp}$	78.2	[g/s]	Fluid mass flow rate in expander
$\dot{M}_{leak}$	5.36	[g/s]	Leakage mass flow rate
$\dot{W}_{pump1}$	121.5	[W]	Pump 1 power consumption
$\dot{W}_{pump2}$	3.3	[W]	Pump 2 power consumption
$\dot{W}_{pump3}$	31.8	[W]	Pump 3 power consumption
$\dot{W}_{pump4}$	24.9	[W]	Pump 4 power consumption
$\dot{W}_{pump}$	181.5	[W]	Total pumps power consumption
$\dot{W}_{el}$	2398	[W]	Electrical power output

$\dot{W}_{net}$	2217	[W]	Net electrical power output
residual	$4.9 \cdot 10^{-11}$	[W]	Residual error
$\dot{Q}_{input}$	68200	[W]	Input heat flow
$\dot{Q}_{HX\_water}$	32588	[W]	Heat flow provided to water loop
$\dot{Q}_{cw}$	64728	[W]	Heat flow provided to cold water
$\dot{Q}_{amb}$	1193	[W]	Heat flow released in ambient
η_{is}	71	[%]	Isentropic efficiency
η_{cycle}	98	[%]	Cycle efficiency
η_{el}	6.8	[%]	Electrical efficiency
φ	1.062	[-]	Filling factor

N.B. The number associated to each pump is reported in Figure 13 as a circled number above the pump.

5.1.2. Parametric Analysis

A parametric analysis has been carried out to evaluate the variation of the output values of the code when the parameters that can be controlled have been modified. The pressure ratio PR has been considered between points 2 and 8, with the pressure at suction port fixed to 1.2 bar and temperature of 140°C. It is better not to have too high PR values, as too high gradients of pressure could lead to a higher leakage flow and eventually to a major stress on the mechanical parts of the machine. The built-in volume ratio was made to vary from 2 to 4, which is approximately the admissible range for this type of machine, considering that the geometry of the scrolls is not too variable from one expander to another. The swept volume has been taken from 22.4 cc which is the same value chosen in the expander initial assumption (see Table 2) and was doubled up to 45 cc which is a suitable value for commercial scroll expanders. The suction area has been tripled to see it's change consequences on output values, since it is a geometrical parameter of the machine that can be optimized. Results are reported in the following pages.

Mass flow rate in expander ($\dot{M}_{exp}$)

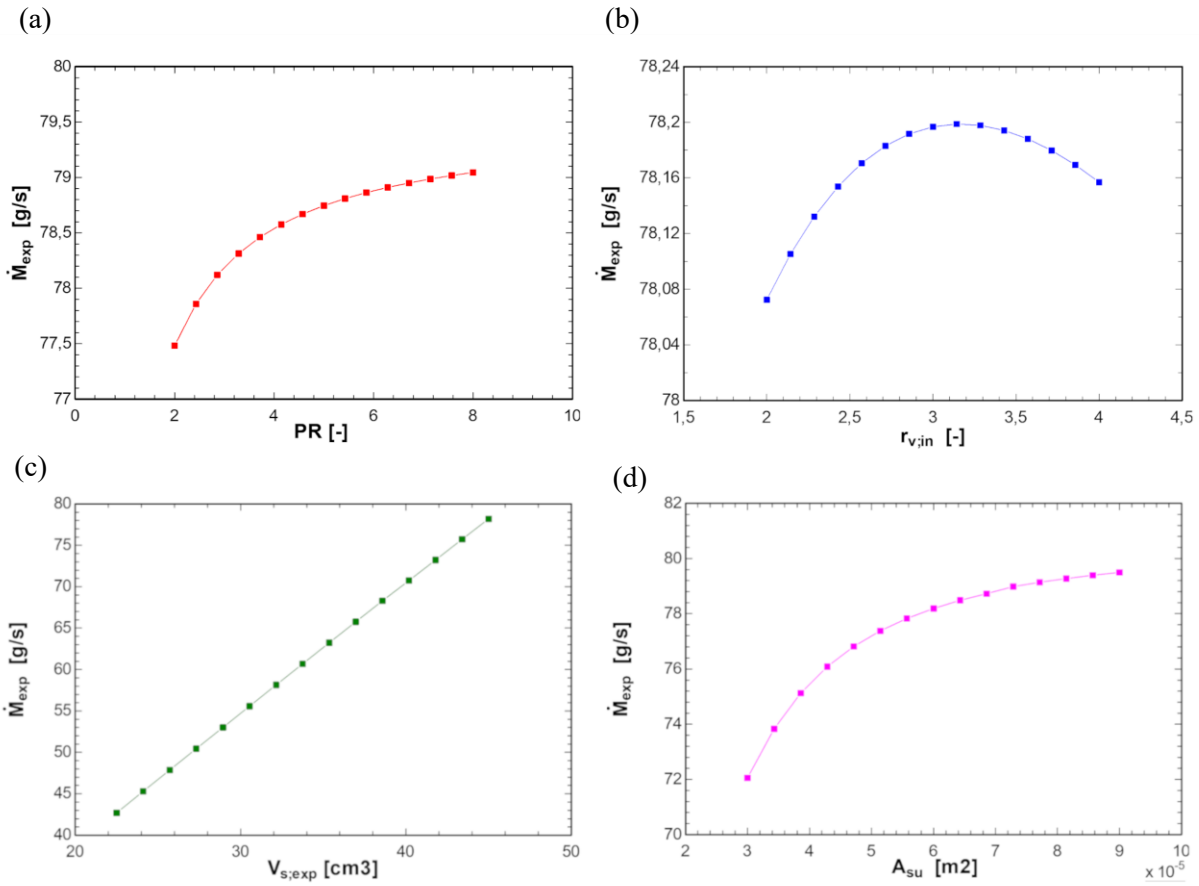

Figure 15: Mass flow-rate as function of **a)** pressure ratio (PR). **b)** built-in volume ratio ($r_{v,in}$). **c)** swept-volume (V_s). **d)** suction area (A_{su}).

Observations:

The trend of graphs a), c) and d) is a general increase of mass flow rate as function of parameters, whereas graph b) presents a maximum value, which corresponds to the adapted built-in volume ratio, even though in absolute terms the mass flow rate is approximately constant.

Leakage mass flow rate ($\dot{M}_{leak}$)

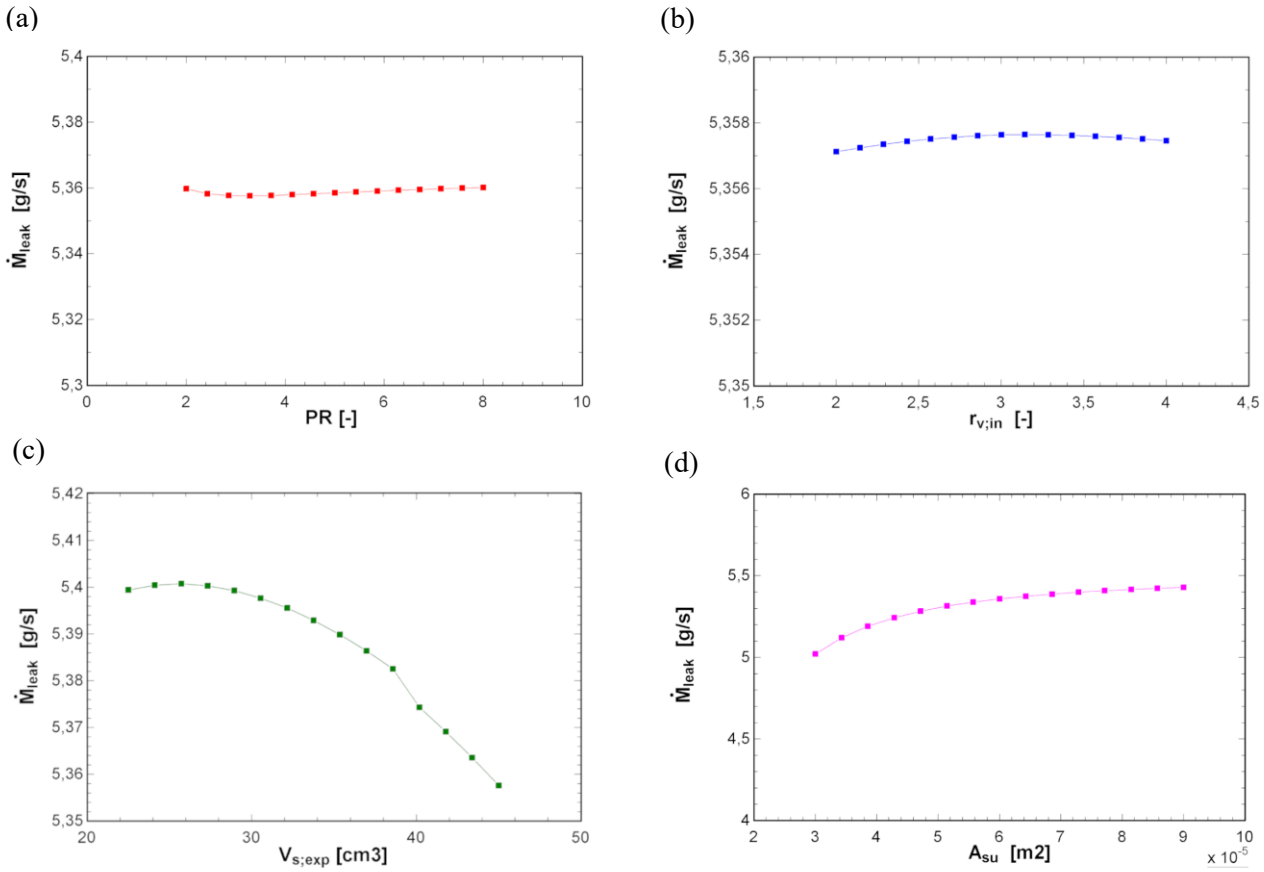

Figure 16: Leakage mass flow-rate as function of **a)** pressure ratio (PR). **b)** built-in volume ratio ($r_{v,in}$). **c)** swept-volume (V_s). **d)** suction area (A_{su}).

Observations:

In absolute terms, the mass flow rate is approximately constant for graphs a), b), c) and d), but in general terms there is a decrease of leakage mass flow rate as function of swept volume (c) and a slight increase in graph d). Anyway, it can be observed that leakage flow is not varying much with the 4 parameters.

Mass flow rate vs Leakage ($\dot{M}_{exp}$ and $\dot{M}_{leak}$)

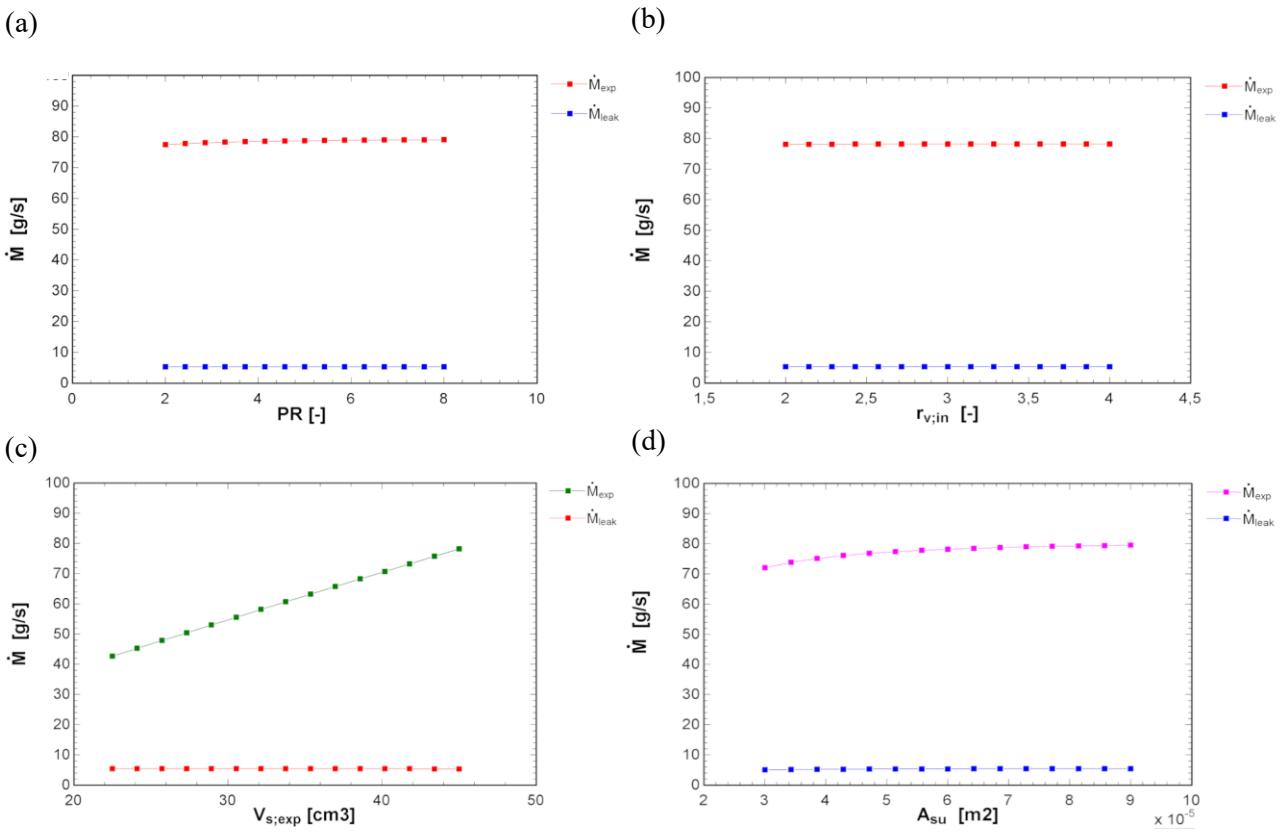

Figure 17: Mass flow-rate and leakage as function of **a)** pressure ratio (PR). **b)** built-in volume ratio ($r_{v,in}$). **c)** swept-volume (V_s). **d)** suction area (A_{su}).

Observations:

The only parameter that increases relevantly the difference between mass flow rate and leakages is the swept volume. This means that a major internal mass flow is available to effectively cross the expander and produce output work. It can be observed that the nost effective way to increase power output is to increase swept volume.

Utility water total mass flow rate ($\dot{M}_{cw}$)

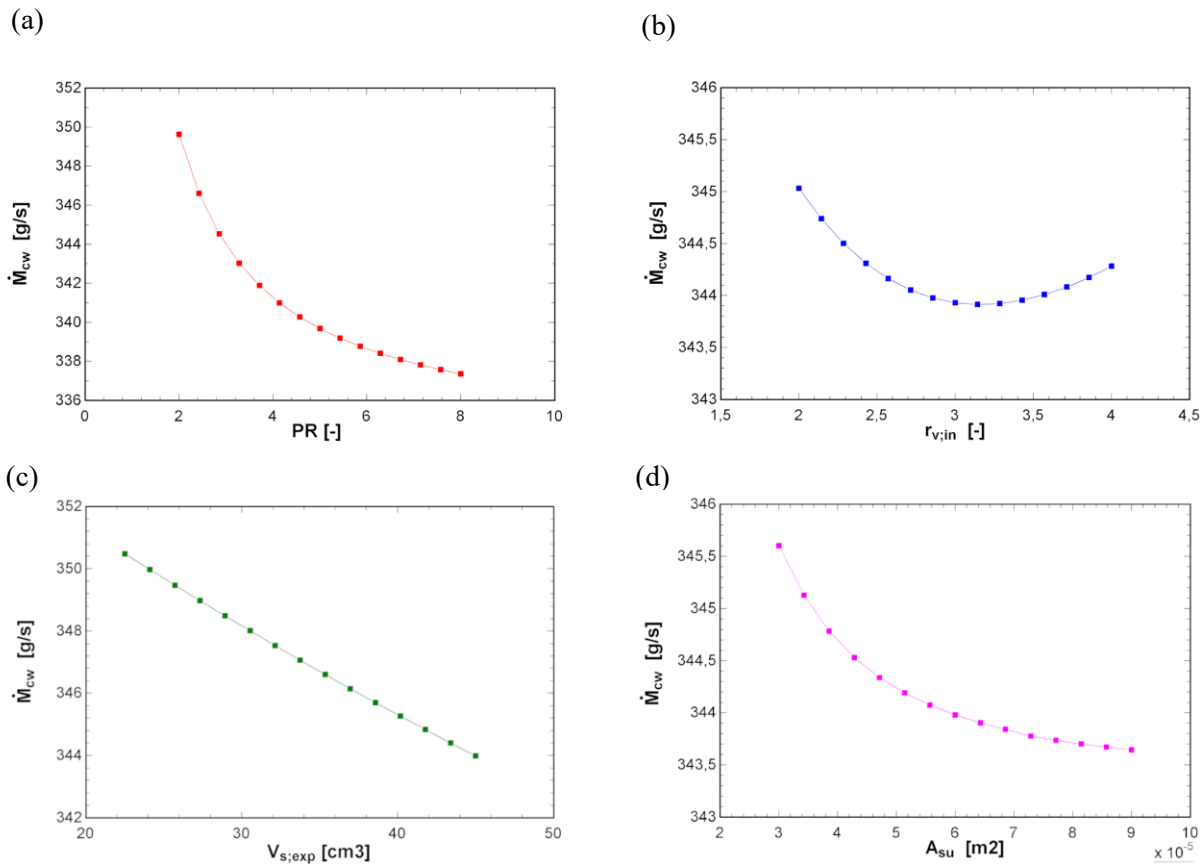

Figure 18: Utility water mass flow-rate and leakage as function of **a)** pressure ratio (PR). **b)** built-in volume ratio ($r_{v,in}$). **c)** swept-volume (V_s). **d)** suction area (A_{su}).

Observations:

The trend is decrescent for almost all the graphs, except graph b) which has a minimum point for a value of $r_{v,in}$ of aproximately 3.15, which corresponds to the adapted value and therefore avoids over/under expansion losses. These losses in fact have an influence on the exhaust heat transfer to the ambient. However, the absolute trend on water mass flow is more or less constant (around 344 g/s).

Utility water mass flow rates ($\dot{M}_{cw}$, $\dot{M}_{cw1}$ and $\dot{M}_{cw2}$)

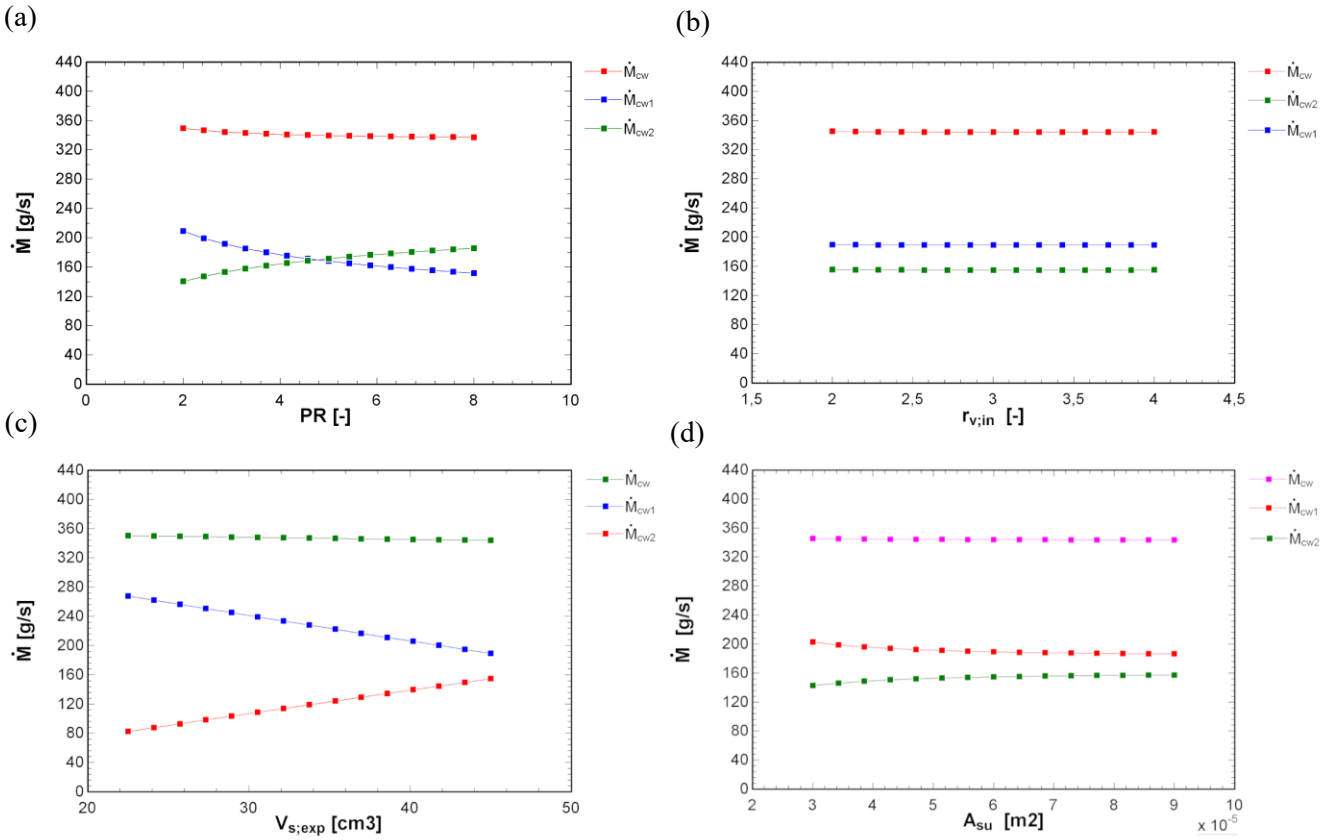

Figure 19: Utilities water mass flow-rate as function of **a)** pressure ratio (PR). **b)** built-in volume ratio ($r_{v,in}$). **c)** swept-volume (V_s). **d)** suction area (A_{su}).

Observations:

The two graphs that are more significant are a) and c). In graph a) for a pressure ratio value of approximately 5, the two utility mass flow rates are the same. In graph c) the two mass flow rates are compensating each other.

Electrical power vs net power ($\dot{W}_{el}$ and $\dot{W}_{net}$)

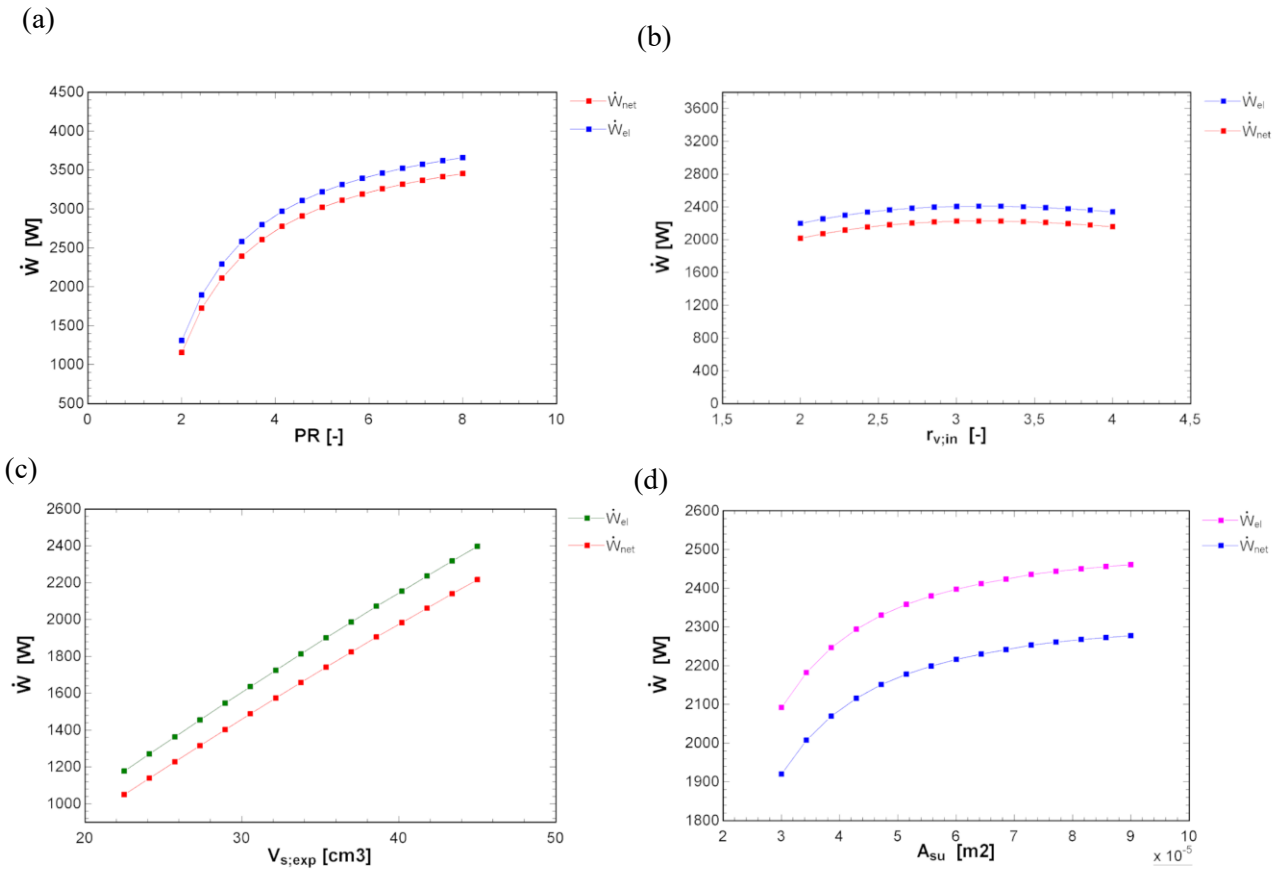

Figure 20: Electrical power output and net power output as function of **a)** pressure ratio (PR). **b)** built-in volume ratio ($r_{v,in}$). **c)** swept-volume (V_s). **d)** suction area (A_{su}).

Observations:

The trend is generally a crescent one, apart from graph b) which includes a maximum value around a value of $r_{v,in}$ of 3, related to the optimum value of adapted pressure.

Temperature at expander exhaust (T_{ex})

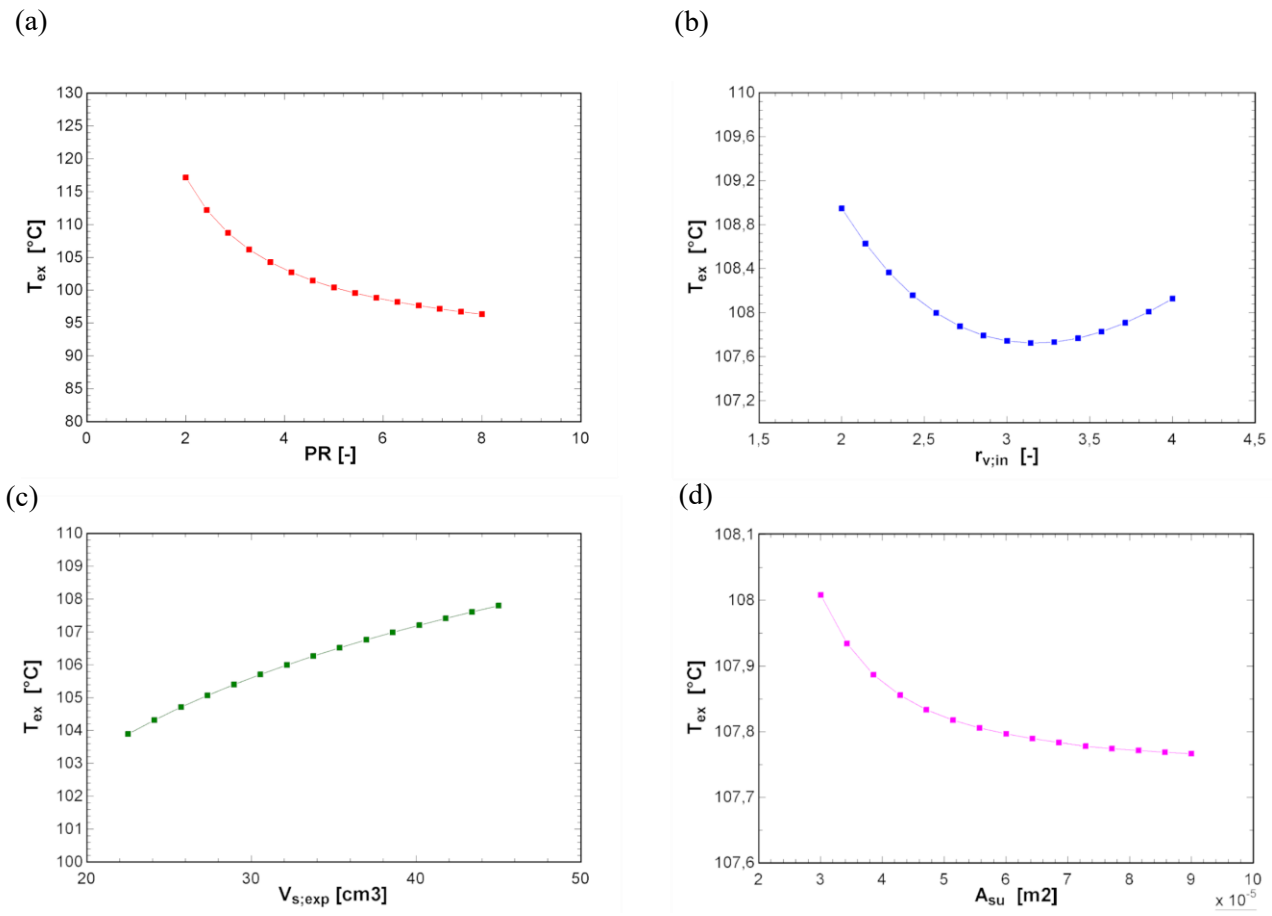

Figure 21: Exhaust fluid temperature as function of **a)** pressure ratio (PR). **b)** built-in volume ratio ($r_{v,in}$). **c)** swept-volume (V_s). **d)** suction area (A_{su}).

Observations:

The only graph that has an increasing trend is c). The others are all decrescent but in b) and d) temperature at the exhaust is not varying in an perceivable way. Exhaust temperature has a minimum value due to the fact that lower heat losses are present in adapted conditions.

Electrical efficiency (η_{el})

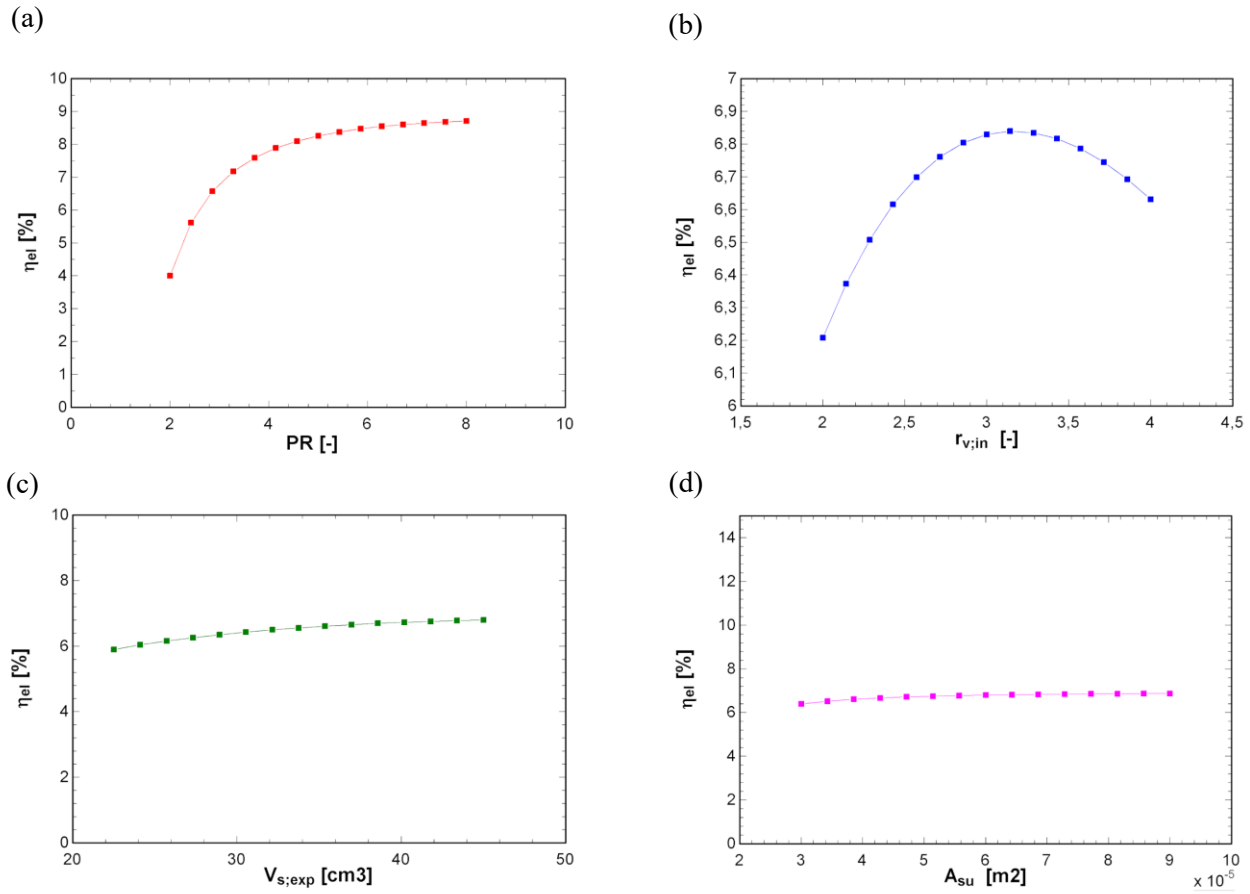

Figure 22: Electrical efficiency as function of **a)** pressure ratio (PR). **b)** built-in volume ratio ($r_{v,in}$). **c)** swept-volume (V_s). **d)** suction area (A_{su}).

Observations:

Graph a) stars a general increase which has an asymptotic trend for high values of PR. Graph b) includes a maximum value around a value of $r_{v,in}$ of 3.2. The other graphs present stable trends. The electrical efficiency obtained is still too low to consider this application valuable. A goal of 10% electrical efficiency is what had been chosen from the start. The configuration presented in the next sub-section tries to fulfill this goal.

Isentropic efficiency (η_{is})

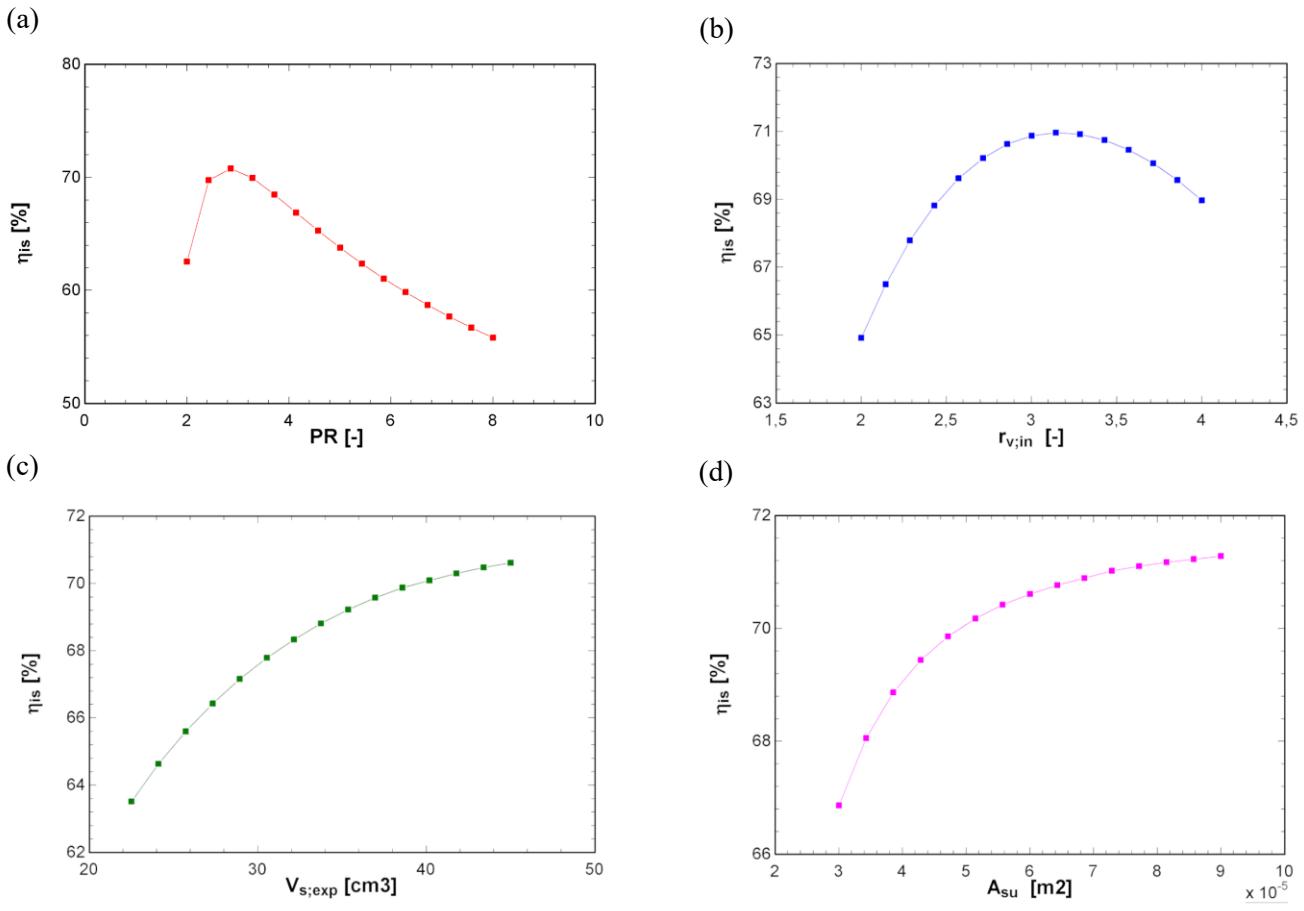

Figure 23: Isentropic efficiency as function of **a)** pressure ratio (PR). **b)** built-in volume ratio ($r_{v,in}$). **c)** swept-volume (V_s). **d)** suction area (A_{su}).

Observations:

It can be noticed that isentropic efficiency is influenced by built-in volume ratio (b) and that graph (a) admits a maximum value of pressure ratio around 3 and then decreases abruptly. This suggests that higher pressure ratios imply lower isentropic efficiencies and therefore must be avoided. The following configuration's parametric analysis in section 5.2.2. has limited pressure ratio to 4 for this specific reason.

Total Pump consumption ($\dot{W}_{pump}$)

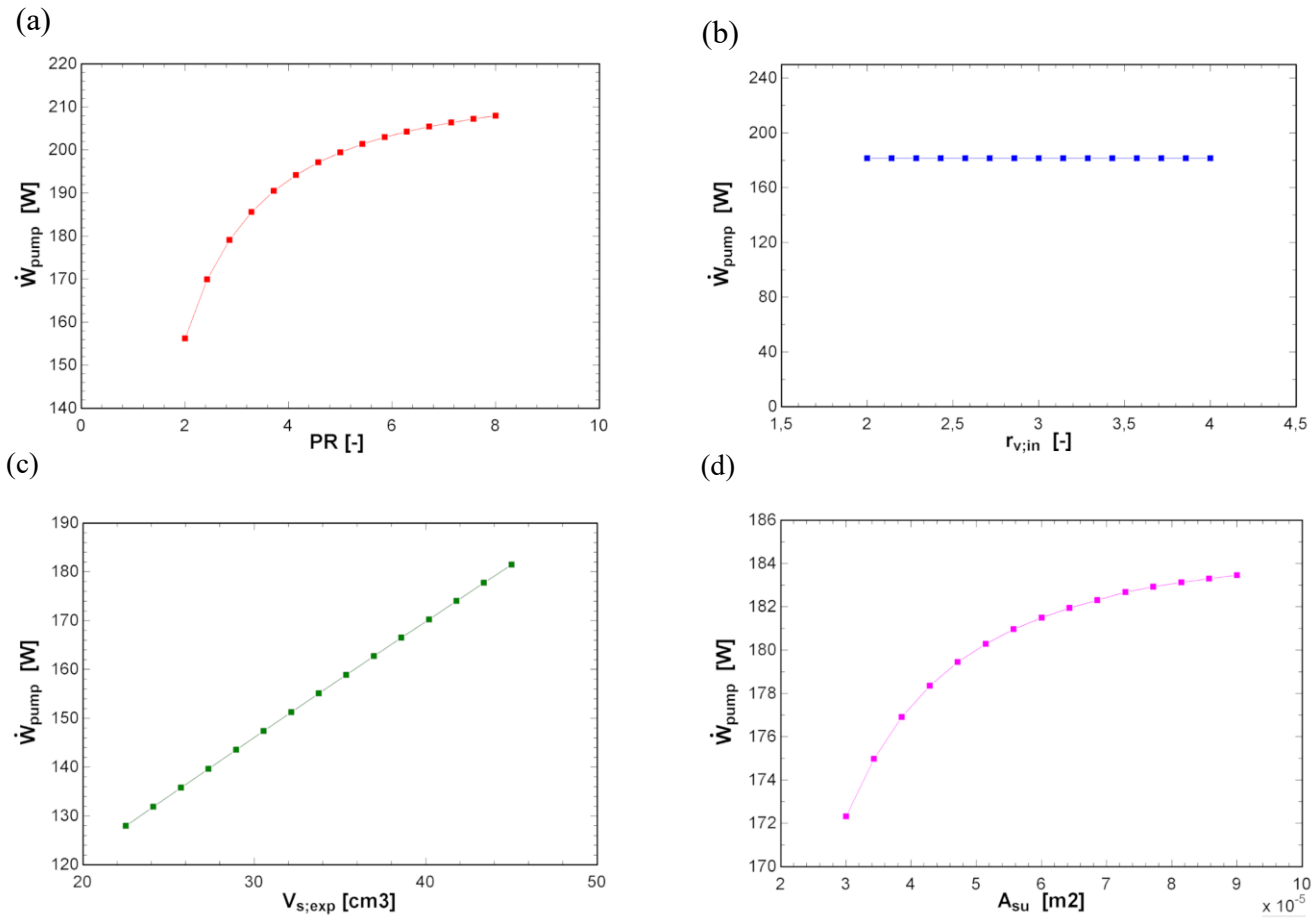

Figure 24: Total pump power supplied as function of **a)** pressure ratio (PR). **b)** built-in volume ratio ($r_{v,in}$). **c)** swept-volume (V_s). **d)** suction area (A_{su}).

Observations:

The trend is crescent, apart from graph b) which is more or less stable. Graphs a) and d) are asymptotic for high values of abscissa. Graph c) is obviously linear due to the fact that pump power depends linearly on mass flow rate and the latter increases linearly with swept volume increase.

Pumps consumption ($\dot{W}_{pump}$, $\dot{W}_{pump1}$, $\dot{W}_{pump2}$, $\dot{W}_{pump3}$ and $\dot{W}_{pump4}$)

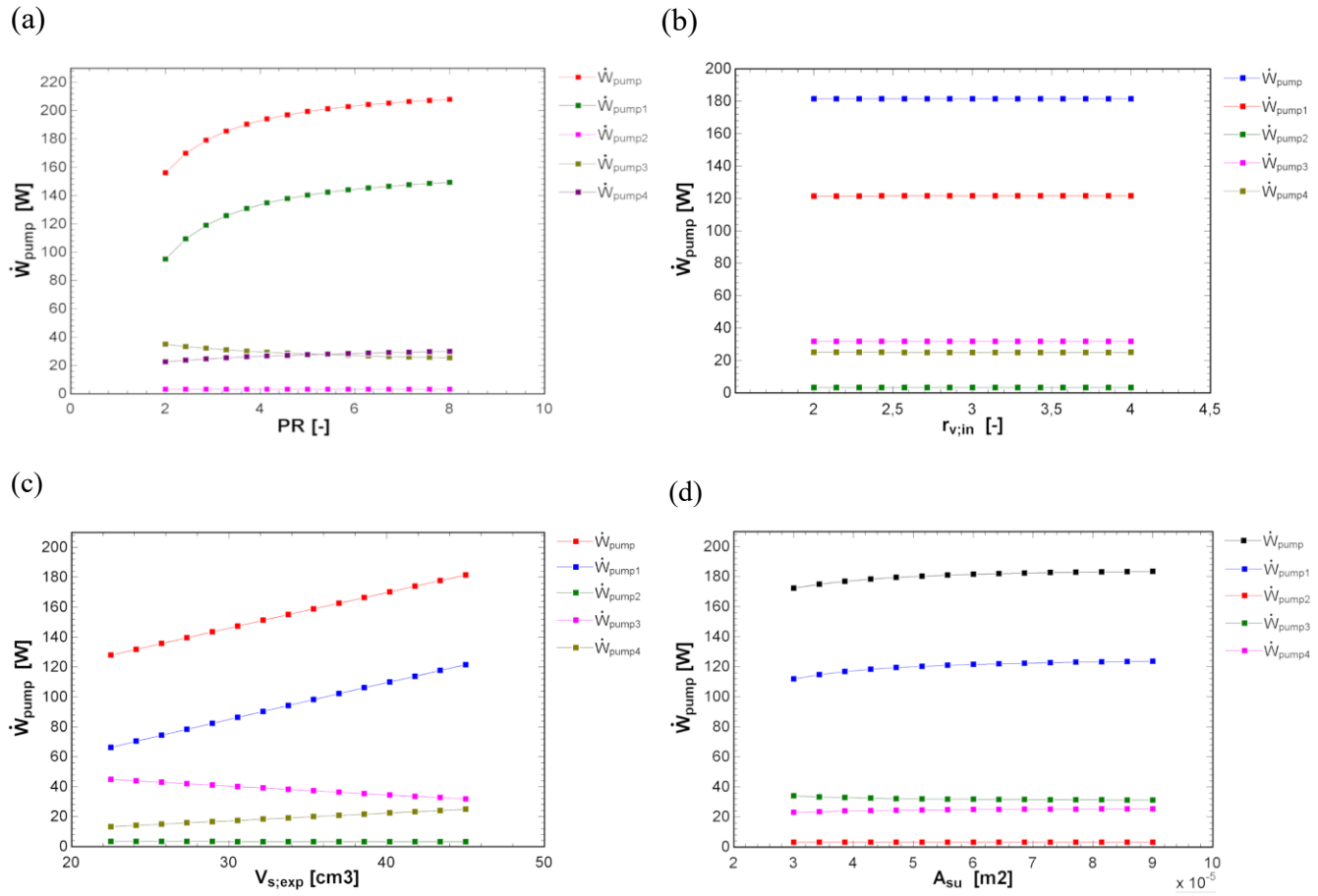

Figure 25: Pumps power supplied as function of **a)** pressure ratio (PR). **b)** built-in volume ratio ($r_{v,in}$). **c)** swept-volume (V_s). **d)** suction area (A_{su}).

Observations:

Results show that pump consumption is more related to the pressure level at the pump outlet than to the mass flow rate. Pump 2 (see Figure 13) has very low power necessity, as it is a closed water circuit in which pressure drops have been assumed to be only in heat exchangers. Increasing swept volume (c) means generally to increase pump power consumption, apart from the case of pump 3 because a lower temperature is achieved in point 6 and so the mass flow rate through that pump will be lower.

5.2. Double-loop configuration

5.2.1. Design conditions

The results obtained in the single-loop configuration in design conditions are reported in Table 11.

Table 11 : Results of double-loop configuration in design conditions

Symbol	Value	UOM	Parameters
T_{ex1}	107.8	[°C]	Scroll exhaust temperature (1)
T_{ex2}	63.3	[°C]	Scroll exhaust temperature (2)
$\dot{M}_{water}$	100	[g/s]	Water-loop mass flow rate
$\dot{M}_{cw}$	324	[g/s]	Utility water mass flow rate
$\dot{M}_{exp1}$	78.2	[g/s]	Fluid mass flow rate in expander (1)
$\dot{M}_{exp2}$	83.6	[g/s]	Fluid mass flow rate in expander (2)
$\dot{M}_{leak1}$	5.36	[g/s]	Leakage mass flow rate (1)
$\dot{M}_{leak2}$	7.48	[g/s]	Leakage mass flow rate (2)
$\dot{W}_{pump1}$	122.5	[W]	Pump 1 power consumption
$\dot{W}_{pump2}$	170.3	[W]	Pump 2 power consumption
$\dot{W}_{pump3}$	4.5	[W]	Pump 3 power consumption
$\dot{W}_{pump4}$	55.4	[W]	Pump 4 power consumption
$\dot{W}_{pump}$	352.7	[W]	Total pumps power consumption
$\dot{W}_{el}$	5243	[W]	Electrical power output
$\dot{W}_{net}$	4891	[W]	Electrical net power output
residual1	$4.9 \cdot 10^{-11}$	[W]	Residual error(1)
residual2	$4.3 \cdot 10^{-10}$	[W]	Residual error(2)
$\dot{Q}_{input}$	68200	[W]	Input heat flow
$\dot{Q}_{HX\_water}$	38676	[W]	Heat flow provided to water loop
$\dot{Q}_{cw}$	60979	[W]	Heat flow provided to cold water
$\dot{Q}_{amb1}$	1193	[W]	Heat flow released in ambient (1)
$\dot{Q}_{amb2}$	1067	[W]	Heat flow released in ambient (2)
η_{is1}	70.6	[%]	Isentropic efficiency (1)
η_{is2}	68.9	[%]	Isentropic efficiency (2)
η_{cycle}	96.5	[%]	Cycle efficiency
η_{el}	13.6	[%]	Electrical efficiency
φ_1	1.062	[-]	Filling factor (1)
φ_2	1.089	[-]	Filling factor (2)

N.B. The number associated to each pump is reported in Figure 14 as a circled number above the pump.

5.2.2. Parametric Analysis

In this parametric analysis, the main assumptions are the same as in the single-loop configuration. Temperatures and pressure at the inlet of expander 1 are therefore the same. The new loop integrates isobutane, which is a fluid that can work to lower temperatures than isobutane. The parameters have been varied in the same way for both expanders (all 4 parameters were the same on both expanders) so that the expanders were identical at each loop of the analysis.

Mass and leakage flow rate in expander 1 ($\dot{M}_{exp1}$ and $\dot{M}_{leak1}$)

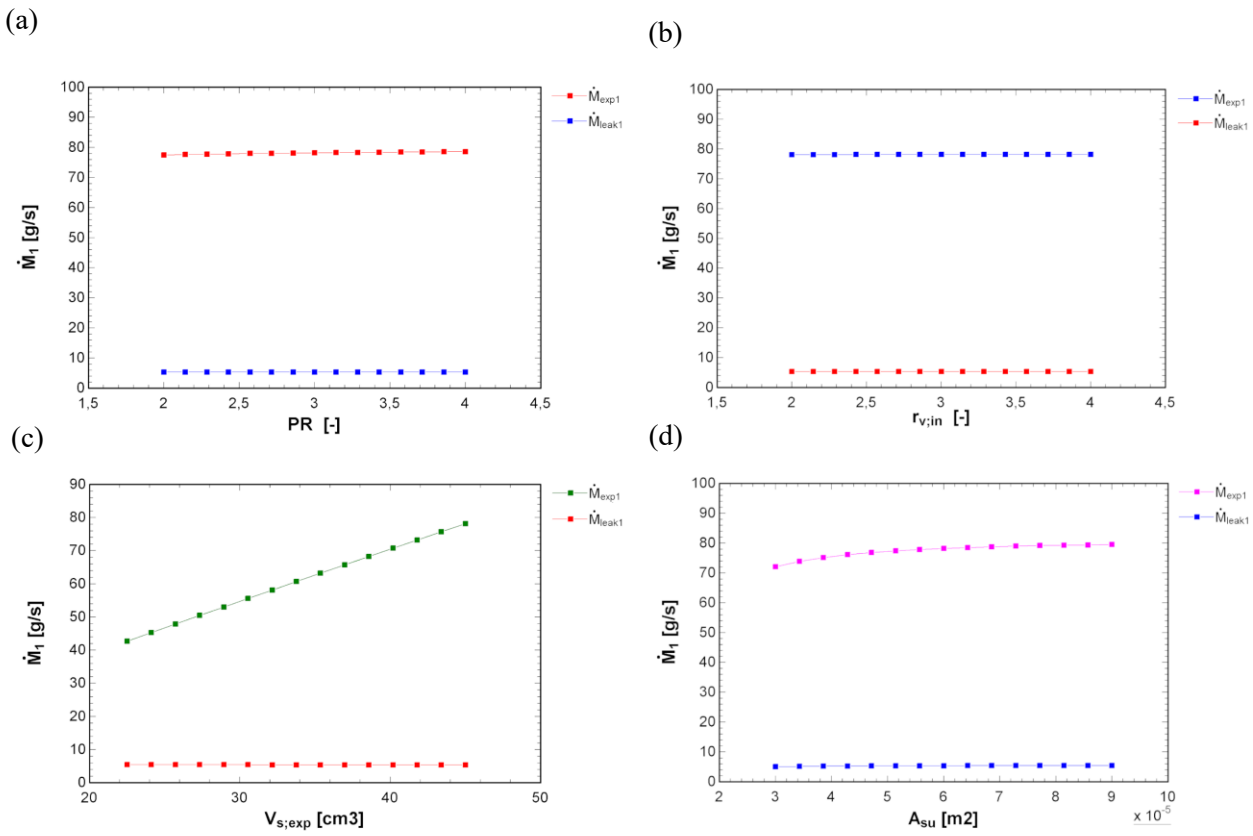

Figure 26: Mass and leakage flow rate in expander 1 as function of **a)** pressure ratio (PR) **b)** built-in volume ratio ($r_{v,in}$). **c)** swept-Volume (V_s). **d)** suction area (A_{su}).

Observations:

The only parameter that increases relevantly the difference between mass flow rate and leakages is the swept volume (c).

Mass and leakage flow rate in expander 2 ($\dot{M}_{exp2}$ and $\dot{M}_{leak2}$)

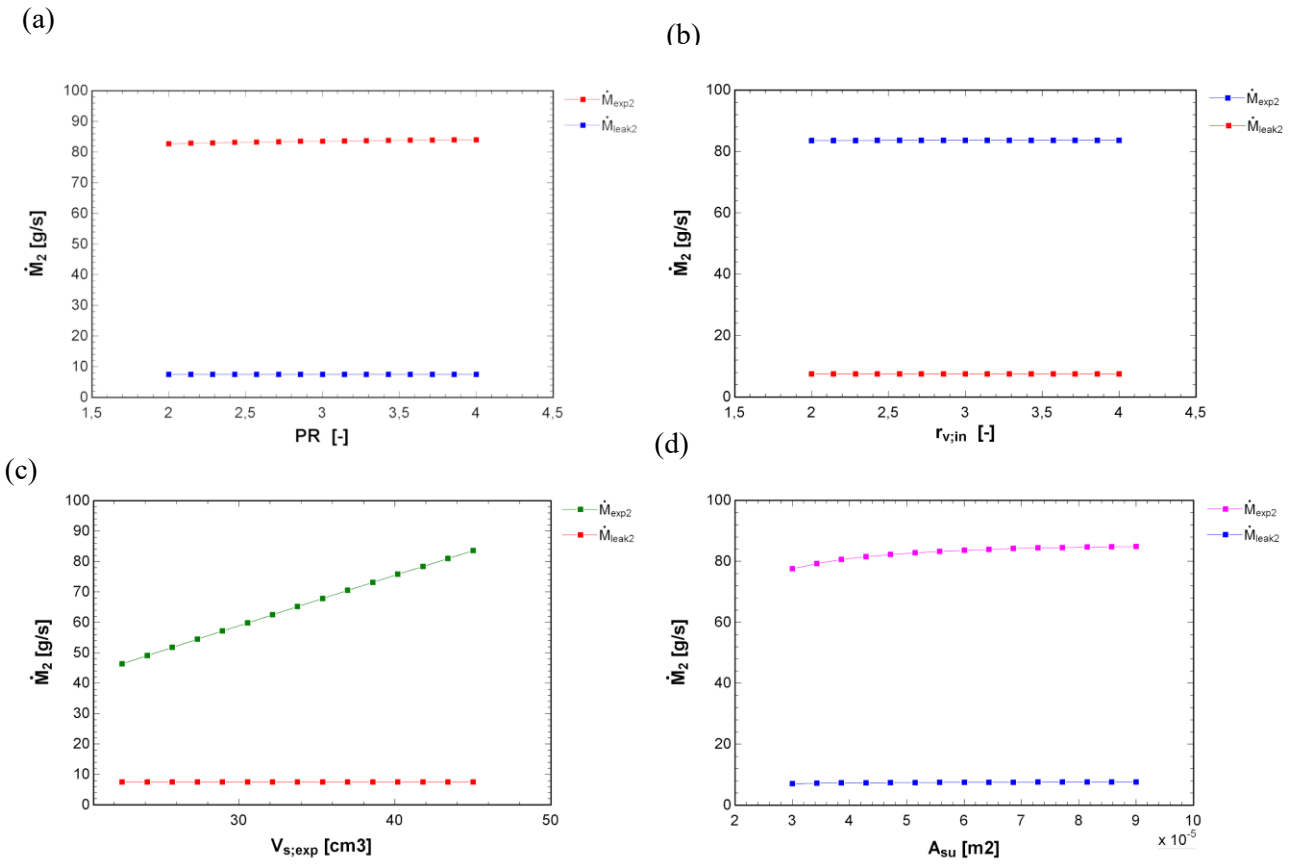

Figure 27: Total pump power supplied as function of **a)** pressure ratio (PR). **b)** built-in volume ratio ($r_{v,in}$). **c)** swept-volume (V_s). **d)** suction area (A_{su}).

Observations:

The graphs are very similar to the ones in the previous page but they are shifted to higher values. These graphs have been reported only to have a perception of the proportions between mass flow rate and leakage mass flow rate.

Mass flow rate in expander 1 and 2 ($\dot{M}_{exp1}$, $\dot{M}_{exp2}$)

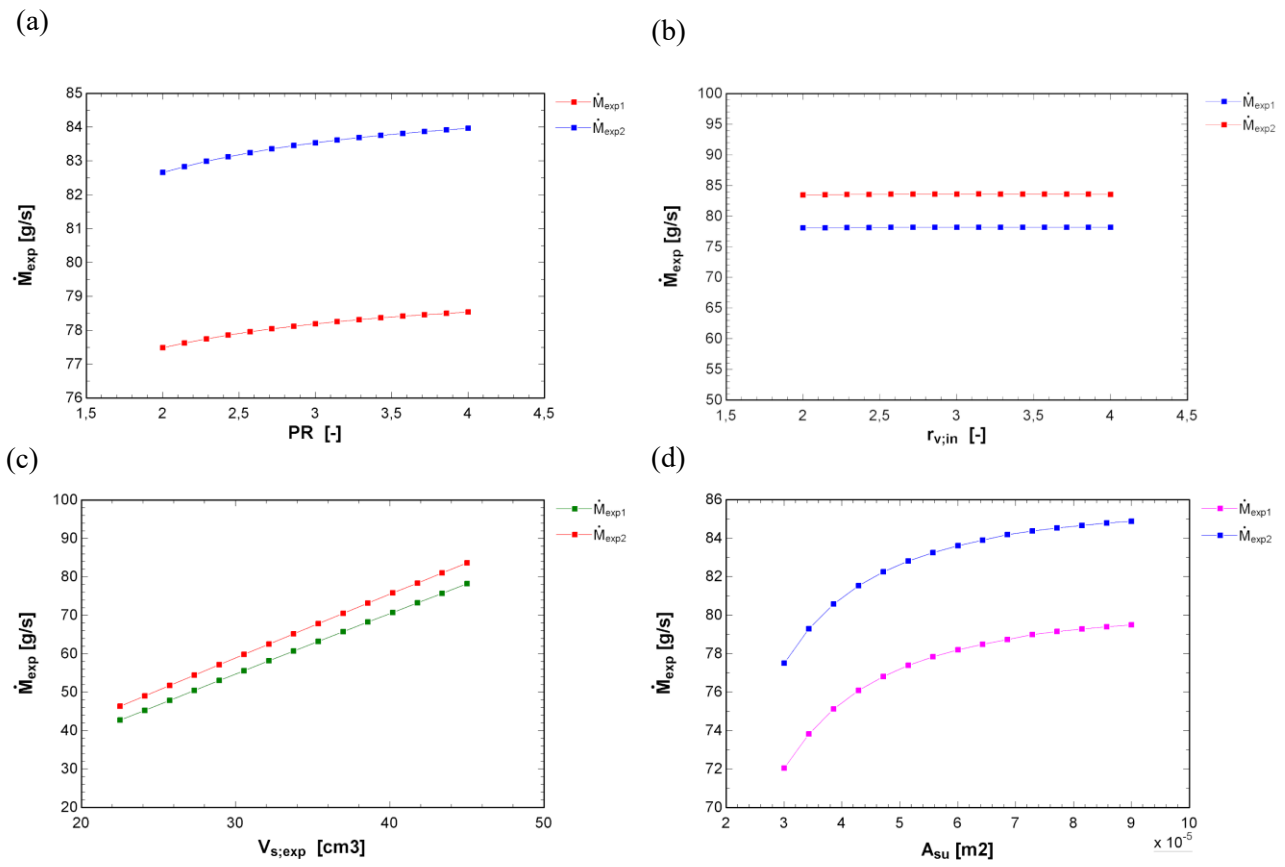

Figure 28: Mass flow rate in expander 1 and 2 as function of **a)** pressure ratio (PR). **b)** built-in volume ratio ($r_{v,in}$). **c)** swept-volume (V_s). **d)** suction area (A_{su}).

Observations

Mass flow rate does not vary much with the pressure ratio. This is because the inlet pressure is kept constant and what varies is the downstream pressure. The inlet pressure, as said before, has been optimized to the consistent temperature of 140 °C in order to avoid an exaggerated super-heating.

Utility water mass flow rate ($\dot{M}_{cw}$)

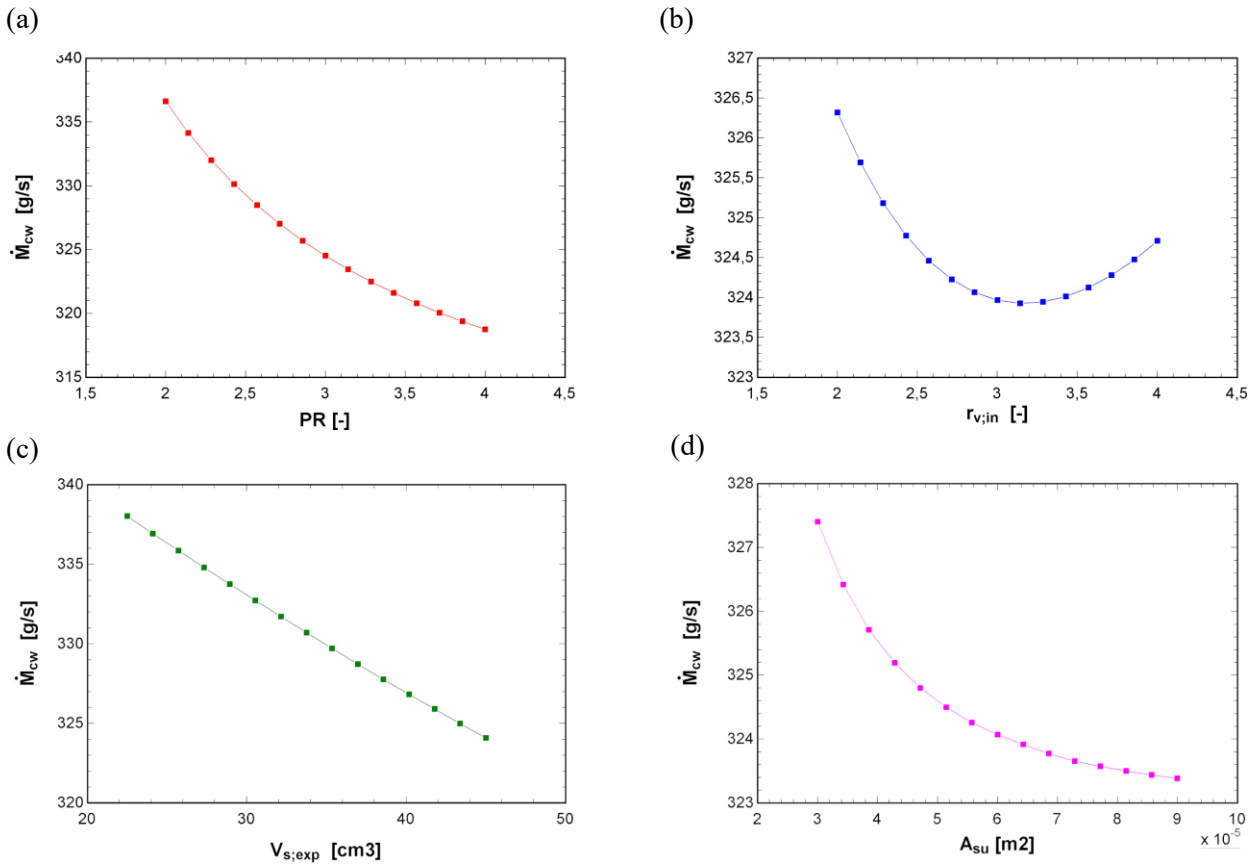

Figure 29: Utility water mass flow rate as function of **a)** pressure ratio (PR). **b)** built-in volume ratio ($r_{v,in}$). **c)** swept-volume (V_s). **d)** suction area (A_{su}).

Observations

In Figure 29 the utility water mass flow is presented as function of the parameters of interest. A general decrescent trend is observed, even though the decrease is not a drastic one. This is an interesting result as it shows that even if the expanders were to be modified, the flow rate at the utility would remain almost unchanged if this model is applied. The higher the electrical power the lower the water mass flow rate, as the total energy balance must be respected.

Net electrical power output ($\dot{W}_{net}$)

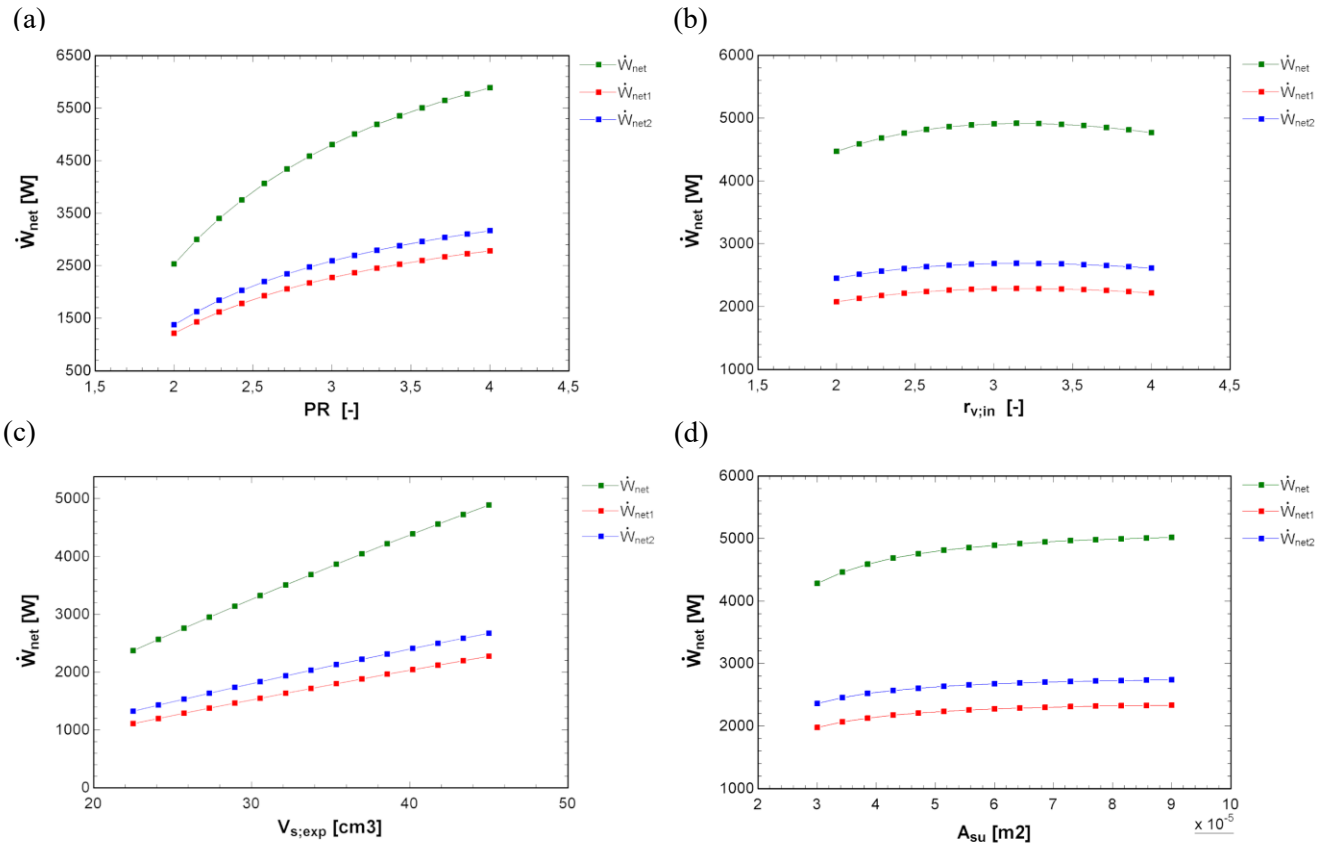

Figure 30: Net electrical power output as function of **a)** pressure ratio (PR). **b)** built-in volume ratio ($r_{v,in}$). **c)** swept-volume (V_s). **d)** suction area (A_{su}).

Observations:

Results obtained from the analysis are presented in Figure 30. It can be noticed that a global crescent trend is present. PR has a non-linear impact on net power output. This non-linearity is mainly due to the leakage. Regarding graphs (b) the outlet pressure is not the adapted pressure and this generates either over or under-expansion losses on both sides of maximum value 3. Results of graph (c) are clearly showing a crescent and linear trend of the net power output as function of swept volume, as definition of the latter implies. Graph (d) illustrates the net power output as function of inlet hole area.

The power increases with the area, and, as mentioned before, the pressure drop diminishes and therefore a higher pressure is available at the end of suction process.

Heat flow towards the ambient ($\dot{Q}_{amb}$)

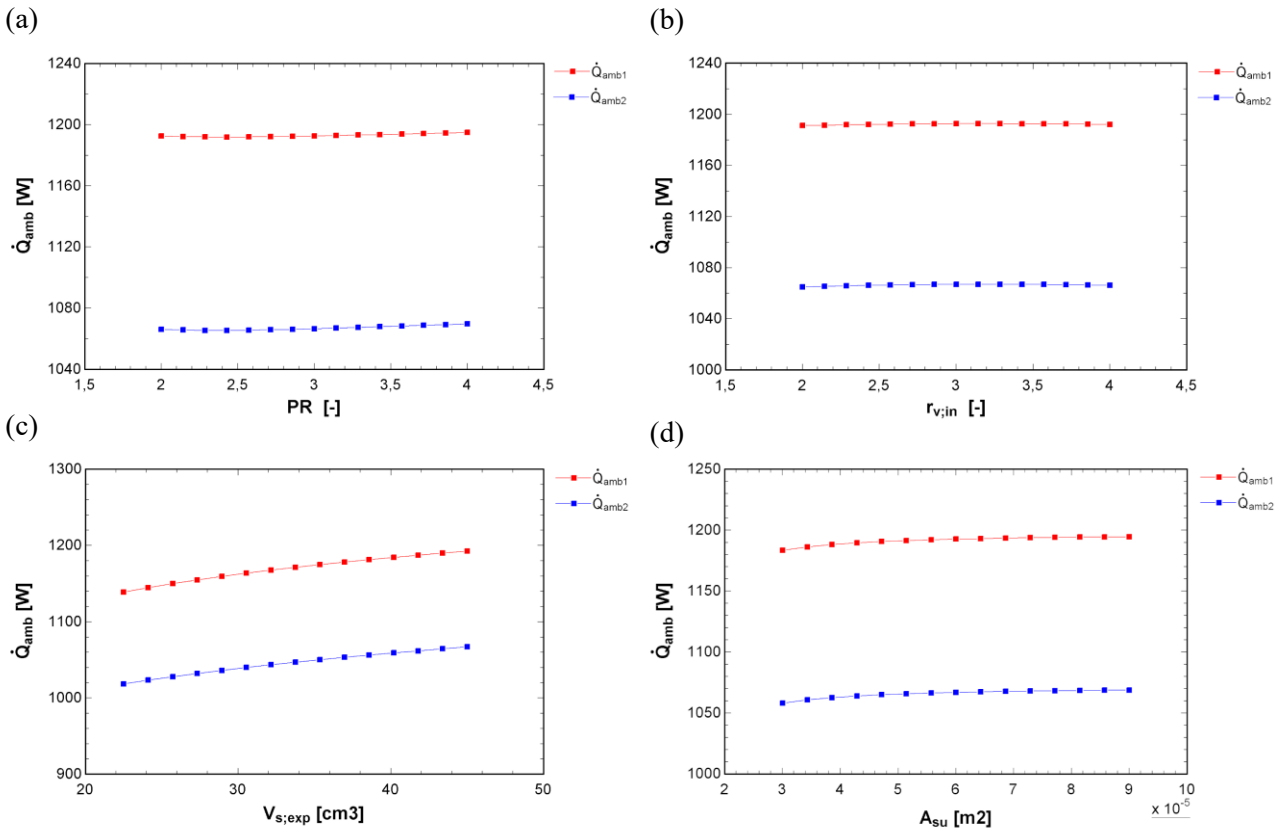

Figure 31: Heat flow towards the ambient ($\dot{Q}_{amb}$) as function of **a)** pressure ratio (PR). **b)** built-in volume ratio ($r_{v,in}$). **c)** swept-volume (V_s). **d)** suction area (A_{su}).

Observations:

The parameter that influences mostly the heat transfer towards the ambient is the swept volume. If there is an increase of the swept volume, the machine will be larger and therefore have a major surface for heat transfer to the ambient. The other parameters do not affect too much the three terms (suction, inside, exhaust) of heat transfer.

Temperature at expander exhaust (T_{ex})

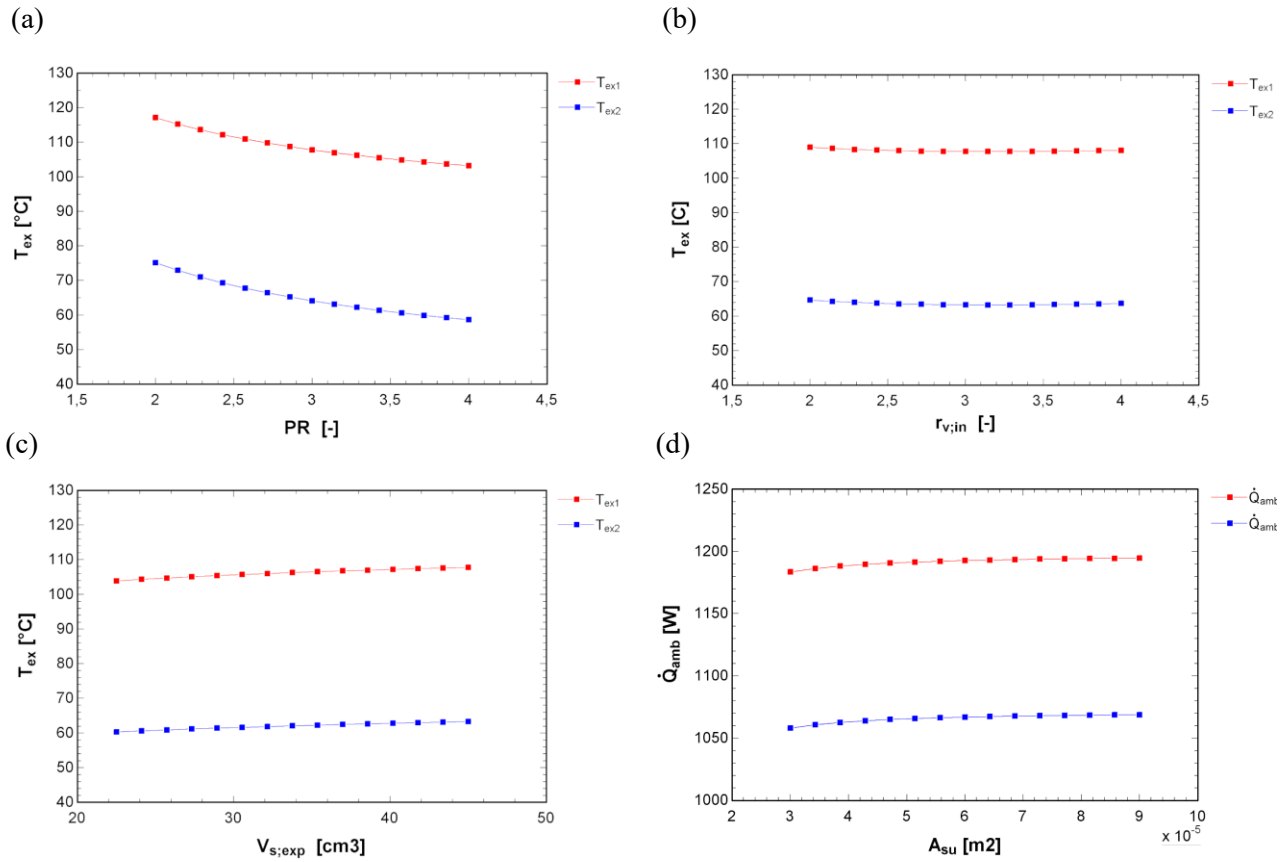

Figure 32: Temperature at the expander exhaust as function of **a)** pressure ratio (PR). **b)** built-in volume ratio ($r_{v,in}$). **c)** swept-volume (V_s). **d)** suction area (A_{su}).

Observations:

The exhaust temperature calculated by the model has the same trend as the heat exchange, which means that this particular temperature has some incidence on heat transfer. There is an exception though for PR. In fact, as PR increases temperature at the exhaust decreases and this is senseful because we are decreasing the exhaust pressure.

Electrical efficiency (η_{el})

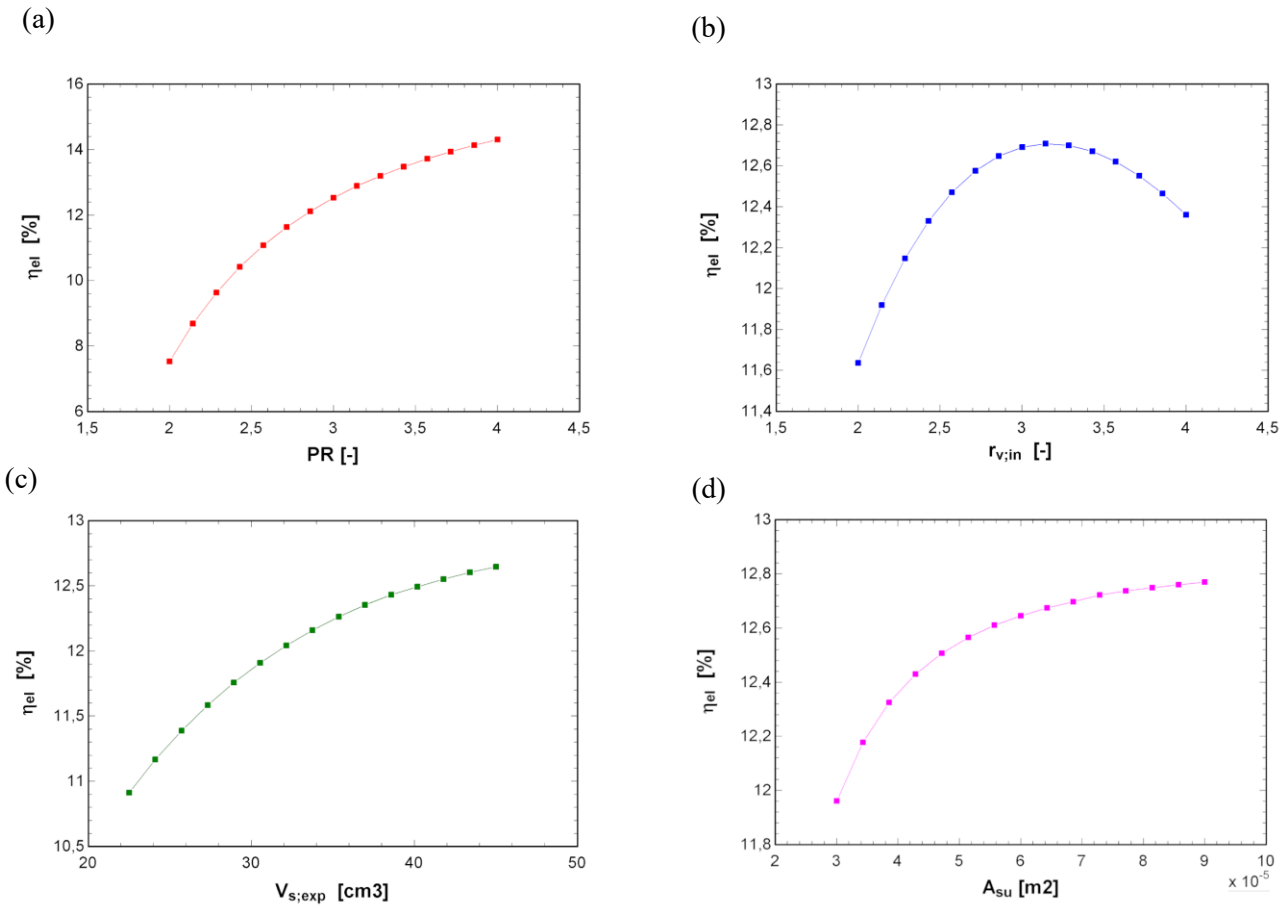

Figure 33: Electrical efficiency as function of **a)** pressure ratio (PR). **b)** built-in volume ratio ($r_{v,in}$). **c)** swept-volume (V_s). **d)** suction area (A_{su}).

Observations:

Like the single-loop configuration, the only parameter that affects relevantly the electrical efficiency is the PR. The electrical efficiency is calculated considering both expanders and an increase with respect to the previous configuration is remarked.

Isentropic efficiency (η_{is})

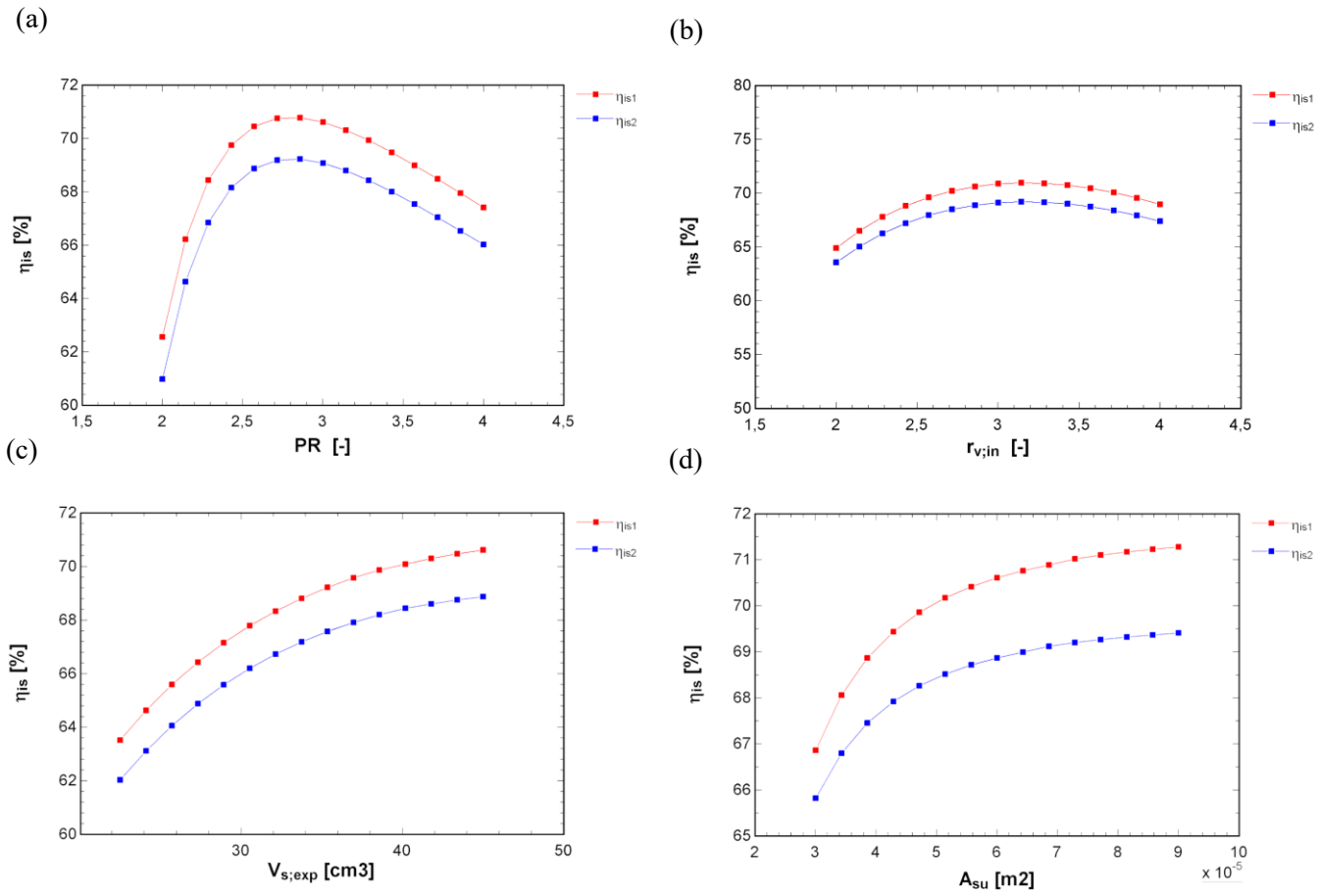

Figure 34: Isentropic efficiency as function of **a)** pressure ratio (PR). **b)** built-in volume ratio ($r_{v,in}$). **c)** swept-volume (V_s). **d)** suction area (A_{su}).

Observations:

Results obtained from the analysis are presented in Figure 34. It can be noticed that a global crescent trend is present. The isentropic efficiency in (a) attains a maximum value and then decreases. This is due to the fact that for PR values lower or higher than approximately 2.7, the outlet pressure is not the adapted pressure and this generates either over or under-expansion losses. Similarly, isentropic efficiency in (b) attains a maximum value (around 72%) which is the value corresponding to the built-in volume which guarantees an adapted pressure at the outlet. Results of graph (c) are clearly showing

a crescent trend of the isentropic efficiency as function of swept volume. Graph (d) illustrates the isentropic efficiency as function of inlet hole area. Isentropic efficiency increases with the area, as the pressure drop diminishes and therefore a higher pressure is available at the end of suction process.

Total pumps power consumption ($\dot{W}_{pump}$)

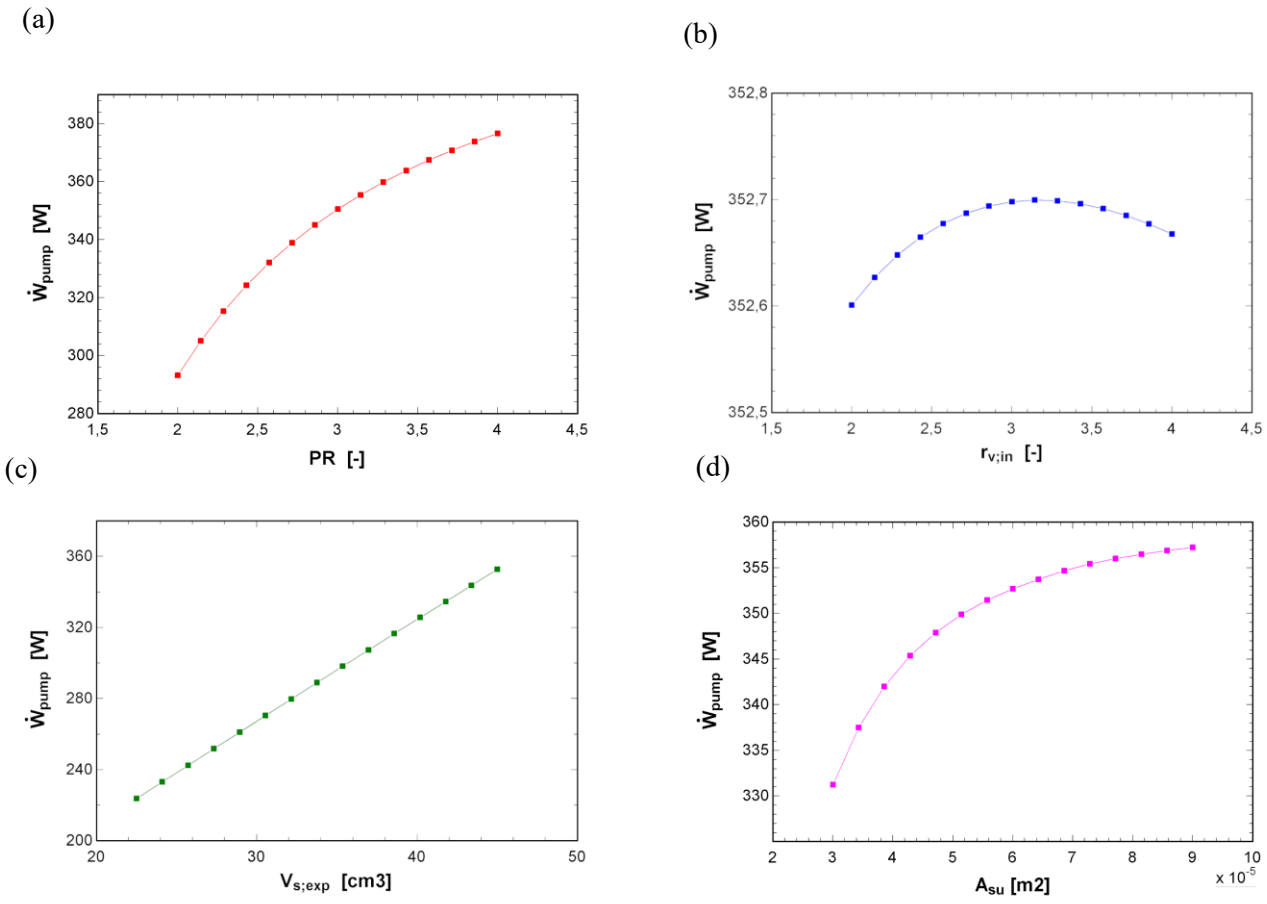

Figure 35: Pump total power as function of **a)** pressure ratio (PR). **b)** built-in volume ratio ($r_{v,in}$). **c)** swept-volume (V_s). **d)** suction area (A_{su}).

Pump total power consumption has evidently a linear dependence on swept volume (c). The dependence on the suction area (d) seems to be asymptotic at this scale. In absolute terms, pump power consumption as function of built-in ratio (b) is stable.

Pumps power consumption ($\dot{W}_{pump}$, $\dot{W}_{pump1}$, $\dot{W}_{pump2}$, $\dot{W}_{pump3}$ and $\dot{W}_{pump4}$)

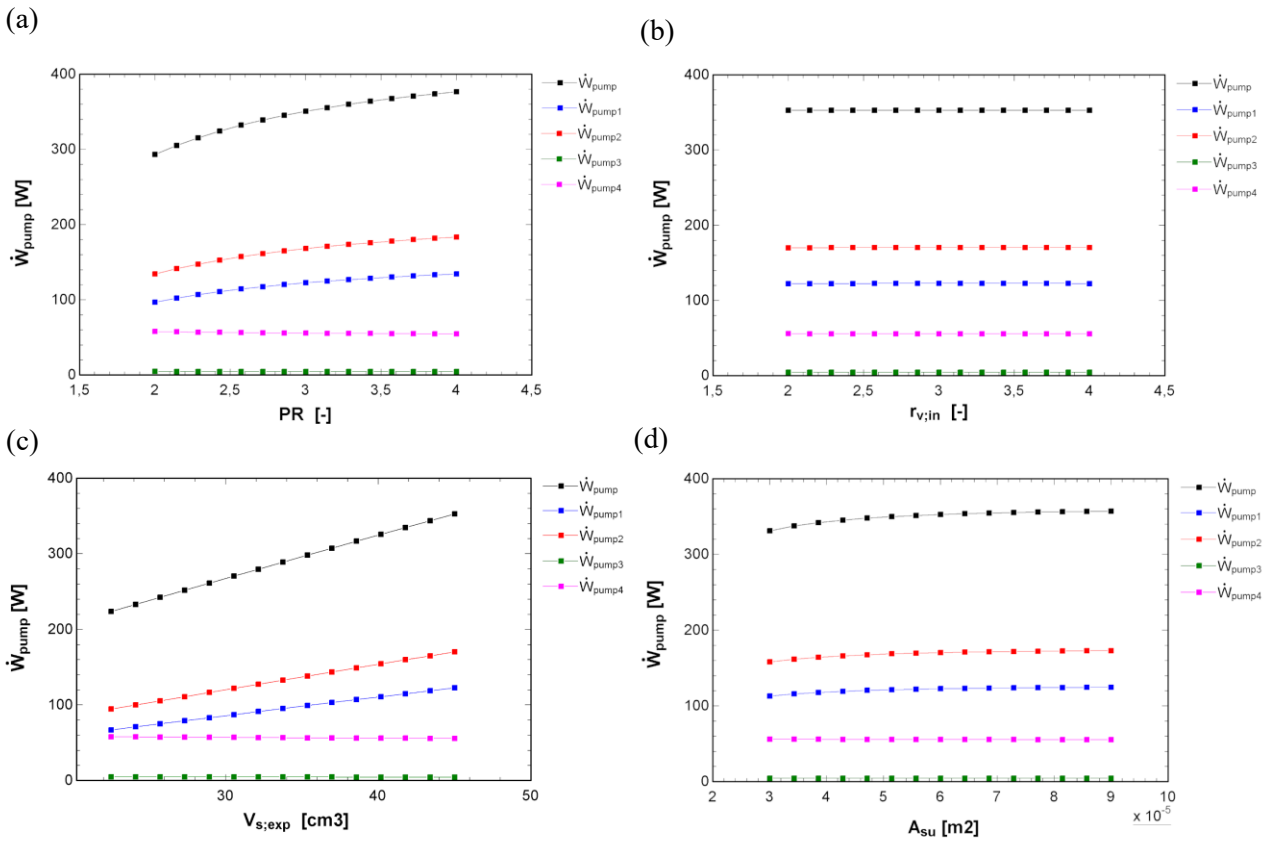

Figure 36: Pumps power as function of **a)** pressure ratio (PR). **b)** built-in volume ratio ($r_{v,in}$). **c)** swept-volume (V_s). **d)** suction area (A_{su}).

Observations:

Pump power consumption as function of built-in volume ratio is stable. As expected, the pumps related to the loops increase their consumption with the swept-volume linearly. Also the pressure ratio has an influence on the pump power as a major pumping work is necessary to obtain the pressure level at the expander's inlet.

5.3. Diagrams of the working fluids in design conditions

In Figure 37 and Figure 38 are represented the enthalpy-entropy diagrams of the two different working fluids in design conditions.

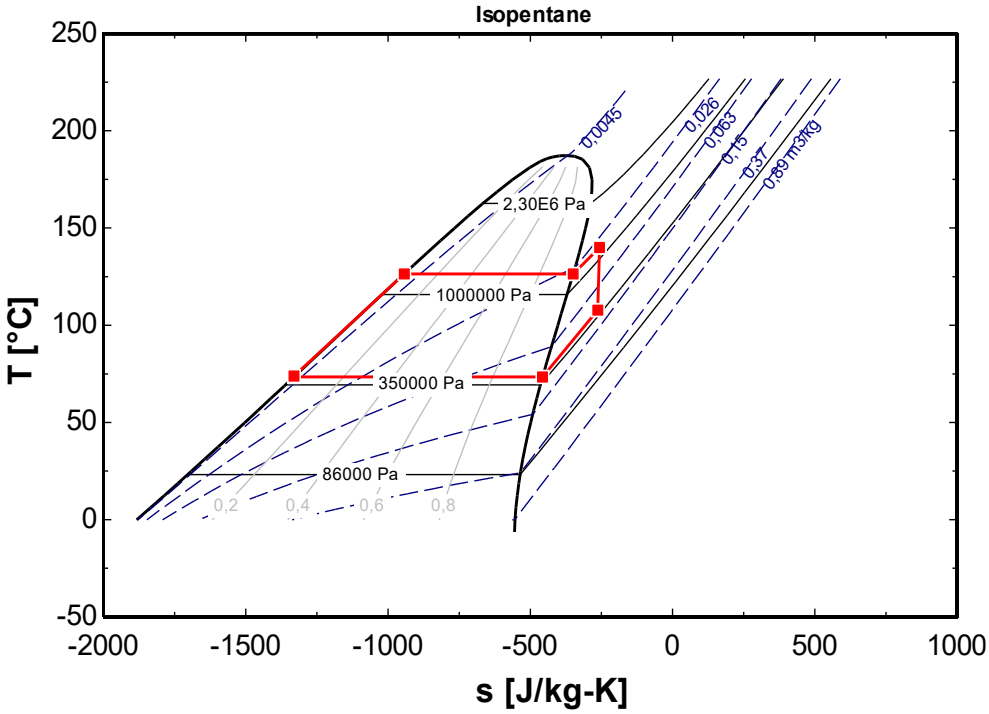

Figure 37: T-s diagram of isopentane in thermodynamic cycle

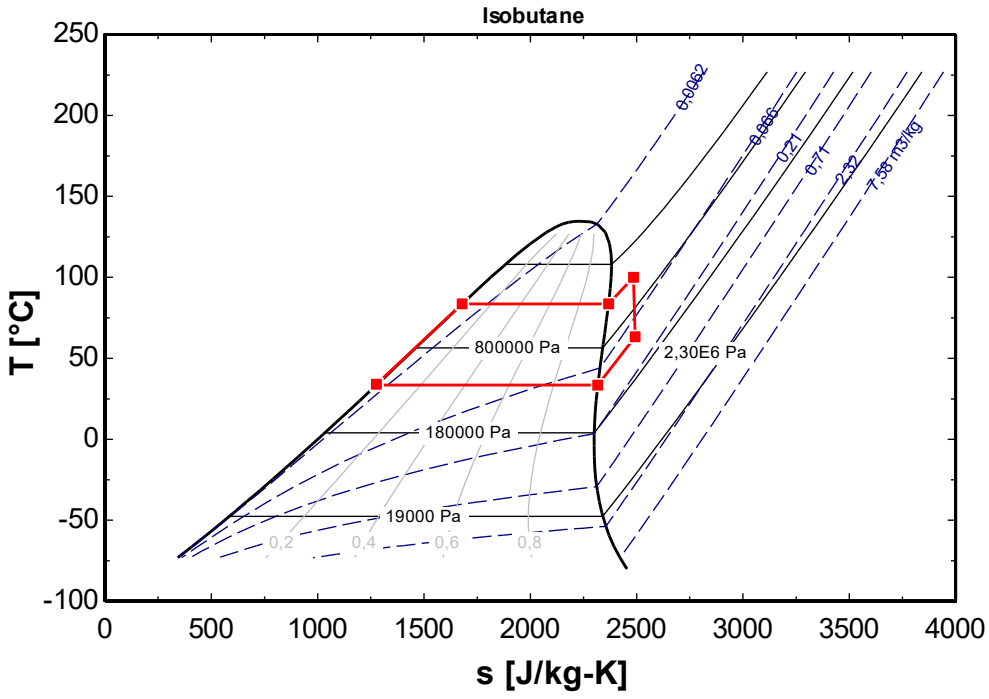

Figure 38: T-s diagram of isobutane in thermodynamic cycle

5.4. Discussion

The outcome of the analysis of the results part shows clearly an advantage in combining two loops. The double-loop configuration is more convenient as it allows a higher electrical efficiency and a doubled net power with almost unchanged water utility conditions. This is possible only because the working fluid is of organic type, and so requires low energy to be superheated and because working fluid pass flow rate are not too high. It is necessary to point out that cycle efficiency is nearly 97%, which is a very high value for this kind of application, considering that maximum cycle efficiencies are usually around 95%. This difference could be explained by the fact that enthalpy losses in pipes and in the heat exchangers have been neglected. The most interesting parameter of the analysis is the built-in volume ratio, which has an influence on the performance of the machine. In particular, in Figure 30 and Figure 33, we can have a visual perception of it. If rv,in varies from 2 to 4, the difference is relevant, considering that the other parameters are kept constant. This confirms that an optimum value is to be found and must be taken into account while designing this machine. The angular speed of the scroll was kept in all the simulations to 3000 rpm, in order to avoid the use of reduction gears or inverters that would either increase the size of the plant or its cost. Regarding the double loop, if this solution were to be produced, the initial investment would be higher, as the plant complexity and the fact that there are two expanders would increase the cost dramatically, but it would result in a higher power regeneration and the investment should have a payback period inferior to the single-loop configuration, which is more inefficient. The electrical and overall efficiency gains in design conditions are reported in Table 12.

Table 12: Efficiency gain

Symbol	Value	UOM	Parameters
$\Delta\eta_{el}$	4.2	[%]	Electrical efficiency gain
$\Delta\eta_{overall}$	57	[%]	Overall efficiency gain

6. Conclusion

A dual-loop ORC system starring scroll expanders has been investigated and analyzed. The results show clearly that there is a net advantage in implementing this solution. Therefore, ORC add-on could be a promising solution for micro-CHP applications. Results show that an electrical efficiency of 13.6% could be achieved in the proposed ORC system, generating a net power output of almost 5kW, provided that the scroll is designed according to the parameters set. The overall system electrical efficiency could increase of approximately 4.2%. From an economic point of view, this CHP solution would imply a higher initial investment but lower operating costs, making it a long-term advantageous solution, given the low maintenance costs. An implementation of this solution could be beneficial to recover heat from exhaust gas of microturbines and prevent the formation of excessive GHG emissions.

The work of Vincent Lemort's research group, in Liège university, has been very useful to fully understand the thermodynamics behind scroll expanders and the code that has been used is the result of years of optimization performed by Lemort's research group. The two configurations used have been successfully tested and analyzed with two working fluids. The results show a clear advantage in using double-loop configuration. The new challenge would be to design a compact double-loop device, which could be more desirable for customers. This type of application with microturbine is likely to be used in vast areas of the world that have a large availability of fossil fuels (e.g. Russian countryside) and could be an effective way to produce also hot water, which is sometimes vital for human survival. Scroll machines are compact devices that have many advantages compared to turbomachines. Their use in industry (as energy recovery systems in great industrial or energy plants) would surely be a breakthrough and would lead to a better energy economy.

7. Bibliography

[1] A. Jaatinen-Varri *et al.*, “Design of a 400 KW Gas Turbine Prototype,” in *Proceedings of the ASME Turbo Expo*, 2016.

[2] “https://www.capstoneturbine.com/services.” .

[3] A. Giuffrida and D. Pezzuto, “Assessing the performance of a scroll expander with a selection of fluids suitable for low-temperature applications,” *Energy Procedia*, vol. 126, pp. 493–500, 2017.

[4] S. Quoilin, M. Van Den Broek, S. Declaye, P. Dewallef, and V. Lemort, “Techno-economic survey of organic rankine cycle (ORC) systems,” *Renew. Sustain. Energy Rev.*, vol. 22, pp. 168–186, 2013.

[5] V. Lemort, S. Quoilin, C. Cuevas, and J. Lebrun, “Testing and modeling a scroll expander integrated into an Organic Rankine Cycle,” *Appl. Therm. Eng.*, vol. 29, no. 14–15, pp. 3094–3102, 2009.

[6] D. Mikielewicz and J. Mikielewicz, “A thermodynamic criterion for selection of working fluid for subcritical and supercritical domestic micro CHP,” *Appl. Therm. Eng.*, 2010.

[7] V. M. Nguyen, P. S. Doherty, and S. B. Riffat, “Development of a prototype low-temperature Rankine cycle electricity generation system,” *Appl. Therm. Eng.*, vol. 21, no. 2, pp. 169–181, 2001.

[8] K. Qiu, M. Thomas, and M. Douglas, “Investigation of a scroll expander driven by compressed air and its potential applications to ORC,” *Appl. Therm. Eng.*, vol. 135, no. January, pp. 109–115, 2018.

[9] R. B. Peterson, H. Wang, and T. Herron, “Performance of a small-scale regenerative Rankine power cycle employing a scroll expander,” *Proc. Inst. Mech. Eng. Part A J. Power Energy*, 2008.

[10] L. Guangbin, Z. Yuanyang, L. Yunxia, and L. Liansheng, “Simulation of the dynamic processes in a scroll expander-generator used for small-scale organic Rankine cycle system,” *Proc. Inst. Mech. Eng. Part A J. Power Energy*, 2011.

[11] T. Yanagisawa, T. Shimizu, M. Fukuta, and T. Handa, “Study on fundamental performance of scroll expander,” *Nippon Kikai Gakkai Ronbunshu, B Hen/Transactions Japan Soc. Mech. Eng. Part B*, 1988.

[12] R. Zanelli and D. Favrat, “Experimental Investigation of a Hermetic Scroll Expander-Generator,” in *International Compressor Engineering Conference*, 1994.

[13] T. Yanagisawa, M. Fukuta, Y. Ogi, and E. Yamada, “Operating performance of scroll expander working with water-mixed air,” in *Fluid Mach. Group Inter. Conf. Compressors Syst.*, 2005.

[14] A. Hiwata, A. Ikeda, T. Morimoto, O. Kosuda, and M. Matsui, “Axial and radial force control for a co2Scroll Expander,” *HVAC R Res.*, 2009.

[15] M. S. Orosz, A. V. Mueller, B. J. Dechesne, and H. F. Hemond, “Geometric Design of Scroll Expanders Optimized for Small Organic Rankine Cycles,” *J. Eng. Gas Turbines Power*, vol. 135, no. 4, p. 042303, 2013.

[16] Z. Liu *et al.*, “Modelling and Optimisation on Scroll Expander for Waste Heat Recovery Organic Rankine Cycle,” *Energy Procedia*, vol. 75, no. 0, pp. 1603–1608, 2015.

[17] P. Song, M. Wei, L. Shi, S. N. Danish, and C. Ma, “A review of scroll expanders for organic rankine cycle systems,” *Appl. Therm. Eng.*, vol. 75, pp. 54–64, 2015.

[18] P. Garg, G. M. Karthik, P. Kumar, and P. Kumar, “Development of a generic tool to design scroll expanders for ORC applications,” *Appl. Therm. Eng.*, vol. 109, pp. 878–888, 2016.

[19] V. Lemort, S. Declaye, and S. Quoilin, “Experimental characterization of a hermeti scroll expander for use in a micro-scale Rankine cycle,” *Proc. Inst. Mech. Eng. Part A J. Power Energy*, vol. 226, no. 1, pp. 126–136, 2012.

[20] V. Lemort, S. Quoilin, and J. Lebrun, “Numerical simulation of a scroll expander for use in a Cycle.pdf,” *Int. Compress. Eng. Conf.*, pp. 1–8, 2008.

[21] E. Winandy, C. S. Saavedra O, and J. Lebrun, “Experimental analysis and simplified modelling of a hermetic scroll refrigeration compressor,” *Appl. Therm. Eng.*, vol. 22, no. 2, pp. 107–120, 2002.

[22] Capstone Turbine Corporation, “Technical Reference - Capstone Model C30 Performance,” no. April, pp. 1–14, 2006.

[23] F. Heberle and D. Brüggemann, “Exergy based fluid selection for a geothermal Organic Rankine

Cycle for combined heat and power generation," *Appl. Therm. Eng.*, vol. 30, no. 11–12, pp. 1326–1332, 2010.

[24] H. Nami, A. Nemati, and F. J. Fard, "Conventional and advanced exergy analyses of a geothermal driven dual fluid organic Rankine cycle (ORC)," *Appl. Therm. Eng.*, vol. 122, pp. 59–70, 2017.

[25] M. O. M. E.W. Lemmon, M.L. Huber, "NIST Standard Reference Database 23 e Version 8.0. Physical and Chemical Properties Division, National Institute of Standards and Technology, Boulder, Colorado, 2002, US Department of Commerce, USA." .

Appendix: Double-loop configuration EES code

```
Function gamma1 (fluid1$; P[1]; T[1] ;P[2])
s[1] := entropy (fluid1$; P = P[1]; T = T[1])
v_1 := volume (fluid1$; P = P[1]; T = T[1])
v_2 := volume (fluid1$; P = P[2]; s = s[1])
r_p := P[1] / P[2]
r_v := v_2 / v_1
gamma1:= LOG10 (r_p) / (LOG10 (r_v) )
gamma_tris:= LN (r_p) / LN(r_v)
End gamma1
Function gamma2 (fluid2$; P[6]; T[6] ;P[7])
s[6] := entropy (fluid2$; P = P[6]; T=T[6])
v[6] := volume (fluid2$; P = P[6]; T = T[6])
v[7] := volume (fluid2$; P = P[7]; s = s[6])
r_p := P[6] / P[7]
r_v := v[7] / v[6]
gamma2:= LOG10 (r_p) / (LOG10 (r_v) )
gamma_tris:= LN (r_p) / LN(r_v)
End gamma2
Procedure Expander1 (r_v_in_1; V_s_exp_cm3_1; AU_amb_exp_1; AU_ex1_exp_n_1; AU_su_exp_n_1;
A_leak_1; d_su_1; M_dot_r_exp_n_1; W_dot_loss_0_1; alpha_1; M_dot_r_exp_guess_1;
T_w_exp_guess_1; W_dot_el_exp_guess_1; P_r_su_exp_1; T_r_su_exp_1; P_r_ex1_exp_1; T_amb_exp_1:
M_dot_r_exp_1; W_dot_el_exp_1; T_r_ex1_exp_1; Q_dot_amb_exp_1; T_w_exp_1; residual_1;
r_p_crit_1; M_dot_r_leak_1; r_p_su_exp_1;epsilon_s_exp_1)
$Common FLUID1$
//3. model
//3,1. Supply status
T_r_sat_su_exp_1 := T_sat (fluid1$ ;  P=P_r_su_exp_1)
DELTA_Toh_su_exp_1 := T_r_su_exp_1 - T_r_sat_su_exp_1
h_r_su_exp_1 := enthalpy(fluid1$; P=P_r_su_exp_1; T=T_r_su_exp_1)
v_r_su_exp_1 := volume(fluid1$; P=P_r_su_exp_1; T=T_r_su_exp_1)
s_r_su_exp_1 := entropy(fluid1$; P=P_r_su_exp_1; T=T_r_su_exp_1)
//3,3. supply pressure drop: su=> su1
```

```
A_thr_su_1 := pi * (d_su_1^2)/4
//incompressible flow model:
DELTA_P_r_su_exp_1 := ((M_dot_r_exp_guess_1/A_thr_su_1)^2)/(2/v_r_su_exp_1)
P_r_su1_exp_1 := P_r_su_exp_1 - DELTA_P_r_su_exp_1
r_p_su_exp_bis_1 := P_r_su1_exp_1 / P_r_su_exp_1
//Compressible flow model:
v_r_thr_su_1 := v_r_su_exp_1
1:
C_thr_su_1 := (M_dot_r_exp_guess_1/A_thr_su_1)* v_r_thr_su_1
h_r_thr_su_1 := h_r_su_exp_1 - (C_thr_su_1^2)/2
P_r_thr_su_1 := Pressure (fluid1$; h= h_r_thr_su_1; s=s_r_su_exp_1)
P_r_su1_exp_1 := P_r_thr_su_1
v_r_thr_su_bis_1 := volume(fluid1$; P=P_r_thr_su_1; h=h_r_thr_su_1)
If  (abs(v_r_thr_su_1 - v_r_thr_su_bis_1)/v_r_thr_su_1> 0,02)  Then
v_r_thr_su_1 := v_r_thr_su_bis_1
GoTo 1
Endif
r_p_su_exp_1 := P_r_su1_exp_1/P_r_su_exp_1
h_r_su1_exp_1 := h_r_su_exp_1
T_r_su1_exp_1 := temperature (fluid1$; P=P_r_su1_exp_1; h= h_r_su1_exp_1)
//3.4 supply cooling down: su1 => su2
cp_r_su1_exp_1 := Cp (fluid1$; P=P_r_su1_exp_1; T=T_r_su1_exp_1)
C_dot_su1_exp_1 := M_dot_r_exp_guess_1 * cp_r_su1_exp_1
AU_su_exp_1 := AU_su_exp_n_1* (M_dot_r_exp_guess_1/M_dot_r_exp_n_1)^0,8
NTU_su_exp_1 := AU_su_exp_1/ C_dot_su1_exp_1
epsilon_su_exp_1 := 1 - EXP( - NTU_su_exp_1)
Q_dot_su_exp_1= epsilon_su_exp_1 * C_dot_su1_exp_1* (T_r_su1_exp_1-T_w_exp_guess_1)
P_r_su2_exp_1 := P_r_su1_exp_1
h_r_su2_exp_1 := h_r_su1_exp_1 -(Q_dot_su_exp_1/M_dot_r_exp_guess_1)
T_r_su2_exp_1  := temperature(fluid1$; P=P_r_su2_exp_1; h=h_r_su2_exp_1)
s_r_su2_exp_1 := entropy (fluid1$; P=P_r_su2_exp_1; h=h_r_su2_exp_1)
v_r_su2_exp_1 := volume (fluid1$; P=P_r_su2_exp_1; T=T_r_su2_exp_1)
//3,5 Mass flow rate
rpm_exp_1 := 3007 + 0,02155 * W_dot_el_exp_guess_1 + 0,000002091 * W_dot_el_exp_guess_1^2
```

```
V_s_exp_1 := V_s_exp_cm3_1 / 1000000
V_dot_s_exp_1 := rpm_exp_1/60 * V_s_exp_1
M_dot_r_in_1 := V_dot_s_exp_1/ v_r_su2_exp_1
//3,6 Leakage flow rate
gamma_r_1 := gamma1(fluid1$; P_r_su2_exp_1; T_r_su2_exp_1; P_r_su2_exp_1 / 1,629)
P_r_crit_1 := P_r_su2_exp_1 * ((2 / (gamma_r_1+1))^(gamma_r_1 / (gamma_r_1-1)))
r_p_crit_1  := P_r_su2_exp_1 / P_r_crit_1
P_r_ex3_exp_1 := P_r_ex1_exp_1
P_r_thr_1 := Max (P_r_ex3_exp_1; P_r_crit_1)
h_r_thr_1 := enthalpy (fluid1$; P=P_r_thr_1; s= s_r_su2_exp_1)
C_thr_1 := (2 * (h_r_su2_exp_1 - h_r_thr_1))^0,5
v_r_thr_1 := volume (fluid1$; P=P_r_thr_1; h=h_r_thr_1)
M_dot_r_leak_1 := A_leak_1 * C_thr_1 / v_r_thr_su_bis_1
// 3,7 total flow
M_dot_r_exp_1 := M_dot_r_in_1 + M_dot_r_leak_1
//3,8 Isentropic expansion: su2=>in
v_r_in_exp_1 := r_v_in_1* v_r_su2_exp_1
P_r_in_exp_1 := pressure(fluid1$; v= v_r_in_exp_1; s= s_r_su2_exp_1)
h_r_in_exp_1 := enthalpy(fluid1$; s=s_r_su2_exp_1; P= P_r_in_exp_1)
T_r_in_exp_1 := temperature(fluid1$; h=h_r_in_exp_1; P= P_r_in_exp_1)
w_exp_1_1 := h_r_su2_exp_1 - h_r_in_exp_1
r_p_in_1 := P_r_su2_exp_1/P_r_in_exp_1
// 3,9 Isochore Expansion
w_exp_2_1:=v_r_in_exp_1*(P_r_in_exp_1-P_r_ex3_exp_1)
h_r_ex3_exp_1 := h_r_in_exp_1 - w_exp_2_1
T_r_ex3_exp_1 := temperature(fluid1$; h=h_r_ex3_exp_1; P=P_r_ex3_exp_1)
x_r_ex3_exp_1 := quality(fluid1$; h=h_r_ex3_exp_1; P=P_r_ex3_exp_1)
//3,10 Total work
w_in_exp_1 :=w_exp_2_1+w_exp_1_1
//3,11. Power
W_dot_in_exp_1 := M_dot_r_in_1 * w_in_exp_1
// 3,12. Shaft Power
W_dot_loss1_1 :=  W_dot_loss_0_1+ alpha_1 * W_dot_in_exp_1
W_dot_sh_exp_1 := W_dot_in_exp_1 - W_dot_loss1_1
```

```
eta_mec_1 :=  W_dot_sh_exp_1 / W_dot_in_exp_1
// 3,13. Electrical Power
rpm_rel_1 := 3002 - rpm_exp_1
W_dot_loss2_1 := 198,7 + 0,4553 * rpm_rel_1 + 0,03699 * rpm_rel_1^2
W_dot_el_exp_1 := W_dot_sh_exp_1 - W_dot_loss2_1
eta_mot_1 := W_dot_el_exp_1 / W_dot_sh_exp_1
W_dot_loss_1 := W_dot_loss1_1 + W_dot_loss2_1
eta_elmec_1 := W_dot_el_exp_1/W_dot_in_exp_1
//3,14. Mixing with leakage at the exhaust ex3=>ex2
h_r_ex2_exp_1 := (M_dot_r_in_1 * h_r_ex3_exp_1 + M_dot_r_leak_1 * h_r_su2_exp_1) / M_dot_r_exp_1
P_r_ex2_exp_1 := P_r_ex1_exp_1
T_r_ex2_exp_1 := temperature(fluid1$ ; h = h_r_ex2_exp_1; P=P_r_ex2_exp_1)
//3,15. Exhaust cooling down: ex2=> ex 1
cp_r_ex2_exp_1:= Cp(fluid1$; P = P_r_ex2_exp_1; T=T_r_ex2_exp_1)
C_dot_ex2_exp_1 := M_dot_r_exp_1 * cp_r_ex2_exp_1
AU_ex1_exp_1 := AU_ex1_exp_n_1 * (M_dot_r_exp_1/M_dot_r_exp_n_1)^0,8
NTU_ex1_exp_1 := AU_ex1_exp_1/ C_dot_ex2_exp_1
epsilon_ex1_exp_1 :=1-exp (-NTU_ex1_exp_1)
Q_dot_ex1_exp_1:= epsilon_ex1_exp_1* C_dot_ex2_exp_1* (T_r_ex2_exp_1 - T_w_exp_guess_1)
h_r_ex1_exp_1 := h_r_ex2_exp_1 - (Q_dot_ex1_exp_1/M_dot_r_exp_1)
T_r_ex1_exp_1 := temperature(fluid1$; h=h_r_ex1_exp_1; P=P_r_ex1_exp_1)
v_r_ex1_exp_1 := volume(fluid1$; h=h_r_ex1_exp_1; P=P_r_ex1_exp_1)
//3,17 heat ballance over the expander
Q_dot_amb_exp_1 := Q_dot_su_exp_1 + Q_dot_ex1_exp_1 + W_dot_loss_1
T_w_exp_1 := (Q_dot_amb_exp_1/AU_amb_exp_1 - 273,15) + T_amb_exp_1
//3,18 Energy balance check
residual_1 := M_dot_r_exp_1* (h_r_su_exp_1 - h_r_ex1_exp_1)  - W_dot_el_exp_1 - Q_dot_amb_exp_1
//3,19 Performance
h_r_ex1_exp_s_1 := enthalpy (fluid1$; P=P_r_ex1_exp_1; s=s_r_su_exp_1)
w_exp_s_1 := h_r_su_exp_1  -  h_r_ex1_exp_s_1
epsilon_s_exp_1 := W_dot_el_exp_1/ (M_dot_r_exp_1* w_exp_s_1)
r_p_exp_1 := P_r_su_exp_1 / P_r_ex1_exp_1
M_dot_r_th_1 := V_dot_s_exp_1/v_r_su_exp_1
phi_exp_1 := M_dot_r_exp_1/M_dot_r_th_1
```

```
End Expander1

Procedure Expander2 (r_v_in_2; V_s_exp_cm3_2; AU_amb_exp_2; AU_ex1_exp_n_2; AU_su_exp_n_2;
A_leak_2; d_su_2; M_dot_r_exp_n_2; W_dot_loss_0_2; alpha_2; M_dot_r_exp_guess_2;
T_w_exp_guess_2; W_dot_el_exp_guess_2; P_r_su_exp_2; T_r_su_exp_2; P_r_ex1_exp_2; T_amb_exp_2:
M_dot_r_exp_2; W_dot_el_exp_2; T_r_ex1_exp_2; Q_dot_amb_exp_2; T_w_exp_2; residual_2;
r_p_crit_2; M_dot_r_leak_2; r_p_su_exp_2;epsilon_s_exp_2)

$Common FLUID2$

//3. model

//3,1. Supply status

T_r_sat_su_exp_2 := T_sat (fluid2$ ;  P=P_r_su_exp_2)

DELTA_Toh_su_exp_2 := T_r_su_exp_2 - T_r_sat_su_exp_2

h_r_su_exp_2 := enthalpy(fluid2$; P=P_r_su_exp_2; T=T_r_su_exp_2)

v_r_su_exp_2 := volume(fluid2$; P=P_r_su_exp_2; T=T_r_su_exp_2)

s_r_su_exp_2 := entropy(fluid2$; P=P_r_su_exp_2; T=T_r_su_exp_2)

//3,3. supply pressure drop: su=> su1

A_thr_su_2 := pi * (d_su_2^2)/4

//incompressible flow model:

DELTA_P_r_su_exp_2 := ((M_dot_r_exp_guess_2/A_thr_su_2)^2)/(2/v_r_su_exp_2)

P_r_su1_exp_2 := P_r_su_exp_2 - DELTA_P_r_su_exp_2

r_p_su_exp_bis_2 := P_r_su1_exp_2 / P_r_su_exp_2

//Compressible flow model:

v_r_thr_su_2 := v_r_su_exp_2

1:

C_thr_su_2 := (M_dot_r_exp_guess_2/A_thr_su_2)* v_r_thr_su_2

h_r_thr_su_2 := h_r_su_exp_2 - (C_thr_su_2^2)/2

P_r_thr_su_2 := Pressure (fluid2$; h= h_r_thr_su_2; s=s_r_su_exp_2)

P_r_su1_exp_2 := P_r_thr_su_2

v_r_thr_su_bis_2 := volume(fluid2$; P=P_r_thr_su_2; h=h_r_thr_su_2)

If  (abs(v_r_thr_su_2 - v_r_thr_su_bis_2)/v_r_thr_su_2> 0,02)  Then

v_r_thr_su_2 := v_r_thr_su_bis_2

GoTo 1

Endif

r_p_su_exp_2 := P_r_su1_exp_2/P_r_su_exp_2

h_r_su1_exp_2 := h_r_su_exp_2

T_r_su1_exp_2 := temperature (fluid2$; P=P_r_su1_exp_2; h= h_r_su1_exp_2)

//3.4 supply cooling down: su1 => su2
```

```
cp_r_su1_exp_2 := Cp (fluid2$; P=P_r_su1_exp_2; T=T_r_su1_exp_2)
C_dot_su1_exp_2 := M_dot_r_exp_guess_2 * cp_r_su1_exp_2
AU_su_exp_2 := AU_su_exp_n_2* (M_dot_r_exp_guess_2/M_dot_r_exp_n_2)^0,8
NTU_su_exp_2 := AU_su_exp_2/ C_dot_su1_exp_2
epsilon_su_exp_2 := 1 - EXP( - NTU_su_exp_2)
Q_dot_su_exp_2= epsilon_su_exp_2 * C_dot_su1_exp_2* (T_r_su1_exp_2-T_w_exp_guess_2)
P_r_su2_exp_2 := P_r_su1_exp_2
h_r_su2_exp_2 := h_r_su1_exp_2 - (Q_dot_su_exp_2 / M_dot_r_exp_guess_2)
T_r_su2_exp_2  := temperature(fluid2$; P=P_r_su2_exp_2; h=h_r_su2_exp_2)
s_r_su2_exp_2 := entropy (fluid2$; P=P_r_su2_exp_2; h=h_r_su2_exp_2)
v_r_su2_exp_2 := volume (fluid2$; P=P_r_su2_exp_2; T=T_r_su2_exp_2)
//3,5 Mass flow rate
rpm_exp_2 := 3007 + 0,02155 * W_dot_el_exp_guess_2 + 0,000002091 * W_dot_el_exp_guess_2^2
V_s_exp_2 := V_s_exp_cm3_2 / 1000000
V_dot_s_exp_2 := rpm_exp_2/60 * V_s_exp_2
M_dot_r_in_2 := V_dot_s_exp_2/ v_r_su2_exp_2
//3,6 Leakage flow rate
gamma_r_2 := gamma2(fluid2$; P_r_su2_exp_2; T_r_su2_exp_2; P_r_su2_exp_2/1,629)
P_r_crit_2 := P_r_su2_exp_2 * ((2 / (gamma_r_2+1))^(gamma_r_2 / (gamma_r_2-1)))
r_p_crit_2  := P_r_su2_exp_2 / P_r_crit_2
P_r_ex3_exp_2 := P_r_ex1_exp_2
P_r_thr_2 := Max (P_r_ex3_exp_2; P_r_crit_2)
h_r_thr_2 := enthalpy (fluid2$; P=P_r_thr_2; s= s_r_su2_exp_2)
C_thr_2 := (2 * (h_r_su2_exp_2 - h_r_thr_2))^0,5
v_r_thr_2 := volume (fluid2$; P=P_r_thr_2; h=h_r_thr_2)
M_dot_r_leak_2 := A_leak_2 * C_thr_2 / v_r_thr_su_bis_2
// 3,7 total flow
M_dot_r_exp_2 := M_dot_r_in_2 + M_dot_r_leak_2
//3,8 Isentropic expansion: su2=>in
v_r_in_exp_2 := r_v_in_2* v_r_su2_exp_2
P_r_in_exp_2 := pressure(fluid2$; v= v_r_in_exp_2; s= s_r_su2_exp_2)
h_r_in_exp_2 := enthalpy(fluid2$; s=s_r_su2_exp_2; P= P_r_in_exp_2)
T_r_in_exp_2 := temperature(fluid2$; h=h_r_in_exp_2; P= P_r_in_exp_2)
w_exp_1_2:=h_r_su2_exp_2 - h_r_in_exp_2
```

```
r_p_in_2 := P_r_su2_exp_2 / P_r_in_exp_2
// 3,9 Isochore Expansion
w_exp_2_2 := v_r_in_exp_2* (P_r_in_exp_2 - P_r_ex3_exp_2)
h_r_ex3_exp_2 := h_r_in_exp_2 - w_exp_2_2
T_r_ex3_exp_2 := temperature(fluid2$; h=h_r_ex3_exp_2; P=P_r_ex3_exp_2)
x_r_ex3_exp_2 := quality(fluid2$; h=h_r_ex3_exp_2; P=P_r_ex3_exp_2)
//3,10 Total work
w_in_exp_2 :=w_exp_2_2 + w_exp_1_2
//3,11. Power
W_dot_in_exp_2 := M_dot_r_in_2 * w_in_exp_2
// 3,12. Shaft Power
W_dot_loss1_2 :=  W_dot_loss_0_2+ alpha_2 * W_dot_in_exp_2
W_dot_sh_exp_2 := W_dot_in_exp_2 - W_dot_loss1_2
eta_mec_2 :=  W_dot_sh_exp_2 / W_dot_in_exp_2
// 3,13. Electrical Power
rpm_rel_2 := 3002 - rpm_exp_2
W_dot_loss2_2 := 198,7 + 0,4553 * rpm_rel_2 + 0,03699 * rpm_rel_2^2
W_dot_el_exp_2 := W_dot_sh_exp_2 - W_dot_loss2_2
eta_mot_2 := W_dot_el_exp_2 / W_dot_sh_exp_2
W_dot_loss_2 := W_dot_loss1_2 + W_dot_loss2_2
eta_elmec_2 := W_dot_el_exp_2/W_dot_in_exp_2
//3,14. Mixing with leakage at the exhaust ex3=>ex2
h_r_ex2_exp_2 := (M_dot_r_in_2 * h_r_ex3_exp_2 + M_dot_r_leak_2 * h_r_su2_exp_2) / M_dot_r_exp_2
P_r_ex2_exp_2 := P_r_ex1_exp_2
T_r_ex2_exp_2 := temperature(fluid2$ ; h = h_r_ex2_exp_2; P=P_r_ex2_exp_2)
//3,15. Exhaust cooling down: ex2=> ex 1
cp_r_ex2_exp_2:= Cp(fluid2$; P = P_r_ex2_exp_2; T=T_r_ex2_exp_2)
C_dot_ex2_exp_2 := M_dot_r_exp_2 * cp_r_ex2_exp_2
AU_ex1_exp_2 := AU_ex1_exp_n_2 * (M_dot_r_exp_2/M_dot_r_exp_n_2)^0,8
NTU_ex1_exp_2 := AU_ex1_exp_2/ C_dot_ex2_exp_2
epsilon_ex1_exp_2 :=1-exp (-NTU_ex1_exp_2)
Q_dot_ex1_exp_2:= epsilon_ex1_exp_2* C_dot_ex2_exp_2* (T_r_ex2_exp_2 - T_w_exp_guess_2)
h_r_ex1_exp_2 := h_r_ex2_exp_2 -(Q_dot_ex1_exp_2/M_dot_r_exp_2)
T_r_ex1_exp_2 := temperature(fluid2$; h=h_r_ex1_exp_2; P=P_r_ex1_exp_2)
```

v_r_ex1_exp_2 := volume(fluid2$; h=h_r_ex1_exp_2; P=P_r_ex1_exp_2)

//3,17 heat ballance over the expander

Q_dot_amb_exp_2 := Q_dot_su_exp_2 + Q_dot_ex1_exp_2 + W_dot_loss_2

T_w_exp_2 := (Q_dot_amb_exp_2/AU_amb_exp_2 - 273,15) + T_amb_exp_2

//3,18 Energy balance check

residual_2 := M_dot_r_exp_2* (h_r_su_exp_2 - h_r_ex1_exp_2) - W_dot_el_exp_2 - Q_dot_amb_exp_2

//3,19 Performance

h_r_ex1_exp_s_2 := enthalpy (fluid2$; P=P_r_ex1_exp_2; s=s_r_su_exp_2)

w_exp_s_2 := h_r_su_exp_2 - h_r_ex1_exp_s_2

epsilon_s_exp_2 := W_dot_el_exp_2/ (M_dot_r_exp_2* w_exp_s_2)

r_p_exp_2 := P_r_su_exp_2 / P_r_ex1_exp_2

M_dot_r_th_2 := V_dot_s_exp_2/v_r_su_exp_2

phi_exp_2 := M_dot_r_exp_2/M_dot_r_th_2

End Expander2

//4. Calling the model1

Call Expander1 (r_v_in_1; V_s_exp_cm3_1 ; AU_amb_exp_1 ; AU_ex1_exp_n_1 ; AU_su_exp_n_1 ; A_leak_1 ; d_su_1 ; M_dot_r_exp_n_1 ; W_dot_loss_0_1 ; alpha_1 ; M_dot_r_exp_guess_1 ; T_w_exp_guess_1 ; W_dot_el_exp_guess_1 ; P_r_su_exp_1 ; T_r_su_exp_1 ; P_r_ex1_exp_1 ; T_amb_exp_1: M_dot_r_exp_1 ; W_dot_el_exp_1 ; T_r_ex1_exp_1 ; Q_dot_amb_exp_1 ; T_w_exp_1 ; residual_1; r_p_crit_1; M_dot_r_leak_1 ; r_p_su_exp_1;epsilon_s_exp_1)

//4. Calling the model2

Call Expander2 (r_v_in_2; V_s_exp_cm3_2 ; AU_amb_exp_2 ; AU_ex1_exp_n_2 ; AU_su_exp_n_2 ; A_leak_2 ; d_su_2 ; M_dot_r_exp_n_2 ; W_dot_loss_0_2 ; alpha_2 ; M_dot_r_exp_guess_2 ; T_w_exp_guess_2 ; W_dot_el_exp_guess_2 ; P_r_su_exp_2 ; T_r_su_exp_2 ; P_r_ex1_exp_2 ; T_amb_exp_2 : M_dot_r_exp_2 ; W_dot_el_exp_2 ; T_r_ex1_exp_2 ; Q_dot_amb_exp_2 ; T_w_exp_2 ; residual_2; r_p_crit_2; M_dot_r_leak_2 ; r_p_su_exp_2; epsilon_s_exp_2)

//first expander

//1. Parameters

M_dot_r_exp_n_1 = 0,1 [kg/s]

AU_amb_exp_1 = 3,4 [W/k]

AU_ex1_exp_n_1=30 [W/k]

AU_su_exp_n_1 = AU_ex1_exp_n_1

A_su_1 = 0,00006 [m2]

W_dot_loss_0_1 = 0 [W]

alpha_1 = 0,1 [-]

r_v_in_1 = 2,85[-]

V_s_exp_cm3_1 = 45 [cm3]

```
A_su_1 = PI*d_su_1^2 / 4        [m2]
A_leak_1 = (0,6845 - 0,11635604 * (10 - P_r_su_exp_1 / 100000)) * 0,000001  [m2]
//2. simulation
 fluid1$ = 'isopentane'
P_r_su_exp_1 = 1200000          [Pa]
P_r_ex1_exp_1 = 400000          [Pa]
T_r_su_exp_1 = 140     [C]
T_amb_exp_1 = 34       [C]
M_dot_r_exp_guess_1 = M_dot_r_exp_1
T_w_exp_guess_1 = T_w_exp_1
W_dot_el_exp_guess_1 = W_dot_el_exp_1
PR_1=P_r_su_exp_1/P_r_ex1_exp_1
//second expander
//Parameters
M_dot_r_exp_n_2 = 0,1           [kg/s]
AU_amb_exp_2 = 3,4   [W/k]
AU_ex1_exp_n_2=30   [W/k]
AU_su_exp_n_2 = AU_ex1_exp_n_2
A_su_2 = 0,00006        [m2]
W_dot_loss_0_2 = 0              [W]
alpha_2= 0,1     [-]
r_v_in_2 = 2,85[-]
V_s_exp_cm3_2 = 45   [cm3]
A_su_2 = PI*d_su_2^2 / 4        [m2]
A_leak_2 = (0,6845 - 0,11635604 * (10 - P_r_su_exp_2 / 100000)) * 0,000001   [m2]
//2. simulation
 fluid2$ ='isobutane'
P_r_su_exp_2 = 1400000          [Pa]
P_r_ex1_exp_2 = 450000          [Pa]
T_r_su_exp_2 = 100     [C]
T_amb_exp_2 = 34       [C]
M_dot_r_exp_guess_2 = M_dot_r_exp_2
T_w_exp_guess_2 = T_w_exp_2
W_dot_el_exp_guess_2 = W_dot_el_exp_2
```

```
PR_2 = P_r_su_exp_2/P_r_ex1_exp_2
//PRESSURE LOSSES ASSUMPTIONS + ATMOSPHERIC PRESSURE
HT_Exch_P_loss = 0,98
LT_Exch_P_loss = 0,97
Cond_P_loss = 0,99
P_atm = 101325       [Pa]
//PUMP PRESSURE RATIO
Beta_1 = P[4] / P[3]
Beta_2 = P[9] / P[7]
//BURNT GAS CONDITIONS
cp_g = 1100      [J/kg·K]
// WORKING FLUID CONDITIONS
"state 1"
P[1] = P_r_su_exp_1
T[1] = T_r_su_exp_1
h[1] = Enthalpy (fluid1$ ; P = P[1] ; T = T[1])
s[1] = Entropy (fluid1$ ; P = P[1] ; T = T[1])
v[1] = Volume (fluid1$ ; P = P[1] ; T = T[1])
"state 2"
P[2] = P_r_ex1_exp_1
T[2] = T_r_ex1_exp_1
h[2] = Enthalpy (fluid1$; P = P[2] ; T = T[2])
s[2] = Entropy (fluid1$; P = P[2] ; T = T[2])
v[2] = Volume (fluid1$; P = P[2] ; T = T[2])
"state 3"
P[3] = P[2] *LT_Exch_P_loss
T[3] = temperature (fluid1$ ; P = P[3] ; x = x[3])
h[3] = Enthalpy (fluid1$ ;P=P[3] ; x = x[3])
 s[3] = entropy ( fluid1$ ; x = x[3] ; P = P[3])
v[3] = volume (fluid1$ ; x = x[3] ; P = P[3])
x[3] = 0
"state 4"
P[4] = P[1] / (HT_Exch_P_loss)
T[4] = Temperature (fluid1$ ; P = P[4] ; h = h[4])
```

```
h[4] = h[3] + v[3] * (P[4] - P[3])
s[4] = s[3]
v[4] = volume ( fluid1$ ; P = P[4] ; h = h[4])
// Second loop points
"state 5"
P[5] = P_r_su_exp_2
T[5] = T_r_su_exp_2
h[5] = Enthalpy (fluid2$ ; P = P[5] ; T = T[5])
s[5] = Entropy (fluid2$ ; P = P[5] ; T = T[5])
v[5] = Volume (fluid2$ ; P = P[5] ; T = T[5])
"state 6"
P[6] = P_r_ex1_exp_2
T[6] = T_r_ex1_exp_2
h[6] = Enthalpy (fluid2$ ; P = P[6] ; T = T[6])
s[6] = Entropy (fluid2$ ; P = P[6] ; T = T[6])
v[6] = Volume (fluid2$ ; P = P[6] ; T = T[6])
"state 7"
P[7] = P[6] * Cond_P_loss
T[7] = temperature (fluid2$ ; P = P[7] ; x = x[7])
h[7] = Enthalpy (fluid2$ ; P = P[7] ; x = x[7])
s[7] = entropy (fluid2$ ; P = P[7] ; x = x[7])
v[7]= volume (fluid2$; T = T[7] ; x = x [7])
x[7] = 0
"state 8"
P[8] = P[9] / LT_Exch_P_loss
T[8] = temperature (fluid2$; P = P[8] ; h = h[8])
h[8] = h[7] + v[7] * (P[8] - P[7])
s[8]= s[7]
v[8] = volume (fluid2$; T = T[8] ; h = h[8])
"state 9"
P[9] = P[5] / LT_Exch_P_loss
T[9] = Temperature (fluid2$ ; P = P[9] ; h=h[9])
s[9] = entropy (fluid2$ ; P = P[9] ; h=h[9])
v[9] = volume (fluid2$ ; P = P[9] ; h=h[9])
```

M_dot_r_exp_2 * (h[5] - h[9]) = M_dot_r_exp_1 * (h[2] - h[3])

//WATER UTILITY POINTS

"state 10"

P[10]= 150000

T[10] = 15 [C]

h[10] = enthalpy (Water; T = T[10] ; P = P[10])

v[10] = volume (Water ; P = P[10] ; T = T[10])

"state 11"

P[11] = P[13] / (LT_Exch_P_loss * Cond_P_loss)

T[11] = Temperature (Water ; P= P[11] ; h=h[11])

h[11] = h[10] + v[10] * (P[11] - P[10])

M_dot_cw * (h[12] - h[11]) = M_dot_r_exp_2 * (h[6] - h[7])

v[11] = volume (Water ; P = P[11] ; T = T[11])

s[11] = entropy (Water ; P = P[11] ; T = T[11])

"state 12"

P[12] = P[13] / LT_Exch_P_loss

T[12] = temperature(Water ; h = h[12] ; P = P[12])

"state 13"

P[13] = 300000

T[13] = 60

h[13] = enthalpy (Water ; P=P[13] ; T=T[13])

M_dot_cw * (h[13] - h[12]) = M_dot_1g * (h[19] - h[20])

// WATER LOOP CONDITIONS

"state 14"

M_dot_water =0,1

P[14] = 600000

T[14] = 150

h[14] = enthalpy (Water ; T=T[14]; P=P[14])

v[14] = volume (Water ; T=T[14]; P=P[14])

s[14] = entropy (Water ; T=T[14]; P=P[14])

"state 15"

P[15] = P[14] * HT_Exch_P_loss

T[15] = temperature (Water ; P = P[15] ; h = h[15])

M_dot_water * (h[14] - h[15]) = M_dot_r_exp_1 * (h[1] - h[4])

"state 16"

P[16] = P[14] * HT_Exch_P_loss * LT_Exch_P_loss

T[16] = temperature (Water ; h=h[16] ; P = P[16])

M_dot_water * (h[15] - h[16]) = M_dot_r_exp_2 * (h[9] - h[8])

v[16] = volume (Water ; h=h[16] ; P = P[16])

"state 17"

P[17] = P[14] / HT_Exch_P_loss

h[17] = h[16] + v[16]* (P[17] - P[16])

T[17] = temperature (Water ; P = P[17] ; h = h[17])

"state 18"

M_dot_1g = 0,31

P[18] = P[20] / (LT_Exch_P_loss * HT_Exch_P_loss)

T[18] = 275

M_dot_1g * (h[18] - h[19]) = M_dot_water * (h[14] - h[17])

h[18] = cp_g * (T[18] + 273)

"state 19"

P[19] = P[20] / LT_Exch_P_loss

h[19] = cp_g * (T[19] + 273)

"state 20"

P[20] = P_atm

T[20] = 75

h[20] = cp_g * (T[20] + 273)

//Exchangers Duty

Q_dot_HX1= M_dot_r_exp_1 * (h[1] - h[4])

Q_dot_HX2= M_dot_r_exp_2 * (h[5] - h[9])

Q_dot_HX3= M_dot_r_exp_2 * (h[9] - h[8])

Q_dot_HX4= M_dot_cw * (h[12] - h[11])

Q_dot_HX5 =M_dot_1g * (h[18] - h[19])

Q_dot_HX6 =M_dot_1g * (h[19] - h[20])

//CHP HEAT RECOVERY SYSTEM

Q_dot_cw = Q_dot_HX4 + Q_dot_HX6

Q_dot_input =M_dot_1g * (h[18] - h[20])

//DUTY RATIO

DR=Q_dot_HX1/Q_dot_HX3

```
// PERFORMANCE
W_dot_pump_1 = M_dot_r_exp_1 * (h[4] - h[3]) / eta_pump
W_dot_pump_2 = M_dot_r_exp_2 * (h[8] - h[7]) / eta_pump
W_dot_pump_3 = M_dot_water * (h[17] - h[16]) / eta_pump
W_dot_pump_4 = M_dot_cw * (h[11] - h[10]) / eta_pump
W_dot_pump = W_dot_pump_1 + W_dot_pump_2 + W_dot_pump_3 + W_dot_pump_4
W_dot_el = W_dot_el_exp_1 + W_dot_el_exp_2
W_dot_net_1 = W_dot_el_exp_1 - W_dot_pump_1
W_dot_net_2 = W_dot_el_exp_2 - W_dot_pump_2
W_dot_net = W_dot_el - W_dot_pump
// EFFICIENCY
eta_pump = 0,95 {pump  efficiency}
eta_el = W_dot_el/ (Q_dot_HX1+Q_dot_HX3)
eta_CHP = (W_dot_net + Q_dot_cw) / (Q_dot_input)
eta_el1= W_dot_net_1/ Q_dot_HX1
eta_el2= W_dot_net_2/ (Q_dot_HX3 + Q_dot_HX2)
eta_cycle_1 = (W_dot_net_1 + Q_dot_HX2)/ Q_dot_HX1
eta_cycle_2 = (W_dot_net_2 + Q_dot_HX4) / (Q_dot_HX3 + Q_dot_HX2)
// PITCH POINTS
deltaT1= T[14] - T[1]
deltaT2= T[2] - T[5]
deltaT3= T[5] - T[9]
deltaT4= T[6] - T[11]
deltaT5= T[18] - T[14]
deltaT6= T[19] - T[13]
//REGENERATION EFFICIENCY
eta_rec= (T[5]-T[9])/(T[2]-T[9])
```